

UNCLASSIFIED

AD NUMBER

AD831579

LIMITATION CHANGES

TO:

Approved for public release; distribution is unlimited.

FROM:

Distribution authorized to U.S. Gov't. agencies and their contractors; Critical Technology; 27 DEC 1967. Other requests shall be referred to Office of Naval Research, 875 North Randolph Street, Arlington, VA 22203-1995. This document contains export-controlled technical data.

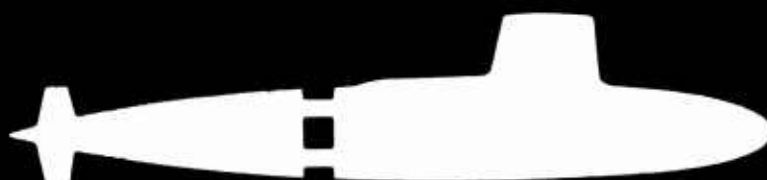
AUTHORITY

ONR ltr, 9 Nov 1973

THIS PAGE IS UNCLASSIFIED

AD831579

# SUBIC



Submarine Integrated Control

OFFICE OF  
NAVAL  
RESEARCH

GENERAL DYNAMICS CORPORATION  
ELECTRIC BOAT DIVISION  
GROTON, CONNECTICUT

STATEMENT #2 UNCLASSIFIED

This document is subject to special export controls and each transmittal to foreign government or foreign nationals may be made only with prior approval of

Code H 66

Office of Naval Research  
NWash, D.C. 20360

PROCESSING OF DATA FROM  
SONAR SYSTEMS  
VOLUME IV  
SUPPLEMENT 1

by

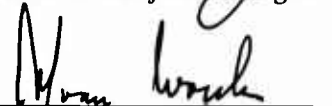
Morton Kanefsky  
F.S. Hill, Jr.  
Peter M. Schultheiss

Yale University

Examined:

  
J.W. Herring  
SUBIC Project Manager

Approved:

  
Dr. A.J. van Woerkom  
Chief Scientist

U417-67-084  
December 27, 1967

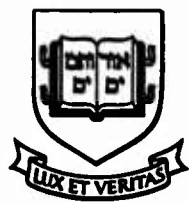
## TABLE OF CONTENTS

<u>Report No.</u>	<u>Title</u>	<u>Page</u>
	Foreword	v
	Introduction	1
23	Adaptive Array Detectors in the Presence of Non-Gaussian Noise	A-1
24	An Automatic Decision Threshold for Polarity Coincidence Arrays	B-1
25	Vertical Directionality of Ambient Noise at a Hydrophone Near the Surface	C-1
27	Detection of Active Sonar Signals by Means of A Crosscorrelator	D-1



## FOREWORD

This is an unclassified supplement to Volume IV of a series of reports describing work performed by Yale University under subcontract to Electric Boat division of General Dynamics Corporation. Volume IV, Report No. C417-67-075, covers the period 1 July 1965 to 1 July 1966. Electric Boat is prime contractor of the SUBIC (Submarine Integrated Control) Program under Office of Naval Research contract NOmr 2512(00). LCDR. E.W. Lull, USN, is Project Officer for ONR; J.W. Herring is Project Manager for Electric Boat division under the direction of Dr. A.J. van Woerkom.



---

ADAPTIVE ARRAY DETECTORS IN THE PRESENCE OF NON-GAUSSIAN NOISE

by

Morton Kanefsky

Progress Report No. 23

General Dynamics Electric Boat division

(8050-33-55001)

August 1965

DEPARTMENT OF ENGINEERING  
AND APPLIED SCIENCE  
YALE UNIVERSITY

## I. Introduction

The standard detector that one considers for the underwater sound problem approximates a monotonic function of the likelihood ratio based on stationary Gaussian inputs when the input signal-to-noise ratio in each channel is small (locally optimum). Very often the variances of the noise processes are unknown but can be assumed to be stationary during the decision time (quasi-stationary). When this occurs, the detection threshold may be adjusted according to an estimate of the noise variance. It has been shown in Report No. 18 that this procedure is desired for CFAR detection and that for large arrays it costs very little in terms of detectability in the presence of Gaussian noise.

It will now be shown that some nonparametric properties are obtained by this procedure. That is, the false-alarm rate can be fixed for any quasi-stationary input and for certain non-Gaussian inputs, of the impulse variety, the cost and hence the miss rate are reduced.

## II. Terminology

We will assume a threshold, m-input, array detector of the following type.

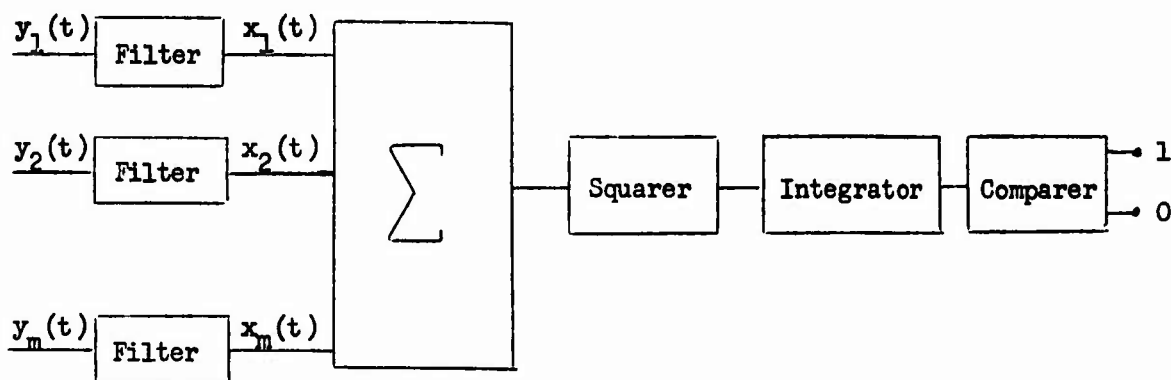


Figure 1

This represents the locally optimum detector (Report No. 10) for detecting a random signal that is common to  $m$  channels each containing stationary Gaussian noise processes that are statistically identical but independent. The filters are identical Eckart-type filters with a transfer function  $S(\omega)/N^2(\omega)$ , where  $S(\omega)$  is the signal spectrum and  $N(\omega)$  is the noise spectrum.

The following assumptions will be made:

- 1) The noise and signal processes which are the components of the vector  $\bar{x}(t)$  have zero mean and normalized time correlation functions given by

$$\rho_n(\tau) = \frac{E\{n_1(t) n_1(t+\tau)\}}{E\{n_1^2(t)\}}$$

$$\rho_s(\tau) = \frac{E\{s_1(t) s_1(t+\tau)\}}{E\{s_1^2(t)\}}$$

- 2) The decision time  $T$ , or integration time, is much larger than the effective width of  $\rho_n(\tau)$ , so that the test statistic can be assumed to be normally distributed with negligible error.

When the variance is unknown, the detector of Fig. 1 is to be modified in the following way.

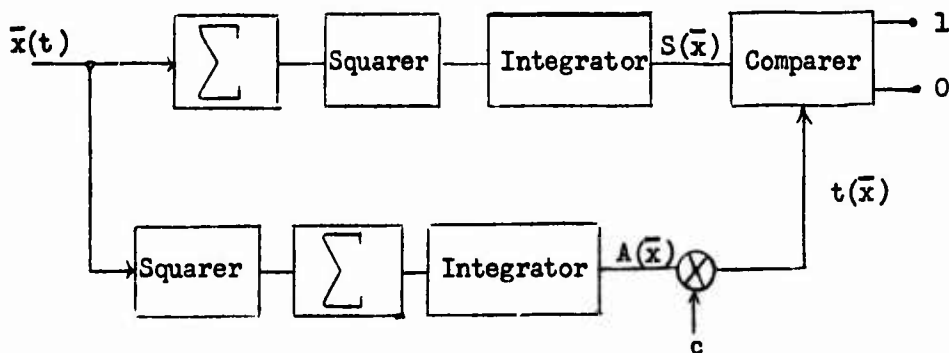


Figure 2

This is the procedure used in Report No. 18 to obtain CFAR detection for Gaussian inputs with unknown variance.

The false-alarm rate ( $\alpha$ ) of this detector is the probability given the hypothesis of no signal present that  $S(\bar{x}) > t(\bar{x})$ . Since  $S(\bar{x})$  and  $t(\bar{x})$  can be assumed to be normally distributed with negligible error, it follows that

$$\alpha = \text{Prob}_H \left\{ S(\bar{x}) - t(\bar{x}) > 0 \right\} \approx 1 - \Phi \left\{ \frac{-E_H \{ S(\bar{x}) - t(\bar{x}) \}}{\left[ \text{Var}_H \{ S(\bar{x}) - t(\bar{x}) \} \right]^{1/2}} \right\},$$

or, conversely,

$$E_H \{ t(\bar{x}) \} \approx E_H \{ S(\bar{x}) \} + \Phi^{-1}(1 - \alpha) \left[ \text{Var}_H \{ S(\bar{x}) - t(\bar{x}) \} \right]^{1/2}, \quad (1)$$

where  $\Phi$  is the normalized Gaussian cumulative distribution function. Since  $E_H \{ S(\bar{x}) \} = E_H \{ A(\bar{x}) \} = Tm\sigma_n^2$ , where  $\sigma_n^2$  is the noise variance, it follows that the multiplier  $c$  should be

$$c \approx 1 + \Phi^{-1}(1 - \alpha) \frac{\left[ \text{Var}_H \{ S(\bar{x}) - t(\bar{x}) \} \right]^{1/2}}{Tm\sigma_n^2}. \quad (2)$$

As  $c \rightarrow 1$  asymptotically, it is sufficient that

$$c = 1 + \Phi^{-1}(1 - \alpha_0) \frac{\left[ \text{Var}_H \{ S(\bar{x}) - A(\bar{x}) \} \right]^{1/2}}{Tm\sigma_n^2}, \quad (3)$$

for the false-alarm rate to approach  $\alpha_0$  as  $T$  gets large. The resulting error in  $\alpha$  is of the same order of magnitude as that implied in assuming that  $S(\bar{x})$  and  $A(\bar{x})$  are normally distributed.

When the signal is present, the shift in the test statistic  $S(\bar{x})$  is given by

$$E_K\{S(\bar{x})\} - E_H\{S(\bar{x})\} = Tm^2\sigma_s^2 ,$$

where  $\sigma_s^2$  is the signal variance. The corresponding shift in  $t(\bar{x})$  is

$$E_K\{t(\bar{x})\} - E_H\{t(\bar{x})\} = Tm\sigma_s^2 .$$

Thus for any  $m \geq 2$  the adaptive detector is consistent. That is, the probability of detection ( $\beta$ ) approaches unity as  $T$  becomes large. In order to calculate the cost of this procedure it is necessary to calculate the output signal-to-noise ratio of the detectors, defined as

$$\text{SNR}_{\text{standard}} = \frac{E_K\{S(\bar{x})\} - E_H\{S(\bar{x})\}}{[\text{Var}_K S(\bar{x})]^{1/2}} , \quad (4)$$

and

$$\text{SNR}_{\text{adaptive}} = \frac{E_K\{S(\bar{x})\} - E_K\{t(\bar{x})\}}{[\text{Var}_K\{S(\bar{x}) - t(\bar{x})\}]^{1/2}} ,$$

where

$$S(\bar{x}) = \int_0^T \left[ \sum_{i=1}^m x_i(t) \right]^2 dt ,$$

$$A(\bar{x}) = \int_0^T \left[ \sum_{i=1}^m x_i^2(t) \right] dt ,$$

and

$$t(\bar{x}) = c A(\bar{x}) .$$

### III. Output Signal-to-Noise Ratio

The following expression can be evaluated under the assumption of stationary noise:

$$\text{Var}_K S(\bar{x}) \approx 2m^2 T \sigma_n^4 h [1 + 2\delta] + 2m T \sigma_n^4 h \psi, \quad (5)$$

where

$$\psi = \frac{\int_0^T \int_0^T E \left\{ n_1^2(t) n_1^2(\xi) - \sigma_n^4 \right\} dt d\xi}{2T \sigma_n^4 h} - 1; \quad (6)$$

and where  $h = 2 \int_0^T \left(1 - \frac{\xi}{T}\right) \rho_n^2(\xi) d\xi$  and is a measure of the "width" of the normalized correlation function of the noise processes; and  $\delta = m \frac{\sigma_s^2}{\sigma_n^2} \frac{h'}{h}$

where  $h'$  is similar to  $h$  except that  $\rho_n^2(\xi)$  is replaced by  $\rho_n(\xi) \rho_s(\xi)$ . The approximation of Eq. (5) is a result of having dropped a  $\delta^2$  term since there is already an error of order  $\delta^2$  inherent in this analysis, as a result of assumption 2). Note that the assumption  $\delta \ll 1$  is also necessary for the standard array detector to approximate the optimum. This assumption is valid for many practical conditions.

When the signal and noise processes have the same spectra, then  $h' = h$ . For Gaussian inputs it is easily shown that  $\psi = 0$ . If the threshold of the standard detector were based on Gaussian inputs, the presence of uncorrelated noise processes for which  $\psi > 0$  would increase the false-alarm rate. It is conjectured that the class of processes for which  $\psi > 0$  contains those processes which correspond to some impulse model. Observe,

however, that the dependence of  $\alpha$  on  $\psi$  is small for large  $m$  ( $m \gg \psi$ ).

The output signal-to-noise ratio for the standard detector and for small  $\delta$  is given by

$$\text{SNR}_{\text{standard}} = \sqrt{\frac{T}{2h}} \frac{\frac{\sigma_s^2}{2}}{\frac{\sigma_n}{\sqrt{1 + 2\delta + \frac{1}{m}\psi}}} \quad (7)$$

For quasi-stationary inputs, one can show that for  $\delta \ll 1$ ,

$$\text{Var}_K \left\{ S(\bar{x}) - A(\bar{x}) \right\} = 2m(m-1)T\sigma_n^4 h \left[ 1 + 2\frac{m-1}{m}\delta \right] \quad (8)$$

It follows from Eqs. (3) and (8) that for arbitrary quasi-stationary inputs,

$$c = 1 + \sqrt{\frac{m-1}{m}} \frac{\Phi^{-1}(1 - \alpha_0)}{\sqrt{\frac{T}{2h}}} \quad (9)$$

Therefore the adaptive detector is asymptotically nonparametric in that  $\alpha$  approaches a constant ( $\alpha_0$ ) as  $T \rightarrow \infty$  for any quasi-stationary input. The rate of convergence is limited by the rate of convergence of the test statistics to the normal distribution. In addition one would expect some improvement in detectability for non-Gaussian noise processes for which  $\psi > 0$ . It can be shown that  $\text{Var}_K \left\{ S(\bar{x}) - t(\bar{x}) \right\}$  differs from  $\text{Var}_K \left\{ S(\bar{x}) - A(\bar{x}) \right\}$  only to order  $\delta^2$  provided  $T$  is sufficiently large so that  $\beta > 50$  per cent. Therefore the output signal-to-noise ratio for the adaptive detector and for small  $\delta$  is



$$\text{SNR}_{\text{adaptive}} \approx \sqrt{\frac{T}{2h}} \frac{\sqrt{m(m-1)} \frac{\sigma_s^2}{2}}{\sqrt{1 + 2\delta - \frac{2\delta}{m}}} \quad (10)$$

#### IV. Cost of Adaptive Procedure

Let us now equate the output signal-to-noise ratios of Eqs. (7) and (10) by considering  $(m-x)$  channels for the standard detector and  $m$  channels for the adaptive detector. Thus  $x$  is defined as the cost in terms of number of channels for estimating the noise variance. Solving for  $x$  yields

$$x = m - m \sqrt{1 - \frac{(1 - \psi + \frac{\psi}{m})(1 - 2\delta)}{m(1 - \frac{2\delta}{m})}} \quad (11)$$

For large  $m$  this can be approximated by

$$x \rightarrow \frac{1}{2} + (\psi - 1)m \frac{\sigma_s^2}{\sigma_n^2} \frac{h'}{h} - \frac{\psi}{2} + O\left(\frac{1}{m} \delta^2\right) \quad (12)$$

Thus for very small input signal-to-noise ratios, Gaussian inputs, and large  $m$ , the cost is approximately  $\frac{1}{2}$  channel (as shown in Report No. 18). Let us now consider an example of a non-Gaussian noise input.

Suppose the input noise consists of a process that has been obtained by squaring a Gaussian process with zero mean and then filtering out the d.c. term. That is,

$$n(t) = \left[ z^2(t) - \sigma_z^2 \right] \quad (13)$$

where  $z(t)$  is Gaussian with zero mean and variance  $\sigma_z^2$ . It follows that  $n(t)$  has a zero mean and a variance of  $2\sigma_z^4$ . From Eq. (6) it is seen that

$$\begin{aligned}
\psi &= \frac{\int_0^T \int_0^T \mathbb{E} \left\{ \left( z^2(t) - \sigma_z^2 \right)^2 \left( z^2(\xi) - \sigma_z^2 \right)^2 - 4\sigma_z^8 \right\} dt d\xi}{2T\sigma_n^4} - 1 \\
&= \frac{\int_0^T \int_0^T \left[ \mathbb{E} \left\{ z^4(t) z^4(\xi) \right\} - 4\sigma_z^2 \mathbb{E} \left\{ z^4(t) z^2(\xi) \right\} + 4\sigma_z^4 \mathbb{E} \left\{ z^2(t) z^2(\xi) \right\} - \sigma_z^8 \right] dt d\xi}{2T\sigma_n^4} - 1 \\
&= \frac{\int_0^T \int_0^T \left[ 32 \sigma_z^8 \rho_z^2(t-\xi) + 24 \sigma_z^8 \rho_z^4(t-\xi) \right] dt d\xi}{2T\sigma_n^4 \int_0^T \left(1 - \frac{\xi}{T}\right) \rho_z^2(\xi) d\xi} - 1 \\
&= \frac{8 \int_0^T \left(1 - \frac{\xi}{T}\right) \rho_z^2(\xi) d\xi + 6 \int_0^T \left(1 - \frac{\xi}{T}\right) \rho_z^4(\xi) d\xi}{2 \int_0^T \left(1 - \frac{\xi}{T}\right) \rho_z^4(\xi) d\xi} - 1 \\
&= 2 + 4 \frac{\int_0^T \left(1 - \frac{\xi}{T}\right) \rho_z^2(\xi) d\xi}{\int_0^T \left(1 - \frac{\xi}{T}\right) \rho_z^4(\xi) d\xi} .
\end{aligned}$$

Since  $\rho_z^4(\xi)$  is narrower than  $\rho_z^2(\xi)$ , it follows that  $\psi > 6$ . For example, if  $\rho_z(\cdot)$  is exponential, then  $\rho_z^4(\xi) d\xi = \rho_z^2(2\xi) d\xi = \frac{1}{2} \rho_z^2(\eta) d\eta$ , and  $\psi = 10$ . It is thus clear from Eq. (12) that for the input of this example  $x$  is negative and of the order of  $-4$  channels. That is, the adaptive

detector is more powerful than the standard detector. This improvement in detection is significant for small to medium-sized arrays. Furthermore, unless the array is large ( $m \gg 10$ ), there will be a significant error in the false-alarm rate of the standard detector.

The process considered in this example has definite characteristics of impulse noise. The amplitude density has a large peak and a slowly (relative to Gaussian) decreasing tail. These characteristics would be exaggerated if we raised the original Gaussian process to a higher power than 2 and correspondingly  $\psi$  would increase further. It is therefore conjectured that the adapted detector is more powerful than the standard detector when the inputs in each channel are uncorrelated impulse noise. This effect is not great, however, for large arrays ( $m \gg 4$ ).



AN AUTOMATIC DECISION THRESHOLD FOR POLARITY COINCIDENCE ARRAYS

by

Morton Kanefsky

Progress Report No. 24

General Dynamics Electric Boat division

(8050-33-55001)

August 1965

DEPARTMENT OF ENGINEERING  
AND APPLIED SCIENCE

YALE UNIVERSITY

### Summary

This report considers the possibility of setting a detection threshold at each bearing angle for the polarity coincidence array. An adaptive threshold employing the number of zero crossings of the hydrophone inputs is shown to greatly reduce the sensitivity of the false-alarm rate to the spectral properties of the noise. The range of usefulness of this procedure is limited to the case when the self-noise of the hydrophones is such as to allow the inputs to be processed to at most 5 times the "nominal" or minimum cut-off frequency of the inputs. The analysis assumes that, in the absence of a target, the hydrophone inputs are all uncorrelated. While this assumption is unreasonable for submarine arrays, it is conjectured that the adaptive procedure can be modified to work in an isotropic noise field with unknown space-time correlation.

## I. Introduction

This report deals with the passive detection of a sonar target in the presence of a gaussian noise background whose spectral properties are unknown. It is common in sonar applications to display the output of some suitable approximation to the likelihood-ratio detector on a cathode ray screen and have an observer reach a decision based on the difference between the on- and off-target detector outputs. This procedure is often carried out in spite of the fact that the likelihood-ratio test is optimum only in the sense that a yes or no decision is made at each bearing angle. There is of course no theory as to the optimum display, primarily because such a theory would involve the subjective nature of the operator. Psychological studies of man's decision-making capabilities are just now beginning. The decision procedure is, however, not automated for a number of reasons. The primary reason is that the detectors are based on a greatly oversimplified model of the actual environment and at the present time do not have the capabilities to distinguish between real and false targets that the operators seem to have. A secondary reason is that a complete statistical knowledge of the noise environment is not available, and the peripheral equipment and computers needed to measure all the necessary parameters are too costly and space-consuming.

As the detectors become more sophisticated, the desirability of an automatic threshold decision made at each bearing angle increases. Sometimes (if we are lucky) certain readily measurable properties of the noise environment contain a large amount of information in just the right form to make an automatic adjustment with minimal peripheral equipment. For example, given a number of simplifying assumptions about the noise

environment, the threshold of a standard array detector can be fixed for non-gaussian noise as well as for gaussian noise simply by using an estimate of the noise variance to set the threshold.\* This procedure assumes that, in the absence of a target, the inputs to the hydrophones are all uncorrelated and have the same known spectral shape. Of course neither of these assumptions is valid and a realistic automatic threshold decision would have to take them into account.

The main conjecture of this report is that the number of zero crossings contains a great deal of information about the space-time correlation of the noise environment and can sometimes be used to automatically adjust the decision threshold. Such a procedure would probably require some additional processing, such as pre-filtering, but hopefully not an unreasonable amount. One might even conjecture that this adaptive procedure could be nonparametric, i.e., not require the gaussian assumption. However, the analysis of this conjecture would require extensive experimentation. This report is far from being a complete study of the problem; rather it presents an example of what can be done.

Consider the use of the Polarity Coincidence Array (PCA), i.e., the Dimus system, for detecting a single sonar target in the presence of an isotropic, gaussian, low-pass noise field. Furthermore, assume that in the absence of the target the hydrophone inputs are all uncorrelated. It will be shown later that this assumption, although reasonable in some respects, is for the purposes of this study prohibitively inaccurate for

---

\*See Report No. 23 for details.

feasible submarine arrays. It is being made, however, to simplify the analysis and to show a possible use of the zero-crossing count. The conjecture is made that the PCA can be made adaptive relative to the spatial correlation by a similar suitable use of the zero-crossing count; however, this conjecture is not examined. The method as well as the restrictiveness of such a procedure are partially indicated by the results presented here for the restricted set of conditions.

It has been shown in Report No. 22 that for the conditions just given the cost of clipping is small when the inputs are sampled rapidly, relative to the cut-off frequency of the noise spectrum. This cost in terms of the input signal-to-noise power ratio is between 0.6 and 1.0 db, depending on the spectral shape. The cost is small in view of the advantages of the PCA, which are (1) ease of implementation and (2) invariance with respect to a nonstationary noise power that varies slowly relative to the inverse bandwidth of the noise spectrum. It was pointed out that in order to set the detection threshold it is necessary to have accurate knowledge of the noise spectrum, that is, of the cut-off frequency as well as the actual shape. It will be demonstrated that an automatic decision threshold can be obtained by using the zero-crossing count in one or more of the hydrophone inputs. This adaptive procedure requires some elementary pre-filtering. Furthermore, this adjustment is not exact, and under certain conditions the false-alarm rate is appreciably different from the designed false-alarm rate. However, in most cases the sensitivity of the false-alarm rate to the spectral shape is significantly reduced.



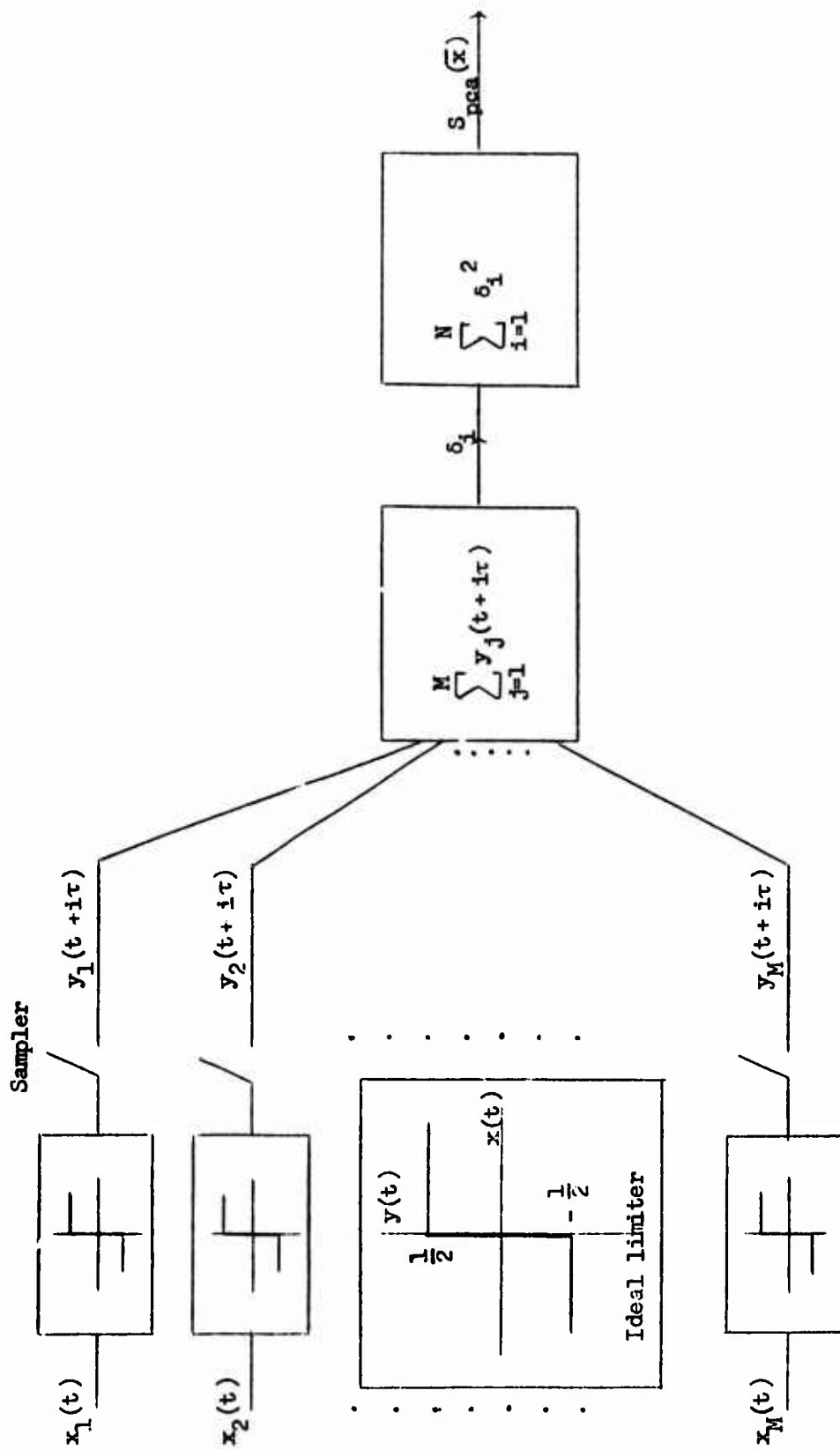


Figure 1 The Polarity Coincidence Array Detector

## II. Terminology

Let us consider the polarity coincidence array detector shown in Fig. 1, which calculates the following test statistic:

$$S_{pca} = \sum_{i=1}^N \left\{ \frac{1}{2} \sum_{j=1}^M \operatorname{sgn}[x_j(t + i\tau)] \right\}^2 \quad (1)$$

The  $x_j(t)$  are the  $M$  inputs to the hydrophones,  $\tau$  is the sampling interval,  $\operatorname{sgn}(\xi) = \begin{matrix} 1 & ; & \xi > 0 \\ -1 & ; & \xi < 0 \end{matrix}$ , and  $N$  is the sample size. This test statistic is compared with a threshold  $t$ , and the detector decides that the signal is present if  $S_{pca} > t$ . The false-alarm probability  $\alpha$  is the probability that  $S_{pca} > t$  given the hypothesis  $(H)$  that the  $x_j(t)$  are all independent gaussian noise processes with the same spectral shape. For large sample sizes and a decision time  $(T)$  large compared with the inverse bandwidth of the noise spectrum,  $S_{pca}$  is approximately normally distributed. Hence

$$\alpha \approx 1 - \bar{\Phi} \left\{ \frac{t - E_H\{S_{pca}\}}{\sqrt{\operatorname{Var}_H\{S_{pca}\}}} \right\}, \quad (2)$$

where  $\bar{\Phi}$  is the normalized gaussian cumulative distribution function, or

$$t \approx E_H\{S_{pca}\} + \bar{\Phi}^{-1}(1 - \alpha) \sqrt{\operatorname{Var}_H\{S_{pca}\}}. \quad (3)$$

From Report No. 22 [Eqs. (10), (27) and (31)] it follows that

$$E_H\{S_{pca}\} = N \frac{M}{L}, \quad (4)$$

and

$$\text{Var}_H\{S_{pca}\} = N \frac{M}{8} (M-1) \left[ 1 + \frac{8}{\pi^2} \sum_{k=1}^N \left(1 - \frac{k}{N}\right) \left\{ \sin^{-1} \left[ \rho_n(k\tau) \right] \right\}^2 \right], \quad (5)$$

where  $\rho_n(\tau)$  is the normalized correlation function of the noise inputs.

It is convenient to define an equivalent sample size  $N_{eq}^*$  as

$$N_{eq} \triangleq \frac{T f_s}{\left[ 1 + \frac{8}{\pi^2} \sum_{k=1}^N \left(1 - \frac{k}{N}\right) \left\{ \sin^{-1} \left[ \rho_n(k\tau) \right] \right\}^2 \right]}, \quad (6)$$

where  $f_s$  is the sampling rate ( $f_s = \frac{1}{\tau}$ ;  $N = T f_s$ ). It follows from the previous four equations that

$$t = f_s T \left[ \frac{M}{L} \left( 1 + \frac{1}{\Phi} (1 - \alpha) \sqrt{\frac{2(1 - \frac{1}{M})}{N_{eq}}} \right) \right]. \quad (7)$$

The equivalent sample size is shown in Figs. 2 and 3 as a function of the sampling rate for a variety of spectral shapes (See Appendix A). It is observed that  $N_{eq}$  varies linearly with the cut-off frequency of the spectrum ( $f_1$ ) and for fast sampling varies considerably with the actual shape of the spectrum. Let us assume that the second break in the spectra shown in Fig. 3 corresponds to the frequency range over which the input data is to be processed. It follows from this figure that continuous

---

\*The output signal-to-noise ratio of  $S_{pca}$  is proportional to  $\sqrt{N}$  for independent samples and to  $\sqrt{N_{eq}}$  for dependent samples; hence the terminology.

Figure 2 Equivalent Number of Uncorrelated Samples for PCA

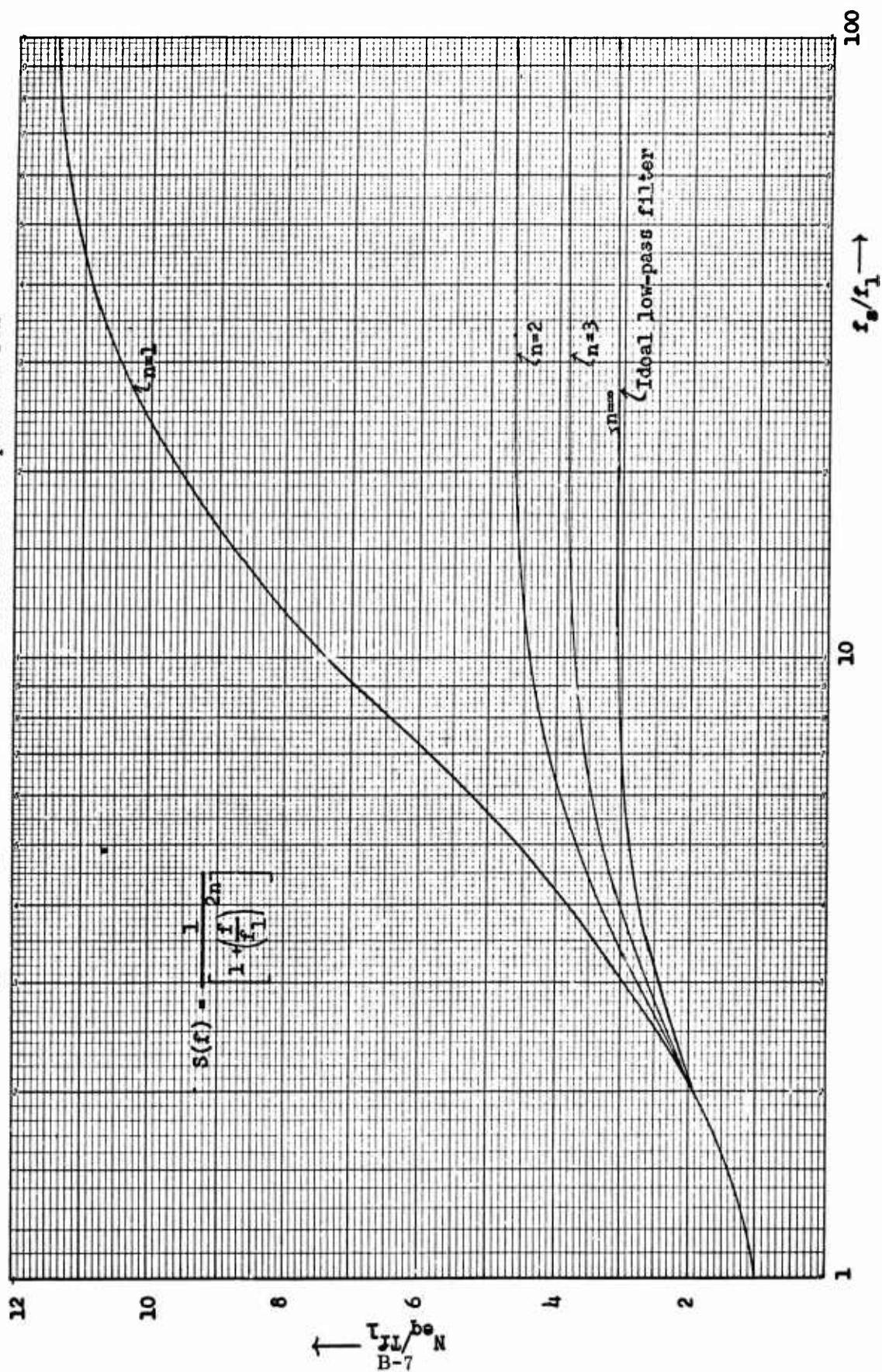
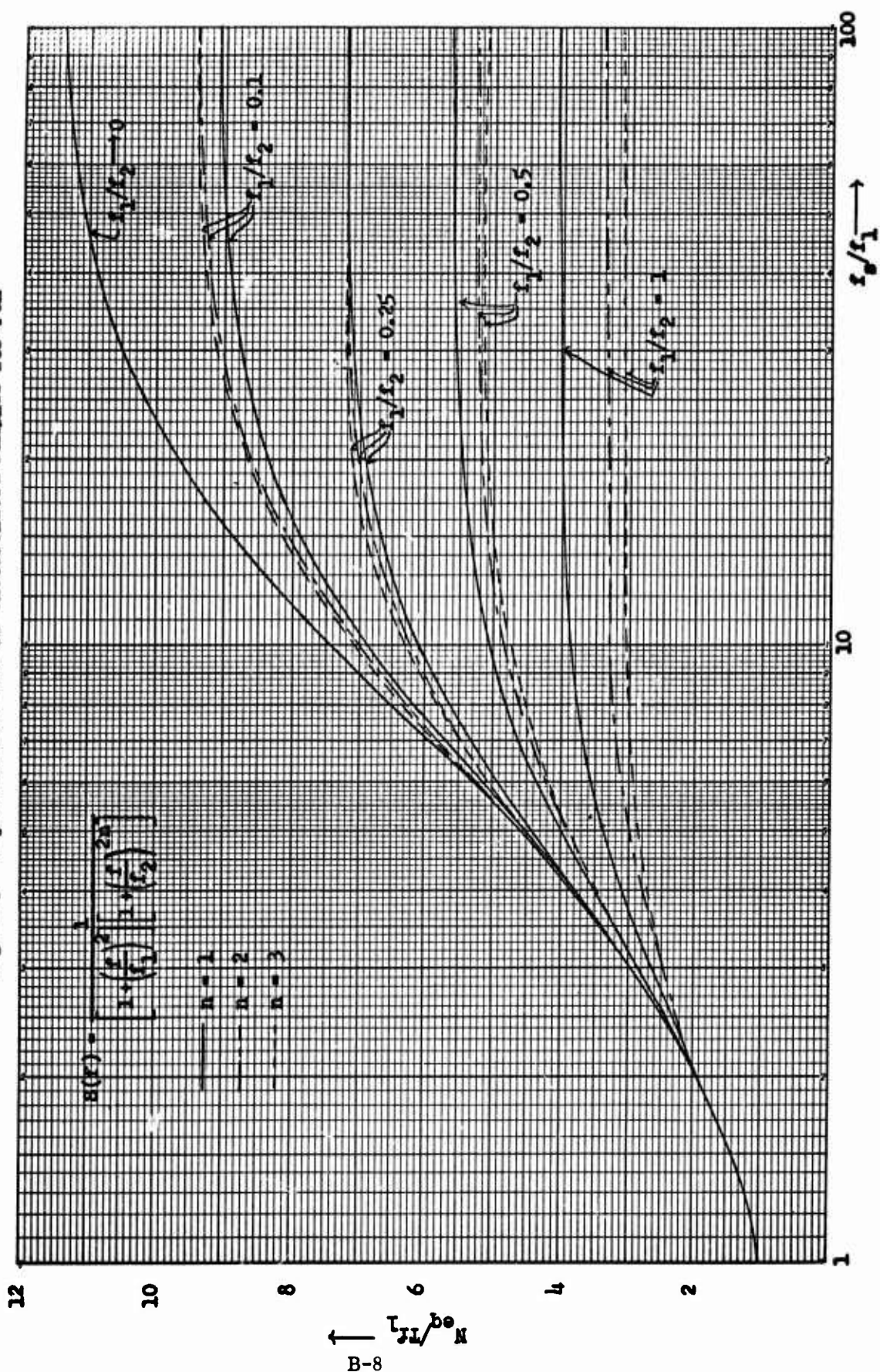


Figure 3 Equivalent Number of Uncorrelated Samples for PCA



operation ( $f_s \rightarrow \infty$ ) is approximately achieved for sampling rates that are at least five times the processing range. It was seen in Report No. 22 that these sampling rates are necessary to achieve the low cost of clipping. In the analysis that follows it will be assumed that the sampling rate is sufficiently fast so that  $N_{eq}$  is essentially equal to its asymptotic value.

### III. An Adaptive Decision Threshold

Let us now consider the following threshold:

$$t' = f_s T \frac{M}{4} \left[ 1 + \Phi^{-1}(1 - \alpha_0) \sqrt{\frac{2(1 - \frac{1}{M})}{K N(0)}} \right], \quad (8)$$

where  $\alpha_0$  is the desired false-alarm probability,  $N(0)$  is the total number of zero crossings in a single channel during the decision time (or the average over more than one channel), and  $K$  is a suitable constant to be determined. The variance of  $t'$  is quite small for large but practical decision times. In fact, the error in the false-alarm probability caused by assuming that  $t'$  is a constant  $[N(0) = \overline{N(0)}; \text{ the average number of zero crossings}]$  vanishes asymptotically as  $T \rightarrow \infty$  in much the same fashion as the error caused by the assumption that  $S_{pca}$  is normally distributed. It is assumed that these errors are small for practical decision times. We will bypass this detail, however, by claiming that we are attempting to set the false-alarm probability asymptotically as the decision time increases (i.e., a learning procedure) and will consider only the error in the asymptotic false-alarm probability. The actual asymptotic false-alarm probability ( $\alpha$ ) is obtained by equating  $t$  of Eq. (7) to  $t'$  of Eq. (8) and replacing  $N(0)$  by  $\overline{N(0)}$ , resulting in

$$\alpha = 1 - \bar{\Phi} \left\{ \bar{\Phi}^{-1} (1 - \alpha_0) - \sqrt{\frac{N_{eq}}{K N(0)}} \right\} . \quad (9)$$

We will now discuss the reasoning behind using  $t'$  as a detection threshold.

The well-known expression for the average number of zero crossings is [1]:

$$\overline{N(0)} = 2T \left[ \frac{\int_0^\infty f^2 S(f) df}{\int_0^\infty S(f) df} \right]^{1/2} , \quad (10)$$

where  $S(f)$  is the spectral shape of the noise inputs. Let us assume that  $S(f)$  can be written in polynomial form and that there exists a first break point in the spectrum denoted by  $f_1$ . If we set  $\frac{f}{f_1} = x$ , we can write

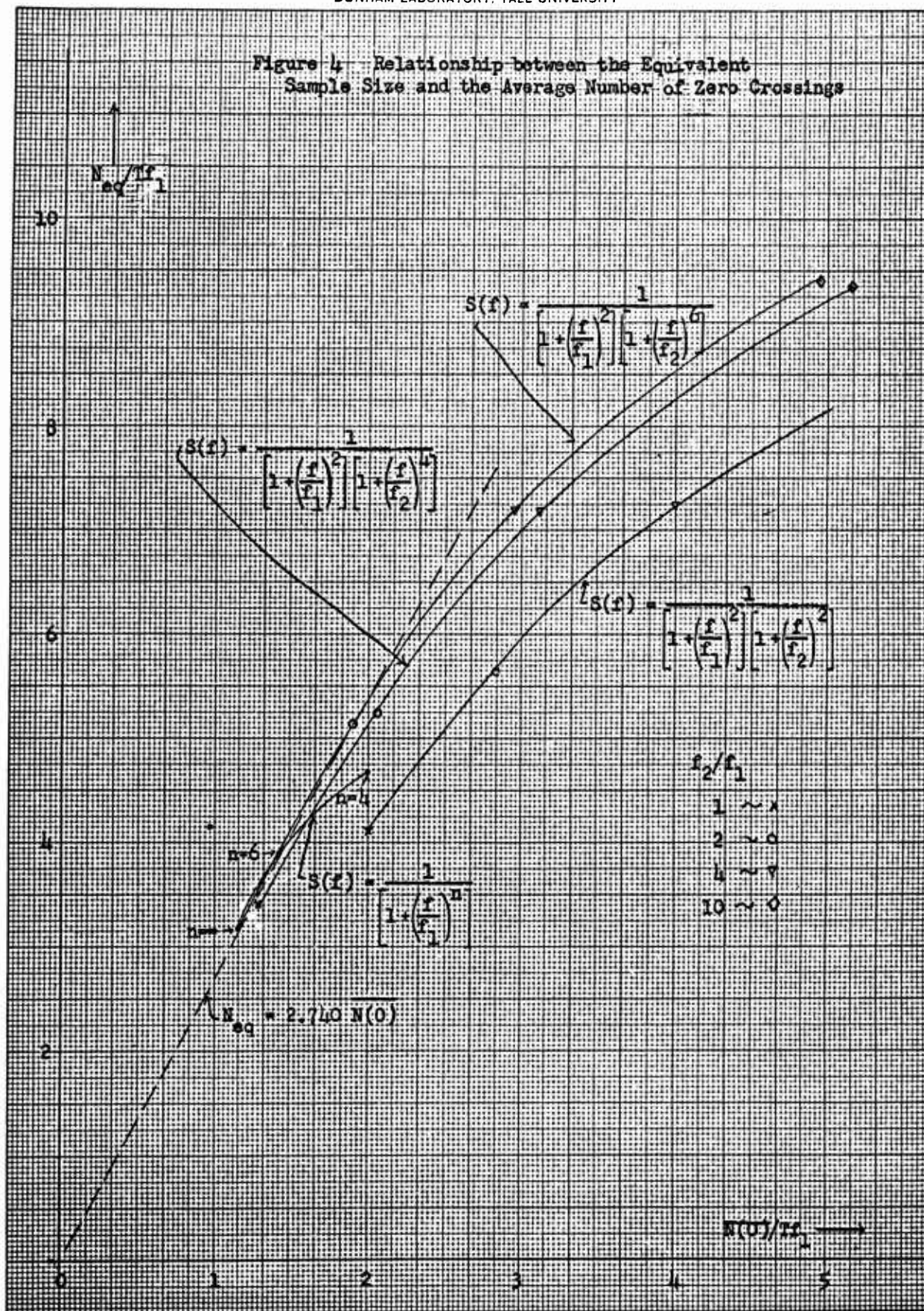
$$\overline{N(0)} = 2Tf_1 \left[ \frac{\int_0^\infty x^2 S(x) dx}{\int_0^\infty S(x) dx} \right]^{1/2} . \quad (11)$$

This expression can be readily evaluated for a variety of low-pass spectral shapes (See Appendix B). Recall [1] that for a "single-pole" spectrum,  $\overline{N(0)} = \infty$ , and our system obviously fails ( $\alpha \rightarrow 50$  per cent). We will assume that there is a processing filter somewhere (maybe the hydrophones themselves) that prevents this possibility.

Figure 4 is a plot of  $\overline{N(0)}$  versus  $N_{eq}$  (large sampling rates) for a variety of spectral shapes that can be obtained by passing white noise through a low-pass filter having no zeros and only real poles. For these



Figure 4 Relationship between the Equivalent Sample Size and the Average Number of Zero Crossings





spectra the following conclusions can be reached. For spectra that fall

off sharply  $\left[ S(f) = \frac{1}{1 + \left(\frac{f}{f_1}\right)^{2n}} ; n \geq 3 \right]$ , there is very nearly a linear

relationship between  $N_{eq}$  and  $\overline{N(0)}$ . For spectra that fall off slowly but

are then cut off sharply at some frequency  $f_2 > f_1$ , the  $\frac{N_{eq}}{\overline{N(0)}}$  curve

has the same linear relationship for  $f_2 < 2f_1$  and falls off somewhat for larger  $f_2$ .

It follows that we should pre-filter the noise inputs with a filter having the transfer function

$$H(j\omega) = \frac{H_0}{1 + \left(\frac{j\omega}{\omega_2}\right)^3}, \quad (12)$$

where  $\omega_2$  is equal to the processing frequency in radians. The constant  $K$  needed for the decision threshold [Eq. (8)] is seen from Fig. 4 to be 2.740. If the noise spectrum begins to fall off slowly at some frequency  $f_1$  considerably less than  $f_2$ , then there will be an error in the asymptotic false-alarm probability given by Eq. (9). This error will be examined in more detail in the next section. In addition to the spectra indicated in Fig. 4, the presence of zeros in the spectrum (filter transfer function) will also be analyzed (spectra restricted to be monotonically decreasing).

It is conjectured that the suboptimum PCA discussed in Report No. 22 will behave similarly with respect to the adaptive threshold and in fact be somewhat better for large arrays. This conjecture is based on the fact that  $N_{eq}$  of the suboptimum device has a larger relative increase than

the optimum PCA as the noise inputs, prior to processing, vary from white to one having a single-tuned spectrum. It follows that the contours of Fig. 4 will probably be even closer to a straight line for the suboptimum PCA.

#### IV. Error in Asymptotic False-Alarm Probability

The actual asymptotic false-alarm probability can be determined from the designed false-alarm probability  $\alpha_0$  and Eq. (9) using Fig. 4 (or the data in the appendices). It will be assumed that the input data are processed according to the previous section. The false-alarm rate is shown in Fig. 5 for a variety of spectral shapes and a designed false-alarm rate of 1 per cent. The abscissa is  $f_1/f_2$ , where  $f_1$  is the cut-off frequency of the noise spectrum and  $f_2$  is the processing frequency. As indicated previously, the only difficulty arises when the noise spectrum falls off slowly and is significantly reduced by the time the processing frequency is reached. The least favorable case ("single-pole" spectrum) is shown again in Fig. 6 for different designed false-alarm rates.

Thus we see that some knowledge of the spectral shape is necessary for an accurate setting of the false-alarm probability. Suppose for instance that we know that the spectral shape is always flat

$$\left\{ \frac{[S(0) - S(f)]}{S(0)} \leq 0.2 \right\} \text{ below some frequency } f_1. \text{ The maximum error in } \alpha$$

caused by processing the inputs out to  $f_2 = 5f_1$  can be obtained from Fig. 6 for the value  $f_1/f_2 = 0.4$ . This is quite a reasonable maximum error. Sometimes one has some other specific knowledge of the noise spectrum that enables one to make an alternate setting of the threshold. Consider the following example.

Figure 5 Error in False-Alarm Rate

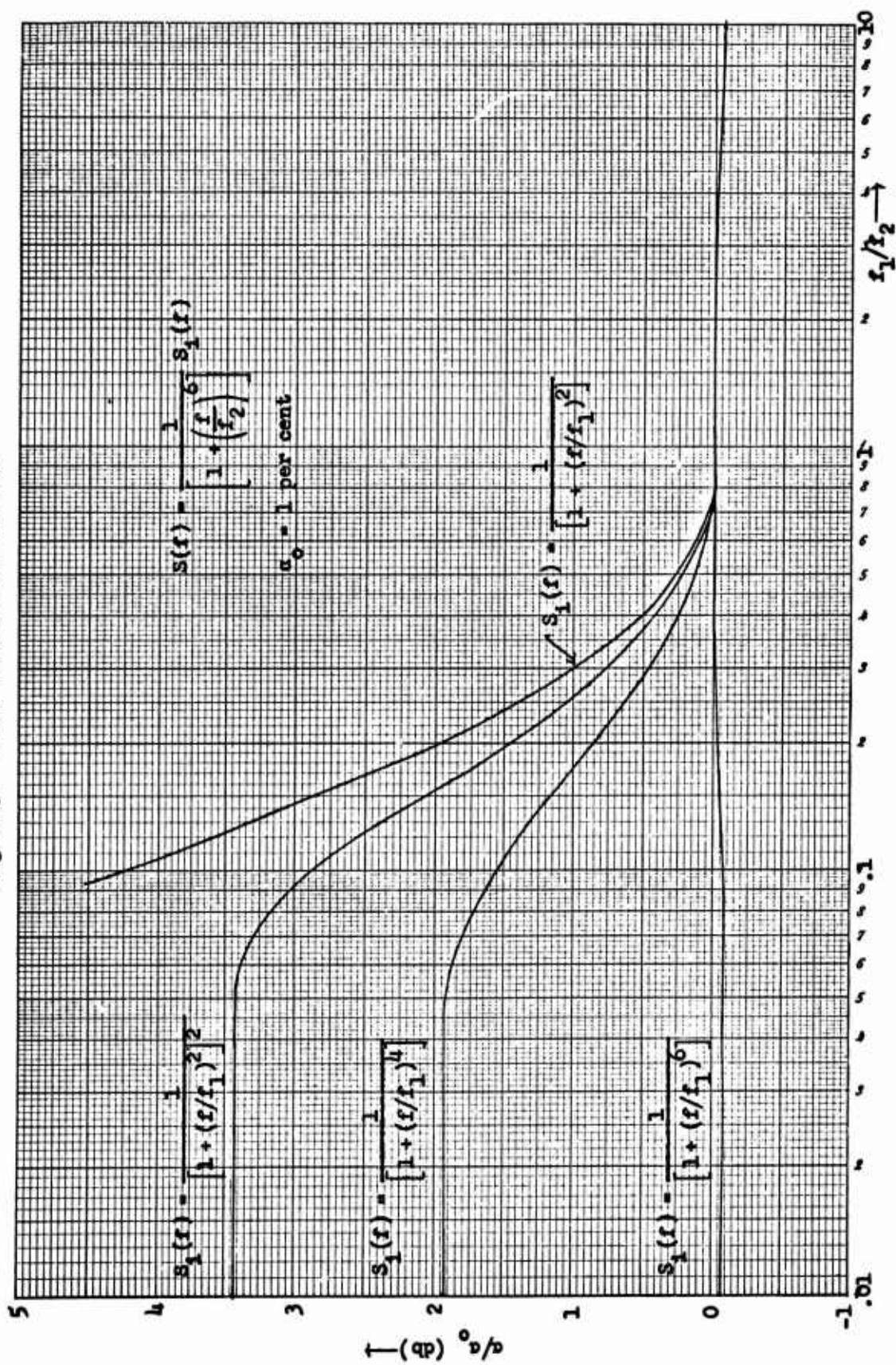
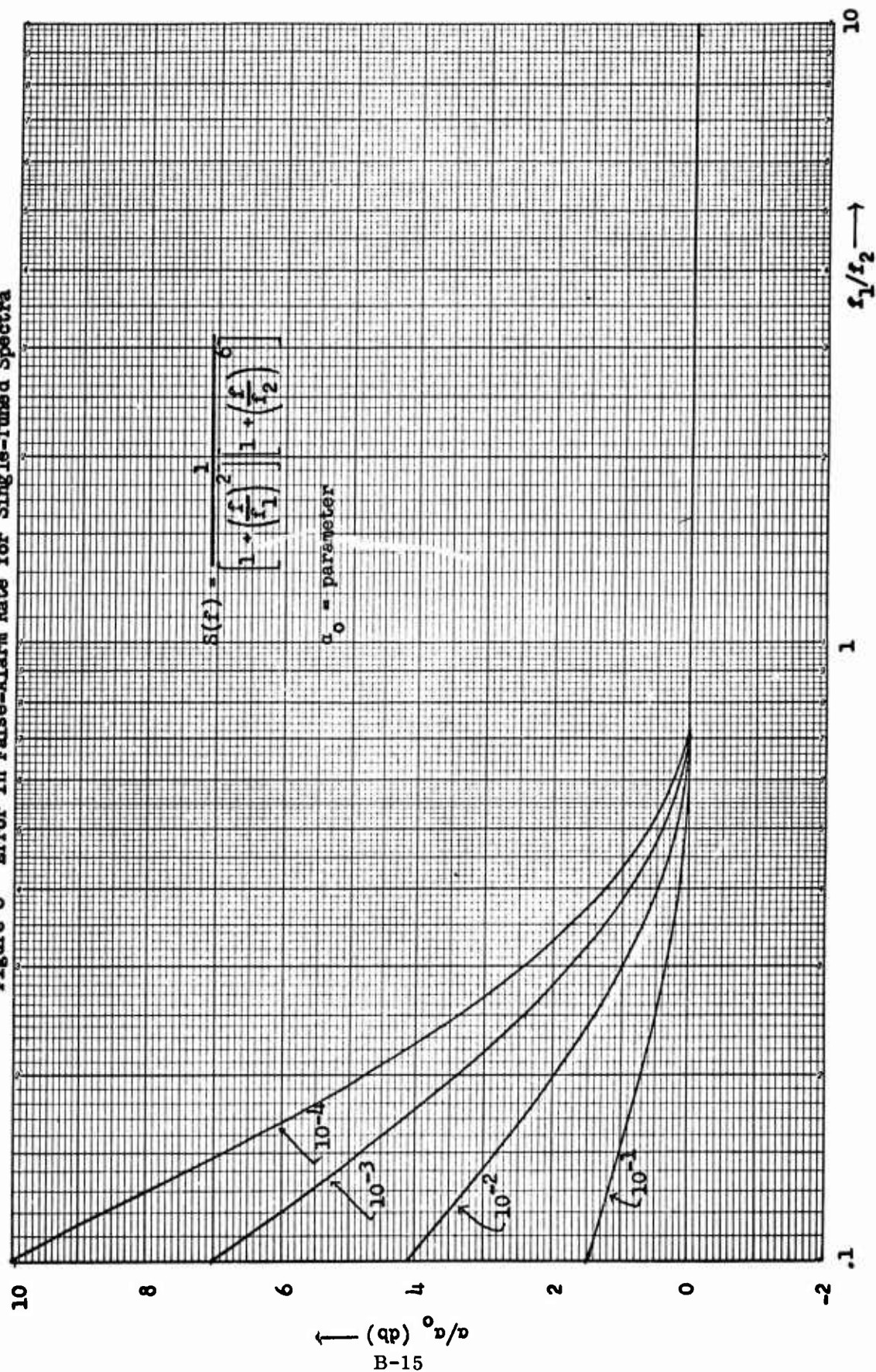


Figure 6 Error in False-Alarm Rate for Single-Tuned Spectra



Let us suppose that the spectrum commonly appears to be "single-tuned" with the cut-off frequency in the vicinity of 1250 cps. Furthermore, let us assume that the self-noise of the hydrophones is such that processing out to 5 kc seems reasonable. Finally assume that the noise spectrum never falls off faster than 12 db/octave. We wish to set the false-alarm probability automatically in such a way that gross errors do not occur for noise spectra other than the nominal one. We therefore process out to 5 kc and set the threshold to give no error for the nominal spectrum ( $K = 2.441$ ). The resulting actual false-alarm probability is shown in Fig. 7 for a designed false-alarm rate of 1 per cent. Included in this figure is the actual false-alarm rate for the non-adaptive detector whose threshold is based on the nominal spectrum. We can reach the following conclusions.

For the non-adaptive detector, the uncertainty in the spectral shape causes a possible variation in  $\alpha$  of 5 db. A similar variation is caused by a 20 per cent uncertainty in the cut-off frequency ( $1 \text{ kc} \leq f_1 \leq 1.5 \text{ kc}$ ). For these uncertainties in the spectral shape, the threshold of the non-adaptive detector can be set to guarantee a maximum error in  $\alpha$  that is less than  $\pm 5$  db. However, the threshold of the adaptive detector can be set to reduce the maximum error in  $\alpha$  to  $\pm 0.7$  db for the same uncertainty in the spectrum. Figure 8 is a similar plot with the only difference being that the inputs are processed only out to the nominal cut-off frequency. With this type of processing the false-alarm rate becomes relatively insensitive to the spectral shape. As a result the non-adaptive detector threshold can be adjusted to guarantee a maximum



Figure 7 Comparison of Adaptive and Non-Adaptive Detectors  
(Nominal spectrum  $S_1(f)$  with  $f_1/f_2 = 0.25$ )

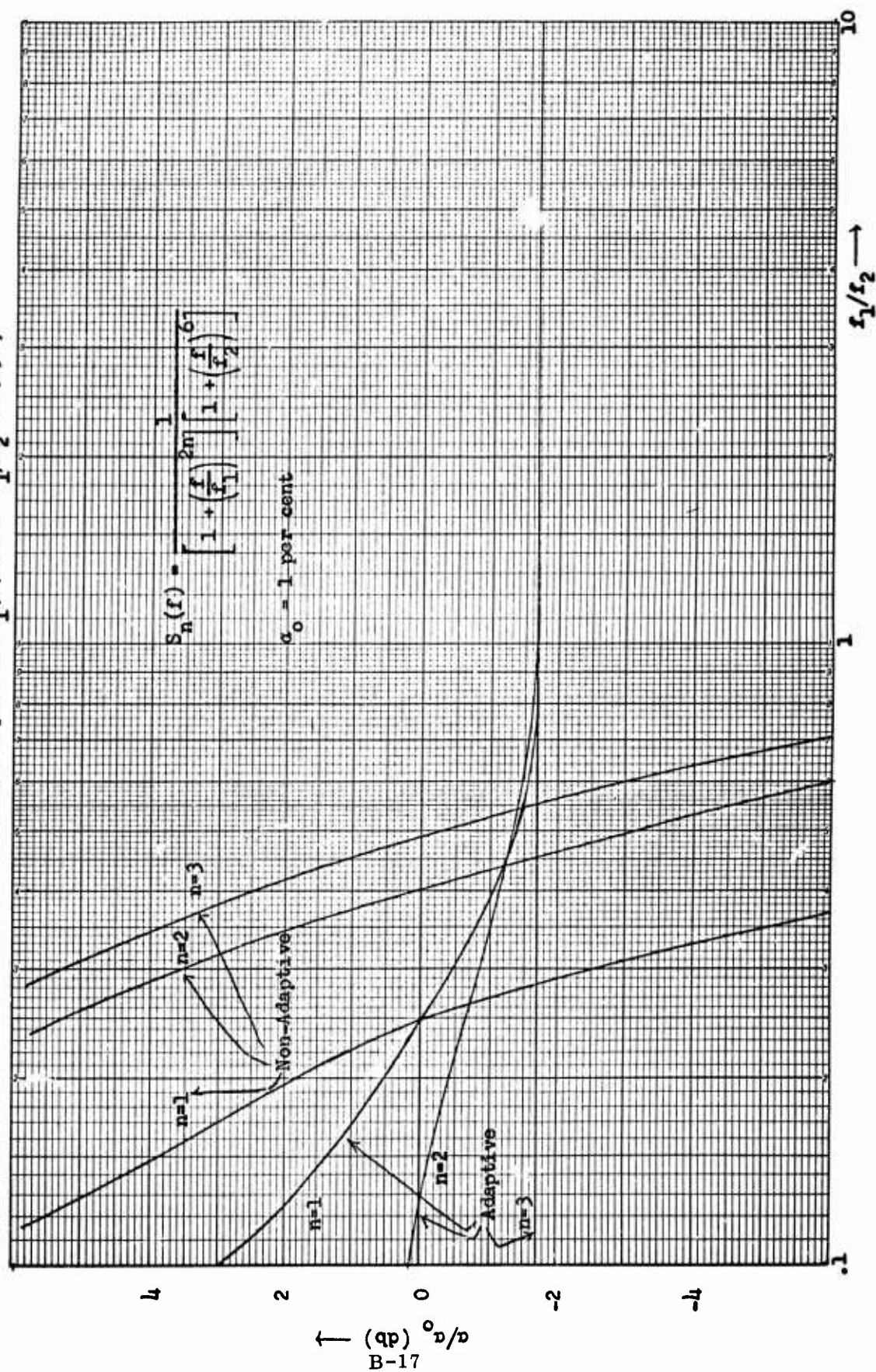
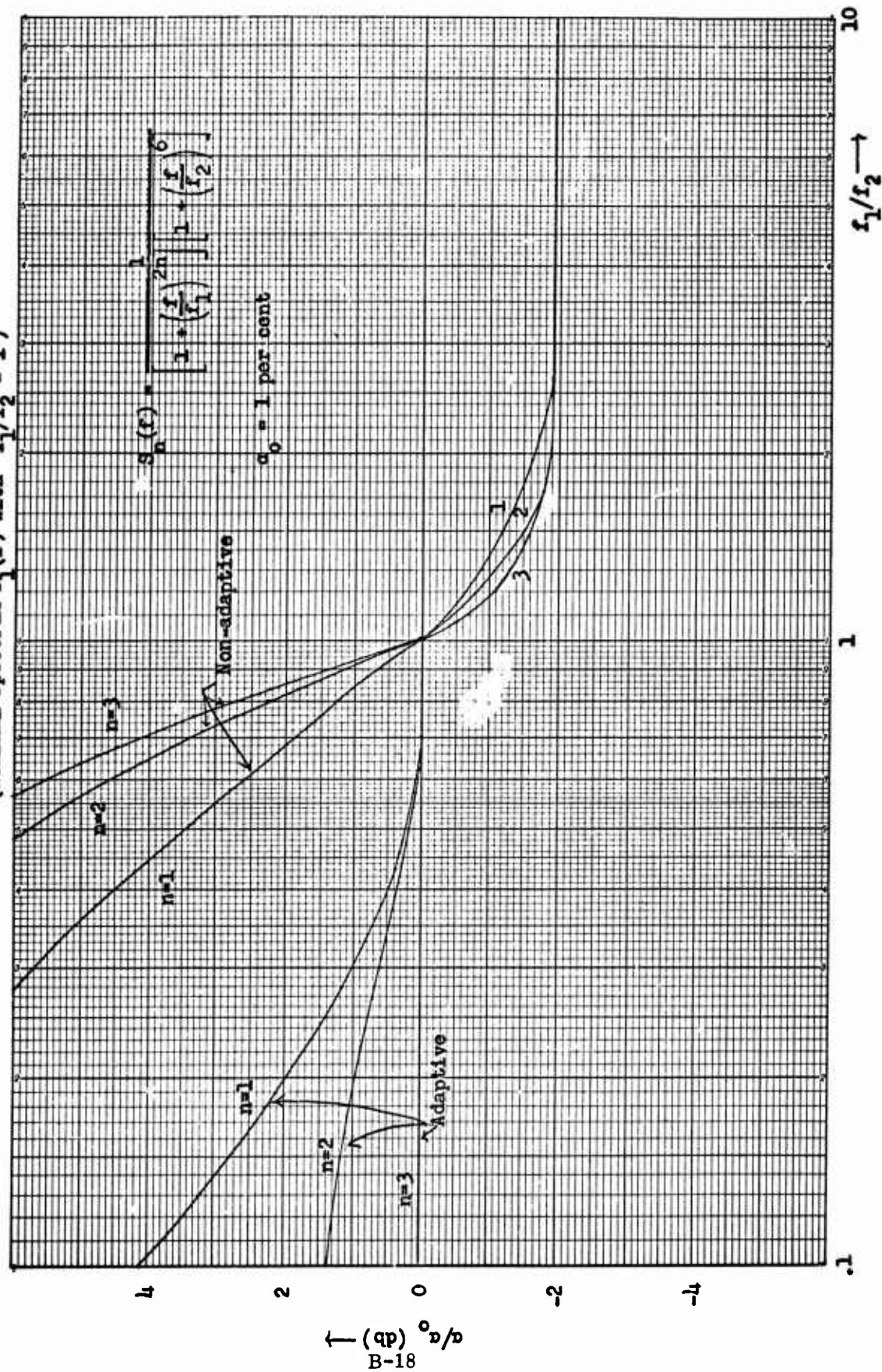


Figure 8 Comparison of Adaptive and Non-Adaptive Detectors  
(Nominal spectrum  $S_1(f)$  with  $f_1/f_2 = 1$ )



error in  $\alpha$  of only  $\pm 1.5$  db for a 20 per cent uncertainty in the cut-off frequency. On the other hand, the adaptive detector introduces virtually no error for this type of processing.

#### V. The Effect of White Self-Noise

Finally we will consider, in a limited way, the effect of allowing a zero in the spectrum. More specifically we will consider a spectrum of the following type:

$$S(f) = \frac{\left[1 + \left(\frac{f}{f_3}\right)^2\right]}{\left[1 + \left(\frac{f}{f_1}\right)^2\right] \left[1 + \left(\frac{f}{f_2}\right)^4\right]}, \quad (13)$$

where  $f_1/f_3 < 1$  and  $f_1/f_2 < 1$ . Hence  $f_1$  is still the first break point in the spectrum. This spectrum can alternatively be written as

$$S(f) = \left[ \frac{1}{\left[1 + \left(\frac{f}{f_1}\right)^2\right]} + q \frac{1}{\left[1 + \left(\frac{f}{f_2}\right)^4\right]} \right] \frac{\left(\frac{f_1}{f_3}\right)^2}{\left[1 + \left(\frac{f_1}{f_3}\right)^2\right]}, \quad (14)$$

where  $q$  is a constant equal to  $\frac{\left(\frac{f_1}{f_3}\right)^2}{\left[1 + \left(\frac{f_1}{f_3}\right)^2\right]}$ . Thus, if the second term

is regarded as the processing filter, the zero of the spectrum corresponds to a minimum level in the noise power spectrum. Small values of  $q$  would always be present as a result of the self-noise generated in the hydrophones. In fact, in the absence of specific knowledge of the signal spectrum, the inputs are normally processed out to some frequency determined by this self-noise ( $f_2 < f_3$ ) in the hope that the signal spectrum is similar to the incoming noise spectrum.

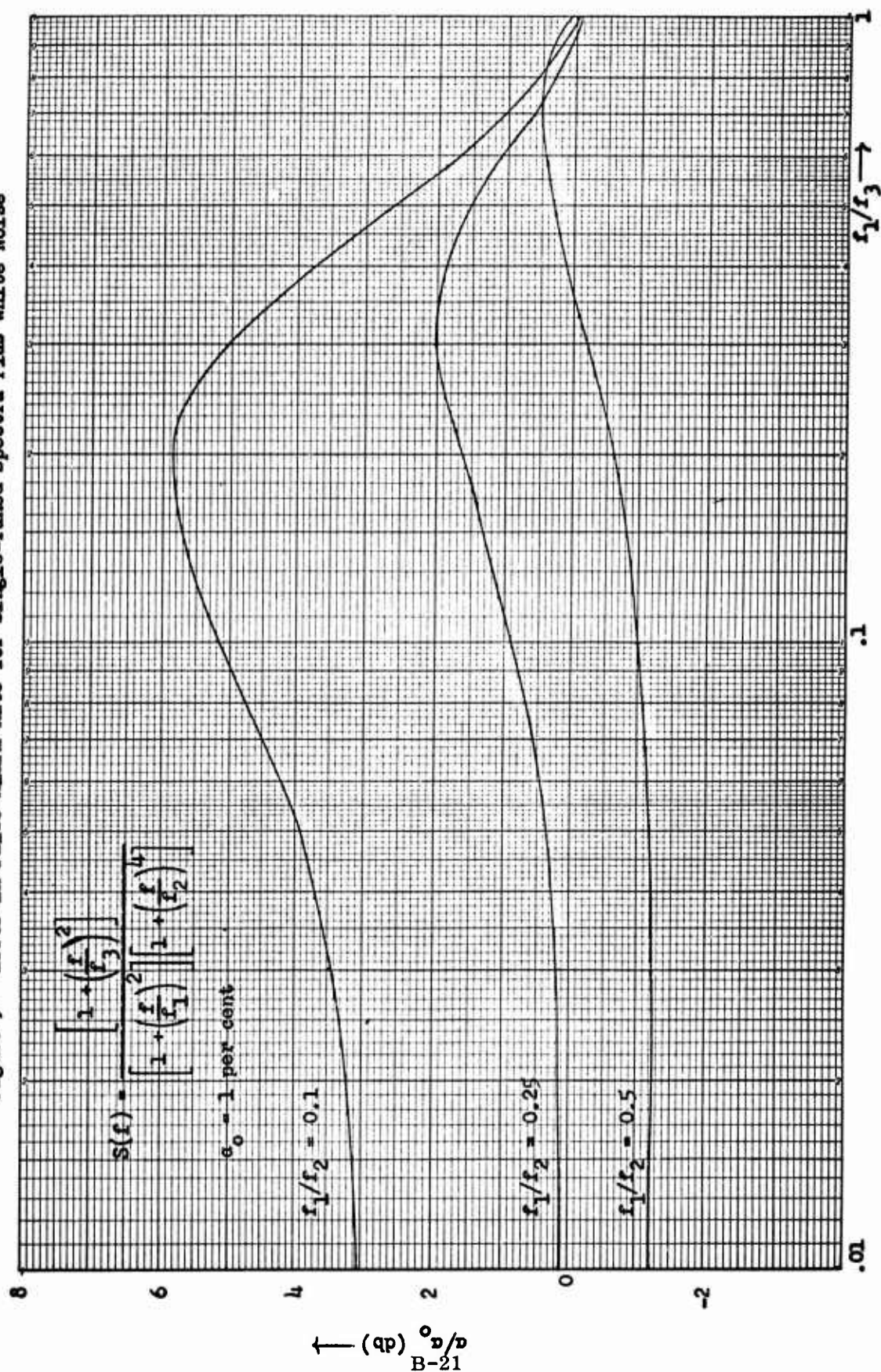


Let us now assume that the adaptive threshold is adjusted under the assumption that the noise spectrum is white (prior to the processing filter) or  $K = 2.3455$ . The actual false-alarm rate ( $\alpha_0 = 1$  per cent) is shown in Fig. 9 for a number of locations of the pole where the abscissa represents the location of the zero. For small values of self-noise ( $f_1/f_3$  small), the spectrum falls off at a rate slightly less than 6 db/octave, and hence the error in  $\alpha$  increases. Since the threshold was designed to give no error for white noise, the error starts to decrease when the self-noise becomes dominant in the vicinity of the processing frequency. Both effects will be far less noticeable for spectra that fall off faster than 6 db/octave. No analysis has been made for higher-order zeros or for a simple zero where  $f_1/f_3 > 1$  (Spectrum increasing in some frequency range).

Let us re-examine our last example (nominal cut-off frequency of 1250 cps). Let us now assume a self-noise -20 db that of the low-frequency noise. Since the spectrum can fall off as fast as 12 db/octave, it seems reasonable to process out to 5 kc. Figure 9 tells us ( $f_1/f_2 = 0.25$ ,  $f_1/f_3 = .1$ ) that for the assumed spectral shape the false-alarm rate is increased by less than 1 db. For sharper spectra this increase is smaller. It follows that the previous decision to set the threshold for the nominal spectrum (no white noise) is about right. This will insure a maximum error in the false-alarm rate of about  $\pm 1$  db within the tolerance limits.

It appears that whether we are setting the threshold on the basis of some lowest cut-off frequency or some nominal cut-off frequency, the adaptive procedure works well for processing frequencies as large as 4 times the nominal (lowest) cut-off frequency. For reasonable amounts of

Figure 9 Error in False-Alarm Rate for Single-Tuned Spectra Plus White Noise



self-noise, there does not appear to be much advantage anyway in processing to some higher frequency. In fact it is the presence of self-noise that makes the adaptive system work. For with extremely small amounts of self-noise, one should process the inputs to some relatively high frequency. If one processes to some frequency  $f_2 > 10 f_1$ , then the adaptive detector is no better than the non-adaptive detector.

#### VI. On the Assumption of Uncorrelated Hydrophone Inputs

Let us assume a linear array of hydrophones. The mean of the PCA detector output is given by

$$E_H\{S_{pca}\} = N \frac{M}{L} \left\{ 1 + \frac{L}{\pi} \sum_{k=1}^M \left( 1 - \frac{k}{M} \right) \sin^{-1}[\rho_s(kd)] \right\}, \quad (15)$$

where  $\rho_s(d)$  is the normalized spatial correlation between two hydrophones spaced  $d$  feet apart. It follows that the threshold [Eq. (7)] should be modified to be

$$t = f_s T \frac{M}{L} \left\{ [1 + R] + \Phi^{-1}(1 - \alpha) \sqrt{\frac{2(1 - \frac{1}{M})}{N'_{eq}}} \right\}, \quad (16)$$

where  $R = \frac{L}{\pi} \sum_{k=1}^M \left( 1 - \frac{k}{M} \right) \sin^{-1}[\rho_s(kd)]$ , and  $N'_{eq}$  is somewhat smaller than

$N_{eq}$  as a result of the spatial correlation. We wish to indicate that the assumption of statistical independence ( $R = 0$ ) is prohibitively inaccurate for feasible submarine arrays, at least as far as setting a detection threshold is concerned. To do this we assume that  $N'_{eq}$  can be accurately determined (say, by the zero-crossing count). It can easily be seen that the error in the false-alarm rate, due to  $R \neq 0$ , can be calculated from

$$\bar{\Phi}^{-1}(1 - \alpha) = \bar{\Phi}^{-1}(1 - \alpha_0) - \sqrt{\frac{N'_{eq}}{2(1 - \frac{1}{M})}} R \quad (17)$$

Let us now place the hydrophones sufficiently far apart so that the error in  $\alpha$  caused by the spatial correlation is "only" +3 db for a designed false-alarm rate ( $\alpha_0$ ) of 1 per cent. [In reality this error is very insensitive to  $\alpha_0$  and varies from 2 db to 4 db as  $\alpha_0$  varies from 10 per cent to .01 per cent.] We will call this spacing the minimum spacing for "uncorrelated" inputs. This spacing is achieved when

$$\sqrt{\frac{N'_{eq}}{2(1 - \frac{1}{M})}} R \leq 0.25 \quad (18)$$

It has been shown in Report No. 1 that for a three-dimensional isotropic noise field and a single pole-spectrum,

$$\rho_s(kd) \leq \frac{c}{2\pi f_1 kd}$$

where  $c$  is the speed of sound in ft/sec. This upper bound is very nearly achieved for small values of  $\rho_s(kd)$  and for arrays that are not steered in the end-fire condition. For these conditions

$$\begin{aligned} R &\approx \frac{2}{\pi^2} \frac{c}{f_1} \frac{1}{d} \sum_{k=1}^M \left(1 - \frac{k}{M}\right) \frac{1}{k} \\ &= \frac{1}{2\pi^2} \frac{c}{f_1} \frac{1}{d} \left[ \frac{1}{2} + \frac{1}{3} + \frac{1}{4} + \dots + \frac{1}{M} \right] \\ &\stackrel{\Delta}{=} \bar{M} \frac{1}{2\pi^2} \frac{c}{f_1} \frac{1}{d} \quad , \end{aligned} \quad (19)$$

where  $\bar{M}$  is very nearly equal to  $M$  for small values of  $M$  ( $M \leq 6$ ) and is less than  $M$  for large arrays. It follows that the "minimum" spacing is given by

$$d > \frac{2}{\pi^2} \frac{\bar{M}}{\sqrt{2(1 - \frac{1}{\bar{M}})}} \frac{c}{f_1} \sqrt{N'_{eq}} \quad (20)$$

The equivalent number of uncorrelated samples is normally quite large, resulting in a large  $d$ . For lightly correlated inputs with single-tuned spectra,  $N'_{eq}$  is of the order of  $10 T f_1$  (see Fig. 2 or 3). If we now assume that  $f_1 \leq 5$  kc, a lower bound for the minimum spacing becomes

$$d > 45 \frac{\bar{M}}{\sqrt{2(1 - \frac{1}{\bar{M}})}} \sqrt{T} \quad (21)$$

The function  $\frac{\bar{M}}{\sqrt{2(1 - \frac{1}{\bar{M}})}}$  varies from 2 to 10 as  $M$  varies from 2 to 50.

The minimum corresponds to  $M = 2$  and hence  $d > 90\sqrt{T}$  ft. Thus for wide spectra ( $f_1 = 5$  kc) and short decision times ( $T \approx 1$  sec), an array with 2 hydrophones spaced 90 ft apart has crudely independent inputs. On the other hand, for a six-element array,  $d > 200\sqrt{T}$  ft, and hence one needs a 1000-ft array even for short decision times. We conclude that the spatial correlation of the noise field must be considered for practical submarine arrays in order to set a decision threshold independently at each bearing angle.

It is speculated, however, that a similar procedure can now be carried out to adapt for the spatial correlation as well as the time correlation. For instance, it would seem reasonable to try an adaptive threshold of the following type:

$$t'' = f_s T \frac{M}{4} \left\{ 1 + \frac{T f_1(M)}{K_1 N(0)} + \Phi^{-1}(1 - \alpha_0) \frac{f_2(M)}{\sqrt{K_2 N(0)}} \right\}, \quad (22)$$

where  $f_1( )$  and  $f_2( )$  are suitable functions and  $K_1$  and  $K_2$  are suitable constants. It should be pointed out that the variance of  $t''$  is no longer negligible and will have to be considered. However, for large arrays, if  $N(0)$  represents the average number of zero crossings over all the inputs, the cost introduced by the variance of  $t''$  should be small. A check of the validity of this modified adaptive threshold would be quite cumbersome and has not been carried out to date.

## Appendix A Calculation of $N_{eq}$

$N_{eq}$  was defined according to Eq. (6) as

$$N_{eq} \triangleq \frac{T f_s}{\left[ 1 + \frac{8}{\pi^2} \sum_{k=1}^N \left( 1 - \frac{k}{N} \right) \left\{ \sin^{-1} [\rho_n(k\tau)] \right\}^2 \right]}$$

where  $\rho_n(\tau)$  is the normalized correlation function of the noise inputs. Given  $\rho_n(\tau)$ ,  $N_{eq}$  can therefore be calculated directly on a computer. The correlation function is obtained via the Wiener-Khintchin theorem from the power spectrum:

$$\rho(\tau) = \int_0^{\infty} S(f) \cos 2\pi f \tau \, df, \quad (A-1)$$

where  $\rho_n(\tau) = \frac{\rho(\tau)}{\rho(0)}$ . Assuming a first break point in the spectrum occurring at  $f_1$  and setting  $x \triangleq \frac{f}{f_1}$ , one obtains

$$\rho(k\tau) = f_1 \int_0^{\infty} S(x) \cos xy \, dx, \quad (A-2)$$

where  $y \triangleq \frac{2\pi k f_1 \tau}{f_s}$ . We will consider three classes of power spectra.

Case 1. Consider spectra of the form

$$S(x) = \frac{1}{1 + x^{2n}} \quad (A-3)$$

where  $n$  is any positive integer. Equation (A-3) can be evaluated directly [2], resulting in

$$\rho(k\tau) = f_1 \frac{\pi}{2n} \sum_{k=1}^n e^{-y \left[ \sin \frac{(2k-1)}{2n} \pi \right]} \sin \left[ \frac{(2k-1)}{2n} \pi + y \cos \frac{(2k-1)}{2n} \pi \right] \quad (A-4)$$

where

$$\rho(0) = f_1 \frac{\pi}{2n} \sum_{k=1}^n \sin \frac{(2k-1)}{2n} \pi$$

The limiting case ( $n \rightarrow \infty$ ) is of course

$$\rho(k\tau) \rightarrow f_1 \frac{\sin y}{y} \quad (A-5)$$

The calculation of Eq. (6) is then straightforward and is plotted in Fig. 2 for  $n = 1, 2, 3$ , and  $\infty$  versus the normalized sampling rate  $f_s/f_1$ . Observe that for  $f_s/f_1 = 100$ ,  $N_{eq}$  has essentially reached its asymptotic value. We will therefore use this calculation of  $N_{eq}$  in order to set the threshold. Below is a table of these results.

n	1	2	3	$\infty$
$N_{eq}/Tf_1$	11.530	4.691	3.883	3.163

Case 2. Consider spectra of the form

$$S(x) = \frac{1}{(1+x^2)(1+p^{2n}x^{2n})}, \quad (A-6)$$

where  $p = f_1/f_2$  and  $n \geq 1$ . This can be factored into the form



$$S(x) = \frac{1}{[1 - (-1)^{n+1} p^{2n}]} \left[ \frac{1}{1+x^2} - \frac{p^{2n} (x^{2n-2} - x^{2n-4} + x^{2n-6} - \dots + (-1)^{n+1})}{1 + p^{2n} x^{2n}} \right] \quad (A-7)$$

This can now be transformed term by term with the correlation function corresponding to  $S'(x) = \frac{x^{m-1}}{1 + p^{2n} x^{2n}}$  for  $0 < m < 2n-1$  being 0 for  $m$  even and

$$p'(k\tau) = f_1 \frac{\pi}{2n} \frac{1}{p^m} \sum_{k=1}^n e^{-\frac{y}{p} \sin \left[ \frac{(2k-1)}{2n} \pi \right]} \sin \left[ \frac{(2k-1)m}{2n} \pi + \frac{y}{p} \cos \frac{(2k-1)}{2n} \pi \right] \quad (A-8)$$

for  $m$  odd. Note that for  $n$  odd and greater than one, this procedure leads to an indeterminate form for the value  $p = 1$ . For other values of  $p$  there is no difficulty.

For example, let us assume that  $n = 2$ . Then it is readily determined from Eqs. (A-7) and (A-8) that

$$\rho(k\tau) = f_1 \frac{\pi}{2} \frac{1}{[1 + p^4]} \left\{ e^{-y} + e^{-\frac{y}{p\sqrt{2}}} \left[ p^3 \sin \left( \frac{\pi}{4} + \frac{y}{p\sqrt{2}} \right) - p \cos \left( \frac{\pi}{4} + \frac{y}{p\sqrt{2}} \right) \right] \right\},$$

and hence

$$\rho_n(k\tau) = \frac{1}{[1 + \frac{\sqrt{2}}{2}(p^3 - p)]} \left\{ e^{-y} + e^{-\frac{y}{p\sqrt{2}}} \left[ p^3 \sin \left( \frac{\pi}{4} + \frac{y}{p\sqrt{2}} \right) - p \cos \left( \frac{\pi}{4} + \frac{y}{p\sqrt{2}} \right) \right] \right\}. \quad (A-9)$$

Thus for a given  $p$  Eq. (6) can be calculated in a straightforward manner. As before, the value for  $N_{eq}$  at  $f_s/f_1 = 100$  will be assumed to be the asymptotic value for  $N_{eq}$ . We will now tabulate the results ( $N_{eq}/Tf_1$ ) for a variety of values of  $n$  and  $p$ .

$\begin{matrix} p \\ n \end{matrix}$	.1	.25	.5	1	5	10
1	9.133	7.2485	5.630	4.103	—	—
2	9.358	7.198	5.230	3.406	4.48	4.62
3	9.401	7.210	5.132	—	—	—

Case 3. Consider spectra of the form

$$S(x) = \frac{1 + q'x^2}{(1 + x^2)(1 + p^{2n}x^{2n})} \quad (A-10)$$

This can alternatively be written (provided  $q' < 1$ , which guarantees that  $f_1$  is still the first break point in the spectrum) as

$$S(x) \propto \frac{1}{(1 + x^2)(1 + p^{2n}x^{2n})} + \frac{q}{(1 + p^{2n}x^{2n})} \quad (A-11)$$

It is clear that the correlation function can now be obtained by a linear superposition of case 1 and case 2. Hence for  $n = 2$ ,

$$\rho(k\tau) = f_1 \frac{\pi}{2} \frac{1}{1 + p^4} \left\{ e^{-y} + e^{-\frac{y}{p\sqrt{2}}} \left[ \frac{p^4 + q(p^4 + 1)}{p} \sin\left(\frac{\pi}{4} + \frac{y}{\sqrt{2}p}\right) - p \cos\left(\frac{\pi}{4} + \frac{y}{\sqrt{2}p}\right) \right] \right\},$$

and hence,

$$\rho_n(k\tau) = \frac{1}{1 + \frac{\sqrt{2}}{2} \left( p^3 - p + \frac{q(p^4 + 1)}{p} \right)} \left\{ e^{-y} + e^{-\frac{y}{p\sqrt{2}}} \left[ \left( p^3 + \frac{q(p^4 + 1)}{p} \right) \sin\left(\frac{\pi}{4} + \frac{y}{\sqrt{2}p}\right) - p \cos\left(\frac{\pi}{4} + \frac{y}{\sqrt{2}p}\right) \right] \right\} \quad (A-12)$$

We will now tabulate the results ( $N_{eq}/Tf_1$ ) for the case  $n = 2$ .

$\begin{array}{c} q \\ p \end{array}$	0	.001	.003	.01	.05	.10	.5	1.778	$\infty$
.1	9.358	9.485	9.750	10.705	15.512	20.436	36.248	—	46.910
.25	7.198	7.240	—	7.350	8.565	9.679	14.177	—	18.764
.5	5.230	—	—	5.308	—	5.888	7.279	8.451	9.382

## Appendix B Calculation of $\overline{N(0)}$

The average number of zero crossings can be calculated directly from the spectral shape from Eq. (11).

$$\overline{N(0)} = 2T f_1 \left[ \frac{\int_0^\infty x^2 S(x) dx}{\int_0^\infty S(x) dx} \right]^{1/2} \quad (B-1)$$

This expression can be evaluated readily from the results of the previous appendix simply by recognizing that

$$\int_0^\infty S(x) dx = \rho(0)$$

and

$$\int_0^\infty x^2 S(x) dx = \rho'(0) , \quad (B-2)$$

where  $\rho'(0)$  is given by Eq. (A-8), where  $m$  is suitably defined. Let us explicitly evaluate  $\overline{N(0)}$  for the same classes of power spectra considered before.

Case 1. For power spectra of the form

$$S(x) = \frac{1}{1+x^{2n}} , \quad (B-3)$$

we obtain from Eqs. (A-4) and (A-8) that

$$\rho(0) = f_1 \frac{\pi}{2n} \sum_{k=1}^n \sin \frac{(2k-1)}{2n} \pi ,$$

and

(B-4)

$$\rho'(0) = f_1 \frac{\pi}{2n} \sum_{k=1}^n \sin \frac{(2k-1)}{2n} 3\pi ,$$

where the latter result is valid only for  $n \geq 2$  [Recall  $\overline{N(0)} = \infty$  for a "single-pole" spectrum.] . Using the identity

$$\sum_{k=1}^n \sin(2k-1) \theta = \frac{\sin^2 n\theta}{\sin \theta} ,$$

one readily evaluates Eq. (B-1) as

$$\overline{N(0)} = 2T f_1 \left[ \frac{\sin \frac{\pi}{2n}}{\sin \frac{3\pi}{2n}} \right]^{1/2} , \quad (B-5)$$

for  $n \geq 2$  . The results are tabulated below.

n	2	3	12	$\infty$
$\overline{N(0)}/Tf_1$	2	1.414	1.216	1.155

Case 2. For power spectra of the form

$$S(x) = \frac{1}{(1+x^2)(1+p^{2n}x^{2n})} , \quad (B-6)$$

$\rho(0)$  is directly determined from Appendix A; however, a different factoring procedure is needed to evaluate  $\rho'(0)$ .

$$x^2 S(x) = \frac{1}{(1+(-1)^{n+1}p^{2n})} \left[ \frac{1}{1+x^2} + \frac{1+p^{2n}x^{2n-2}-p^{2n}x^{2n-4}+\dots+(-1)^{n+1}p^{2n}x^2}{1+p^{2n}x^{2n}} \right] \quad (B-7)$$

One can now use Eq. (A-8) to determine  $\rho'(0)$ . For example, let us assume that  $n = 2$ . Then

$$\rho'(0) = f_1 \frac{\pi}{2} \frac{1}{1+p^4} \left\{ -1 + p \frac{\sqrt{2}}{2} + \frac{1}{p} \frac{\sqrt{2}}{2} \right\}, \quad (\text{B-8})$$

and from Eq. (A-9),

$$\rho(0) = f_1 \frac{\pi}{2} \frac{1}{1+p^4} \left\{ 1 + p^3 \frac{\sqrt{2}}{2} - p \frac{\sqrt{2}}{2} \right\}. \quad (\text{B-9})$$

Hence from Eq. (B-1),

$$\overline{N(0)} = 2T f_1 \sqrt{\frac{1+p^2 - \sqrt{2}p}{p^4 - p^2 + \sqrt{2}p}}. \quad (\text{B-10})$$

These results  $\left[ \overline{N(0)}/Tf_1 \right]$  will now be tabulated for a variety of values of  $n$  and  $p$ .

$\begin{matrix} p \\ n \end{matrix}$	.1	.25	.5	1	5	10
1	6.3246	4	2.8284	2	—	—
2	5.140	3.100	2.044	1.288	1.766	1.9215
3	4.955	2.954	1.908	—	—	—

Case 3. For power spectra of the form

$$S(x) = \frac{1}{(1+x^2)(1+p^{2n}x^{2n})} + \frac{q}{(1+p^{2n}x^{2n})}, \quad (\text{B-11})$$

we can use superposition of the previous results to obtain  $\overline{N(0)}$ . From Eq. (A-12) we have for  $n = 2$

$$\rho(0) = f_1 \frac{\pi}{2} \frac{1}{1+p^4} \left\{ 1 + \frac{\sqrt{2}}{2} \left[ p^3 - p + \frac{q}{p} (p^4 + 1) \right] \right\} \quad (B-12)$$

From Eqs. (B-8) and (A-8) we readily obtain

$$\begin{aligned} \rho'(0) &= f_1 \frac{\pi}{2} \frac{1}{1+p^4} \left\{ -1 + \frac{\sqrt{2}}{2} \left( p + \frac{1}{p} \right) \right\} + f_1 \frac{\pi}{2} \frac{q}{p^3} \\ &= f_1 \frac{\pi}{2} \frac{1}{1+p^4} \left\{ \frac{1}{p^2} \left\{ -p^2 + \frac{\sqrt{2}}{2} \left[ p^3 + p + \frac{q}{p} (p^4 + 1) \right] \right\} \right\} \quad (B-13) \end{aligned}$$

Hence from (B-1),

$$\overline{N(0)} = 2 T f_1 \sqrt{\frac{\frac{\sqrt{2}}{2} \left[ p^3 + p + \frac{q}{p} (p^4 + 1) \right] - p^2}{\frac{\sqrt{2}}{2} p^2 \left[ p^3 - p + \frac{q}{p} (p^4 + 1) \right] + p^2}} \quad (B-14)$$

We will now tabulate the results  $\left[ \overline{N(0)} / T f_1 \right]$  for the case  $n = 2$ .

$\frac{q}{p}$	0	.001	.003	.01	.05	.10	.5	1.778	$\infty$
.1	5.140	5.405	5.892	7.267	11.372	13.697	17.950	—	20
.25	3.100	3.128	—	3.376	4.180	4.840	6.620	—	8
.5	2.044	—	—	2.102	—	2.486	3.185	3.720	4

### References

1. Rice, S. O., "Mathematical Analysis of Random Noise," B.S.T.J., vol. 23 (1944), p. 282; vol. 24 (1945), p. 46.
2. Bateman Manuscript Project (California Institute of Technology), Tables of Integral Transforms, vol. I, McGraw-Hill Book Company, 1954.



VERTICAL DIRECTIONALITY OF AMBIENT NOISE  
AT A HYDROPHONE NEAR THE SURFACE

by

F. S. Hill, Jr.

Progress Report No. 25

General Dynamics Electric Boat division

(8050-31-55001)

September 1965

DEPARTMENT OF ENGINEERING  
AND APPLIED SCIENCE  
YALE UNIVERSITY



### Summary

The ambient noise model proposed by Talham (JASA 36, 1541, 1964) is used to estimate the vertical directionality of ambient noise for a variety of velocity profiles and hydrophones located 100-500 feet below the ocean surface. Except when the hydrophone is located in a region of negative velocity gradient, the model indicates that much of the ambient noise arrives from a near-horizontal direction. The calculated difference between horizontal and vertical intensities exceeds 20 db in a number of cases. When the hydrophone is located in a region of negative velocity gradient, there is a null in the noise directivity pattern in the immediate neighborhood of the horizontal. Aside from this obvious effect of ray geometry, the pattern is not markedly different from that of a hydrophone located in a region of positive velocity gradient.

## I. Introduction

In underwater sound detection systems, ambient noise plays a major role in limiting target detectability. It has been suggested by several researchers that a large contribution to the total ambient noise is generated at the surface, both by wave splashing and by wind blowing across wave tops. In particular, R. J. Talham<sup>(1)</sup> has used a model in which the ocean surface is considered planar and covered by a uniform distribution of independent noise sources. The purpose of that paper was to determine the vertical distribution of ambient noise as received by a hydrophone located at the bottom of the ocean. Curves presented there compared the model with some actual measurements<sup>(2)</sup> and showed good agreement at low sea state. It was shown that the largest amount of noise power was received at nearly horizontal angles, and that the noise intensity decreased as the vertical angle increased, reaching a value 10-20 db lower when the array was beamed straight up.

The question arose as to whether this same general vertical distribution of noise would be observed by a hydrophone array near the surface, say between 100 and 500 feet below the surface. This paper undertakes to answer that question. The model of surface noise discussed by Talham is used as is the general fabric of his derivation. However, since the hydrophone is near the surface, the fine structure of the sound velocity profile near the surface becomes important, and consequently different profiles are used. The one employed by Talham ignored this fine structure near the surface as being insignificant to measurements made at the bottom of the ocean.

## II. Derivation of Vertical Distribution

The geometry used by Talham with slight modifications is shown in Figure 1. A hydrophone located at depth  $H$  is directed at an angle  $\theta$  from the horizontal, and for simplicity is considered to be omnidirectional with respect to azimuth. Noise sources are assumed to be located uniformly over the surface with density  $D$  sources per unit area. The sources are statistically independent, and each emits  $P \cdot g(\theta_1)$  watts per unit solid angle into the water at an angle  $\theta_1$  with respect to the horizontal.

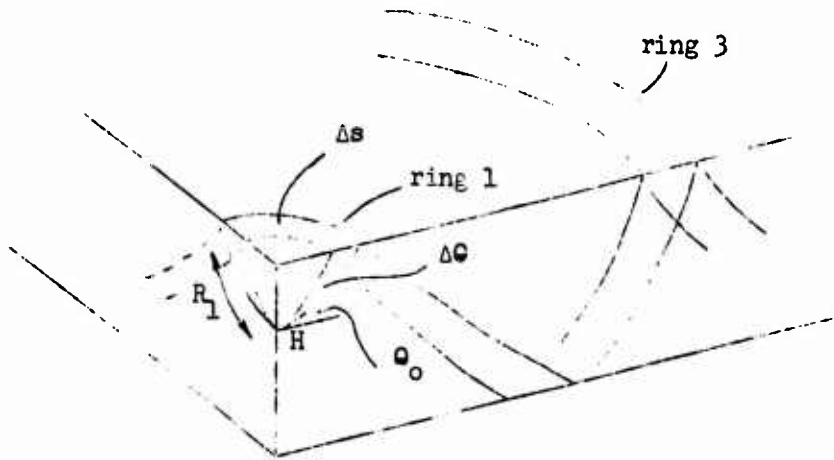


Figure 1 Geometry of the Model

Talham shows that the intensity (watts per unit area) of noise arriving at the hydrophone between the angles  $\theta_0$  and  $\theta_0 + \Delta\theta$ , and due to those sources lying in the innermost surface ring (ring no. 1) of area  $\Delta S$ , is

$$\Delta I_1 = D P g(\theta_1) W \exp[-2\alpha R_1] [\sin \theta_1]^{-1} [2\pi \cos \theta_0 \Delta\theta] \quad (1)$$

where  $P$  and  $D$  are defined above and  $W$  is the ratio of backward-to-forward spreading loss, which plays a significant role in Talham's derivation and is given by

$$W = W(\theta_0) = \left( \frac{\cos \theta_1}{\cos \theta_0} \right)^2 \quad (2)$$

The attenuation of the noise energy is given by the exponential function where  $\alpha$  is the attenuation constant and  $R_1$  is the ray path length from the hydrophone to the surface. The factor  $2\pi \cos \theta_0 \Delta\theta$  is the solid angle at the hydrophone inside of which noise from  $\Delta s$  can reach the hydrophone. The factor  $2\pi \cos \theta_0$  accounts for the fact that this solid angle decreases as  $\theta_0$  becomes larger. The inverse  $\sin \theta_1$  dependence takes into account the rapid increase in  $\Delta s$  as  $\theta_1$  decreases, and therefore the rapid increase in the number of noise sources contributing to  $\Delta I$ . This dependence is most clearly seen in the following argument, where for simplicity the rays are taken as straight lines. Thus  $\theta_1 = \theta_0$ , and as shown in two dimensions in Fig. 2, the areas  $\Delta A$  and  $\Delta s$  are related by  $\Delta A = \Delta s \sin \theta_1$  for small  $\Delta\theta$ .

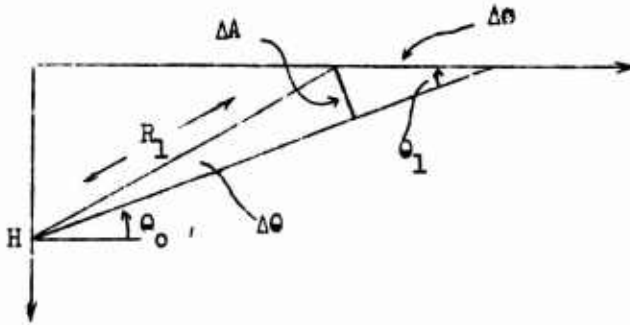


Figure 2 Simplified Geometry Illustrating  $[\sin \theta_1]^{-1}$  Dependence

Ignoring attenuation and considering the usual inverse square law for spreading loss, each noise source in  $\Delta s$  produces at H an intensity proportional to  $1/R_1^2$ . However,  $\Delta A$  is proportional to  $R_1^2 \cos \theta_0$  for a fixed  $\Delta\theta$  and consequently  $\Delta s$  is proportional to  $R_1^2 \cos \theta_0 / \sin \theta_1$ .

Thus the number of noise sources in  $\Delta s$  is proportional to  $R_1^2 \cos \theta_0 / \sin \theta_1$  and the aggregate intensity at H varies as  $\cos \theta_0 / \sin \theta_1$ .

Finally,  $\theta_1$  and  $R_1$  are related to  $\theta_0$  by standard ray tracing relations. For instance, by Snell's law we have

$$\frac{c_{\text{hyd}}}{\cos \theta_0} = C_V = \frac{c_{\text{surf}}}{\cos \theta_1} \quad (3)$$

where  $c_{\text{hyd}}$  and  $c_{\text{surf}}$  are the velocities of sound at the hydrophone and surface respectively. The constant  $C_V$  is peculiar to the ray arriving at the hydrophone at angle  $\theta_0$  and is normally called the 'ray parameter.'

Also contributing to the total noise arriving at angle  $\theta_0$  is energy that arrives at  $\Delta s$  along rays originating at greater distances on the surface, as shown in Fig. 3 in two dimensions.

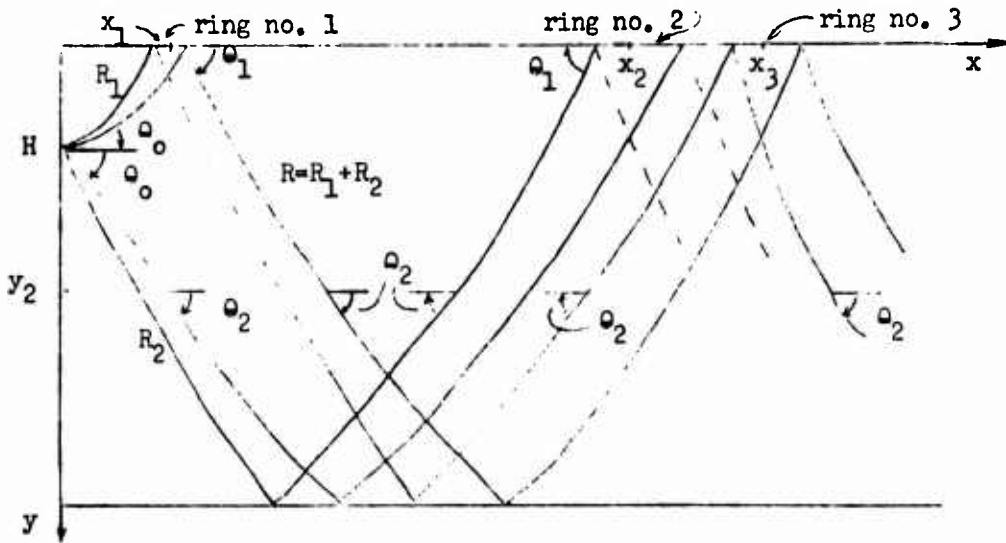


Figure 3 Contributions to Intensity from Distant Sources

The cases of angles  $\theta_0$  below horizontal are also shown to indicate the similarities and differences between the two cases. Since a given ray has associated with it a particular parameter  $c_v$  by (3), at each depth all the rays that finally reach the hydrophone at angle  $\pm\theta_0$  exhibit this parameter, and thus in Fig. 3 all rays shown have angle  $\theta_2$  as illustrated, where

$$\cos \theta_2 = \frac{c(y_2)}{c_v} \quad (4)$$

and  $c(y_2)$  is the speed of sound at depth  $y_2$ . (Note that since  $y_2$  is positive downward, angles are measured positive in a clockwise direction.) This symmetry, which requires that the surface and bottom be parallel, simplifies the addition of ray components. We now consider the two cases separately.

### III. Upward-Looking Case ( $\theta_0 \leq 0$ )

From Fig. 3 it is seen that there exist components of the total intensity at angle  $\theta_0$  originating at  $x_1$ ,  $x_3$ , etc. The ray originating at  $x_3$  travels a total path length of  $2R + R_1 = 3R_1 + 2R_2$  before reaching the hydrophone, and makes a reflection off both the bottom (reflection coefficient  $\beta$ ) and the surface (reflection coefficient  $\gamma$ ). Since the geometry is otherwise the same as for  $\Delta I_1$ , and since phase shift is unimportant (the noise sources are independent), the contribution due to the sources at  $x_3$  is, from (1):

$$\Delta I_3 = \Delta I_1 \beta \gamma \exp[-4 \alpha R] \quad (5)$$

Consequently the total intensity at H due to all such contributions is

$$\Delta I = \Delta I_1 \sum_{i=1}^{\infty} \gamma^i \beta^i \exp[-4i \alpha R] = \frac{\Delta I_1}{1 - \gamma \beta \exp[-4 \alpha R]} \quad (6)$$

To obtain the final form, we remove the dependence on the size of the solid angle at the hydrophone by deleting  $2\pi \cos \theta_o$  in (1), divide through by  $\Delta\theta$ , and let  $\Delta\theta \rightarrow 0$ . This yields for the (upward-looking) vertical noise distribution  $N_{up}(\theta_o)$

$$N_{up}(\theta_o) = \frac{D P g(\theta_1) W \exp(-2\alpha R_1)}{(\sin \theta_1) [1 - \beta \gamma \exp(-4\alpha R)]} \quad (7)$$

Another way of considering the deletion of  $2\pi \cos \theta_o$  is to consider the hydrophone array to be no longer azimuthally omnidirectional, but to have an azimuthal beam width of, say,  $\sigma$ , measured normal to the ray entering at angle  $\theta_o$ . This replaces  $2\pi \cos \theta_o$  in (1) by the single term  $\sigma$ , which then of course is retained in (7). As the final results are to be normalized anyway, the two approaches are equivalent.

It is possible that the hydrophone can be located at a depth such that rays arriving at angle  $\theta_o$  cannot reach the bottom. This is true whenever

$$C_v < c_{bottom} \quad (8)$$

where  $c_{bottom}$  is the speed of sound at the ocean bottom. A typical example is shown in Fig. 4 along with a velocity profile. For a given  $\theta_o$ ,  $C_v$  given by (3) is a sound speed which is equal to the speed of sound at, say, depth  $d$ . Thus by (4) the ray angle must be zero at depth  $d$ . Since  $\cos \theta_2$  in (4) cannot exceed unity, no ray with parameter  $C_v$  as shown can penetrate beneath depth  $d$ . Thus in  $N_{up}(\theta_o)$  of (7), the term  $\beta$  is removed (or set to unity), and path length  $R$  is as shown.

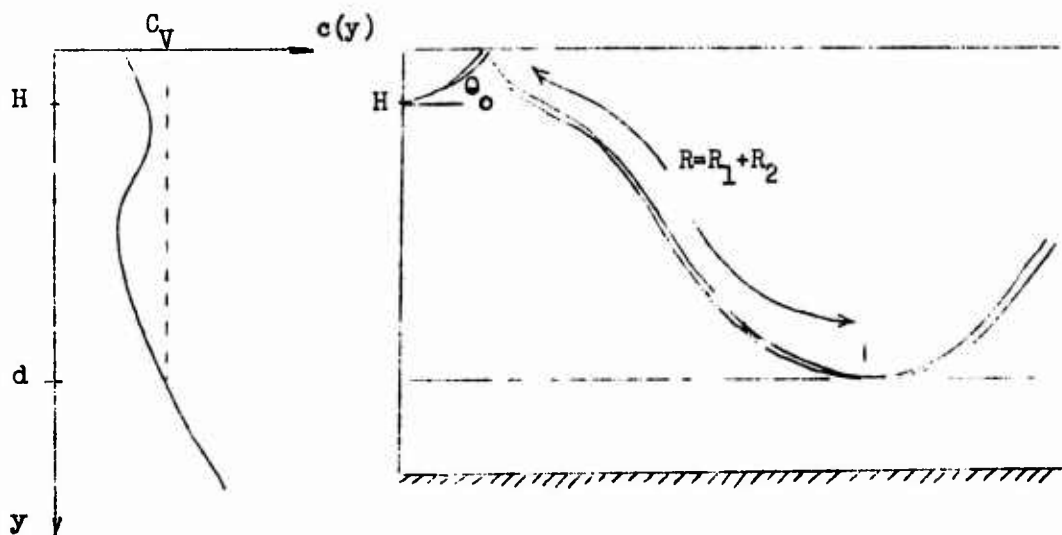


Figure 4 A Situation with No Bottom Reflection

#### IV. Downward-Looking Case ( $\theta_o > 0$ )

Following the derivation for the upward-looking case, it is clear that the only difference in the two cases is that the ray reaching the hydrophone at an angle below horizontal must have travelled further, and if the bottom is reachable, will have sustained an additional bottom reflection.

Thus from Fig. 3 it is seen that a ray must travel further by a distance  $R + R_2 - R_1 = 2R_2$  than a ray arriving above the horizontal, and that

$$N_{\text{down}}(\theta_o) = N_{\text{up}}(-\theta_o) \beta \exp(-4 \alpha R_2) \quad (9)$$

Again, if the bottom cannot be reached,  $\beta$  is set equal to unity.

#### V. Various Propagation Situations

As was suggested by the sample velocity profile given in Fig. 4 above,  $c_v = c_{\text{hyd}}/\cos \theta_o$  determines a velocity of sound for each angle  $\theta_o$ . Given a particular profile,  $c_v$  thus delineates various regions in the ocean in which the given ray may exist. It is interesting to consider the possibilities as a function of  $\theta_o$ .



A typical contour is given in Figure 5 along with two different hydrophone depths,  $H_1$  and  $H_2$ . Associated with  $H_1$  are three rays 1,2,3 showing the three possibilities for rays arriving at  $H_1$ . Ray 1 is confined to the region near the surface because  $c_{V_1} < c_{mode}$ , where  $c_{mode}$  is the speed of sound at the peak in the profile. Ray 2 has a very long path length for all contributions but the nearest, and also ray 2 does not reach the bottom since  $c_{V_2} < c_{bottom}$ . Ray 3 is seen to reach the bottom, as will all rays arriving at angles greater than that of ray 3.

Clearly for  $H_1$  all rays do reach the surface and thus there is no null in the intensity due to surface noise. This is not true in the case of a hydrophone at  $H_2$ , as shown by ray A, which cannot reach the surface (or originate at the surface) since  $c_{V_A} < c_{mode}$ . Thus a null in surface noise is expected for all angles  $\theta_o$  satisfying

$$\cos \theta_o > \frac{c_{H_2}}{c_{mode}} \quad (\text{null exists}) \quad (10)$$

where  $c_{H_2}$  is the speed of sound at  $H_2$ . As  $\theta_o$  increases further, so that this condition is no longer satisfied, then rays similar to ray B or ray C are observed.

Combining these thoughts into a single representation, one expects that a polar plot of  $N_{up}(\theta_o)$  and  $N_{down}(\theta_o)$  vs.  $\theta_o$  will exhibit fairly well-defined regions, each corresponding to one of the ray types discussed. This is suggested in Figure 6, where the contour and depths from Figure 5 have been used.

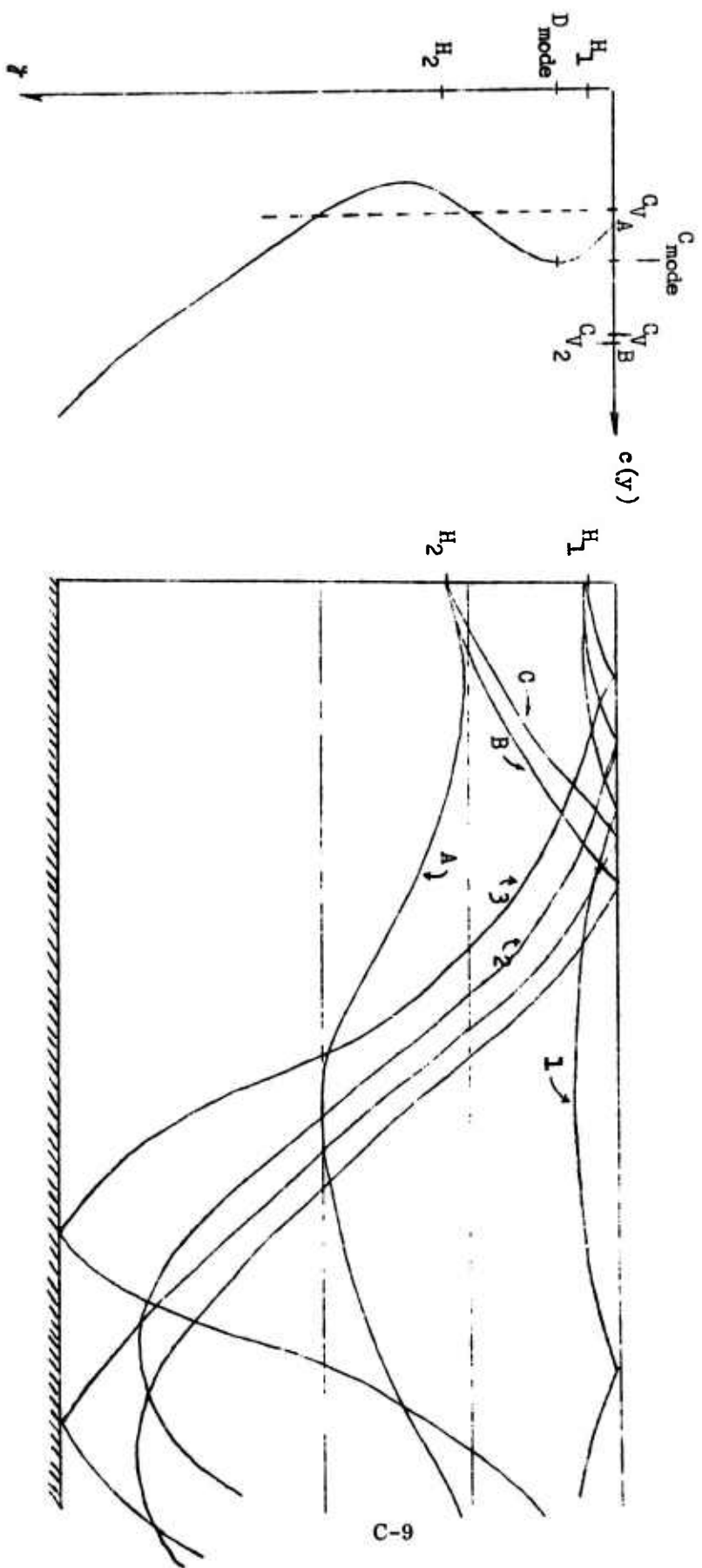


Figure 5. Various Propagation Situations.

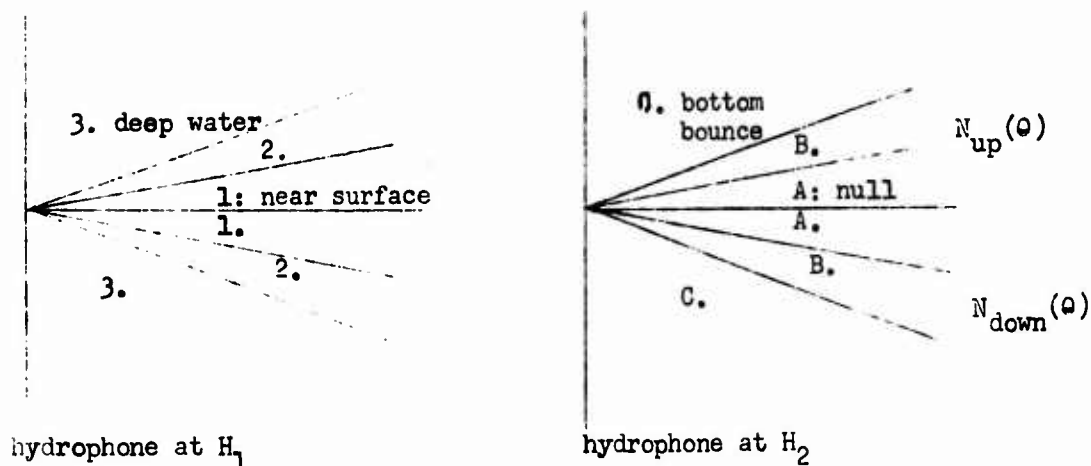


Figure 6 Polar Delineation of Ray Type Regions

It is expected that there will be a rather rapid decrease in  $N_{up}(\theta_0)$  and  $N_{down}(\theta_0)$  at the boundary between regions 1 and 2, since the path length abruptly becomes much larger, and consequently contributions  $\Delta I_3$ ,  $\Delta I_5$ , etc., are more attenuated. Such a rapid decrease is not expected at the boundary separating regions 2 and 3, however, since of necessity the grazing angle with the bottom is very small near this boundary, and consequently the reflection coefficient is near unity.

For completeness it should be remarked that for profiles where  $c_{bottom} < c_{mode}$ , regions 2 and B are absent, since then any ray penetrating into deep water will always reach the bottom.

#### VI. Computation of Noise Distribution

It is noted from (7) that the vertical distribution  $N_{up}(\theta_0)$  [and consequently  $N_{down}(\theta_0)$ ] requires that  $\theta_1$ ,  $R_1$ ,  $R$ , and  $\beta = \beta(\theta_{bottom})$  be known. To this end a ray tracing program was written, and this was applied to several profiles approximated piece-wise by straight lines.

The ray tracing program is described in the Appendix. The significant outputs of this program are  $R_1$  and  $R_2$ , the ray path lengths from the hydrophone to the surface and bottom, respectively.  $\beta$  was found using the curves shown in Figure 7, originally reported by Marsh and Schulkin.<sup>(3)</sup> The same surface reflection coefficient  $\gamma$  and attenuation constant  $\alpha$  as used by Talham were also used, namely,  $\gamma = 1$ , and  $\alpha = .0038 f^{3/2}$  Np/kyd, where  $f$  is in kilocycles per second. A different value of  $\gamma$  is also tried, as discussed below. Two source directionality functions  $g(\theta_1)$  were used,  $g(\theta_1) = 1$  and  $g(\theta_1) = \sin \theta_1$ , although others were checked and showed no peculiar features. Talham showed that at least on the ocean bottom, and at low sea states,  $g(\theta_1) = 1$  agreed most closely with available data.

The results obtained are presented in Figures 10-18 as polar plots of  $N_{up}(\theta_o)$  and  $N_{down}(\theta_o)$ . All plots are in db relative to unity, with P and D normalized to one. Two values of frequency were used, 400 cps and 1000 cps, as being representative of the range of interest. Four sound velocity profiles<sup>(4)</sup> were used, as given in Fig. 8. Attention was concentrated on the Bermuda profiles, while the Iceland profiles are included for purposes of comparison. Various features of these graphs are discussed below.

Certain situations can be handled analytically for comparison with computer results, and to show the major effects contributing to  $N_{up}(\theta_o)$ . In particular the cases where  $\theta_o$  is near  $0^\circ$  or  $90^\circ$  can be studied. Assume that  $\theta_o = \frac{\pi}{2}$ . Then from (7) we have, since  $\theta_1 = \theta_o = \frac{\pi}{2}$ ,

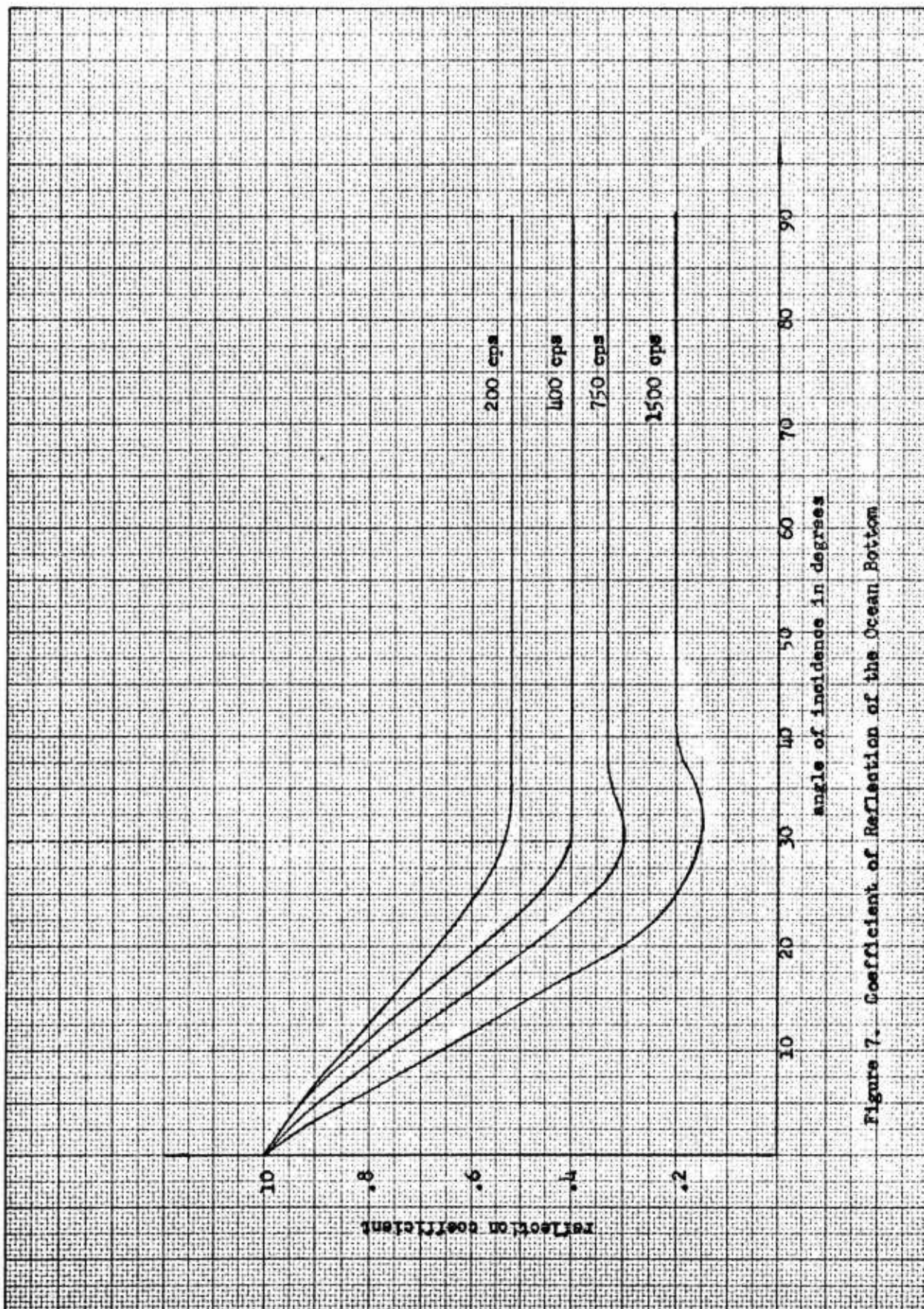
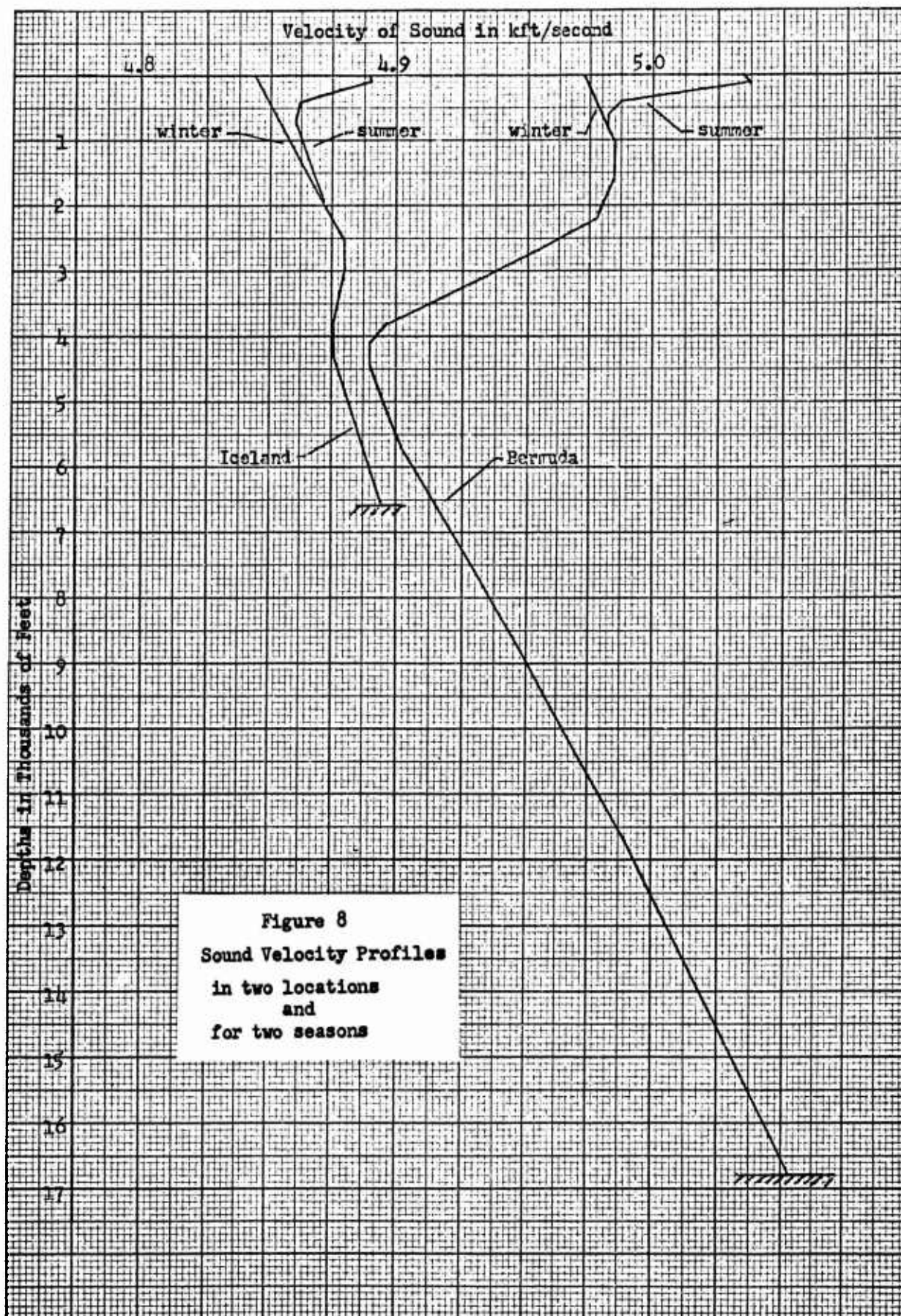


Figure 7. Coefficient of Reflection of the Ocean Bottom





$$N_{up}(\frac{\pi}{2}) = \frac{D P g(\frac{\pi}{2}) e^{-2\alpha H}}{1 - \gamma \beta(\frac{\pi}{2}) e^{-4\alpha B}} \quad (11)$$

$$\approx \frac{D P g(\frac{\pi}{2})}{1 - \gamma \beta(\frac{\pi}{2})} \quad (12)$$

where H and B are the depths of the hydrophone and bottom respectively, and the dependence of  $\beta$  on the bottom angle is indicated as  $\beta(\frac{\pi}{2})$ . The approximation in (12) stems from the fact that at frequencies in the hundreds of cycles the exponents in (11) are very small.

At the other extreme, when the hydrophone lies in a region of positive gradient, as at  $H_1$  in Fig. 5, and  $\theta_0$  is small enough so that the ray is confined to depths less than  $D_{mode}$  (region 1 of Fig. 6), then  $R_1$  and  $R_2$  are reasonably small,  $W \approx 1$ , and  $\beta = 1$ . Thus from (7)  $N_{up}(\theta_0)$  becomes approximately, with  $\gamma = 1$ ,

$$N_{up}(\theta_0) \approx \frac{D P g(\theta_1)}{\sin \theta_1 (4\alpha R)} \quad (\theta_0 \text{ small}) \quad (13)$$

This may be reduced further if the velocity gradient G at the hydrophone is approximately constant up to the surface. Then the radius of curvature r of the ray may be shown<sup>(5)</sup> to be  $r = C_v/G$ . Using the geometry of Fig. 9, where  $R_2$  is the distance from H to the maximum depth reached, it is seen that

$$R_1 = r(\theta_1 - \theta_0) \quad , \quad R_2 = r\theta_0 \quad , \quad R = r\theta_1 \quad (14)$$

and

$$\cos \theta_0 - \cos \theta_1 = \frac{H}{r} \quad (15)$$

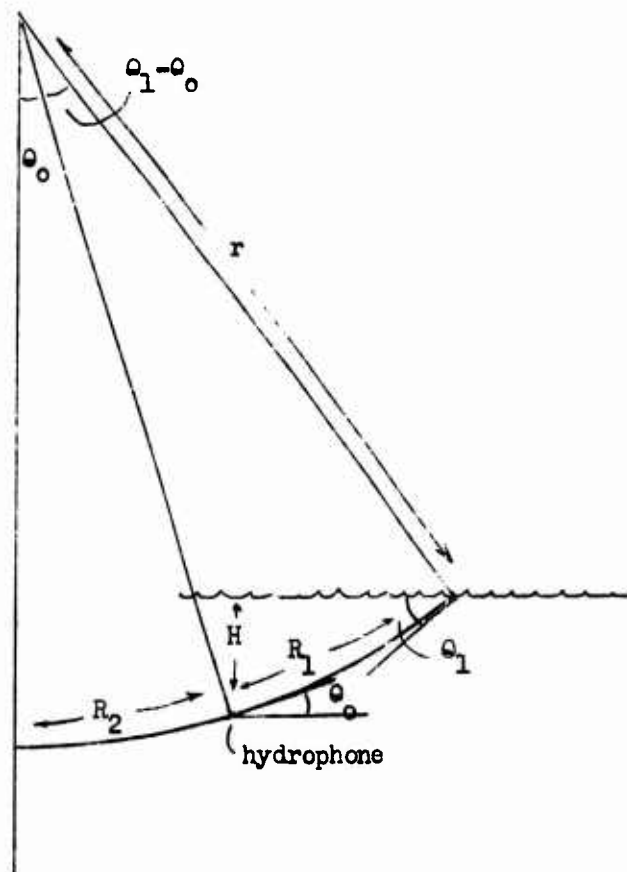


Figure 9 Ray Path Geometry for A Constant Positive Velocity Gradient From The Surface to The Hydrophone



But since  $c_v = c_{hyd} / \cos \theta_o$ , (15) yields

$$\cos \theta_1 = (1 - k) \cos \theta_o \quad (16)$$

where

$$1 - k = 1 - \frac{HG}{c_{hyd}} = \frac{c_{surf}}{c_{hyd}} \quad (17)$$

Thus (13) now becomes

$$N_{up}(\theta_o) = \frac{DP g(\theta_1)}{4a \sin \theta_1 r \theta_1} \quad (18)$$

Using  $\cos \theta = 1 - \frac{\theta^2}{2}$  twice in (16), (18) then yields

$$N_{up}(\theta_o) = \frac{DP g(\theta_1) G \cos \theta_o}{4a \sin \theta_1 c_{hyd} \sqrt{2k + (1 - k) \theta_o^2}} \quad (\theta_o \text{ small}) \quad (19)$$

The two forms for  $g(\theta_1)$  treated here are  $g(\theta_1) = 1$  and  $g(\theta_1) = \sin \theta_1$ . These forms yield the results

$$N_{up}(\theta_o) = \frac{DP G \cos \theta_o}{4a c_{hyd} [2k + (1 - k) \theta_o^2]} \quad \text{if } g(\theta_1) = 1 \quad (20)$$

$$N_{up}(\theta_o) = \frac{DP G \cos \theta_o}{4a c_{hyd} \sqrt{2k + (1 - k) \theta_o^2}} \quad \text{if } g(\theta_1) = \sin \theta_1 \quad (21)$$

The approximation  $\sin \theta_1 = \theta_1$  is used in (20). As an example, for the Bermuda winter profile, with the hydrophone located at 100 ft,  $k$  has the value .0003. Thus the term  $2k$  is less than  $(1 - k)\theta_o^2$  if  $\theta_o \geq 1.4$  degrees. The forms of (20) and (21) show that as  $\theta_o \rightarrow 0$ ,  $N_{up}(\theta_o)$  approaches the values

$$N_{up}(0) = \begin{cases} \frac{DP}{8 \alpha H} & \text{if } g(\theta_1) = 1 \\ \frac{DP}{8 \alpha H} \sqrt{2k} & \text{if } g(\theta_1) = \sin \theta_1 \end{cases} \quad (22)$$

It is noted that the only dependence on the velocity profile for  $\theta_0 = 0$  occurs in  $k$ . Thus, for example, in any ocean for which a constant positive velocity gradient exists from the surface to the hydrophone, and for  $H = 100$  ft and  $f = 400$  cps, we have in db (with  $P = D = 1$ )

$$N_{up}(0) \Big|_{db} = \begin{cases} 35.9 \text{ db} & \text{if } g(\theta_1) = 1 \\ 35.9 - 5 \log_{10} \frac{c_{hyd}}{2HG} \text{ db} & \text{if } g(\theta_1) = \sin \theta_1 \end{cases} \quad (23)$$

For both the Bermuda and Iceland winter profiles (23) yields 19.8 db for the  $g(\theta_1) = \sin \theta_1$  case. These agree closely with the computer results, as seen in Figures 10 and 15. When the hydrophone lies in an ocean region for which the gradient is negative, as at  $H_2$  in Fig. 5, the simple geometric techniques used above fail due to the complicated ray path. Shadow regions are easily found, as mentioned in Section IV, but actual results for  $N_{up}(\theta_0)$  require a computer. In all cases  $N_{down}(\theta_0)$  is easily found from  $N_{up}(\theta_0)$  by means of (9).

It is instructive to consider the physical causes for the various results obtained in (22). Beginning with (13), it is seen that there are two separate contributions to  $N_{up}(\theta_0)$ . The first is the inverse  $\sin \theta_1$  effect, which arises geometrically (see Fig. 2) and relates the number of noise source elements spanned by the beam of the hydrophone. This effect is cancelled, of course, if it is assumed that  $g(\theta_1) = \sin \theta_1$ . Thus the

magnitude of this effect can be judged from a comparison of the graphs with  $g(\theta_1) = 1$  and  $g(\theta_1) = \sin \theta_1$ , as in Figs. 10, 11, 15, and 16. The effect is present in the other cases as well, of course, but (22) is only applicable to the cases corresponding to these figures. The second effect is that of the inverse path length dependence, which is easily traced to (6) and is due to the summation of contributions from remote surface elements. It is thus seen that these remote sources add up significantly at small values of  $\theta_0$ , producing as in (18) an inverse  $\theta_1$  dependence (where  $\theta_1$  is small when  $\theta_0$  is small). This is true for low frequencies since attenuation is then small. The magnitude of this effect is demonstrated in Fig. 14, where the complete  $N_{up}(\theta_0)$  and  $N_{down}(\theta_0)$  are compared with the corresponding ambient noise levels when only the first contribution to the noise, that from ring no. 1 (see Fig. 1), is considered. These values were obtained by setting  $\gamma = 0$  in (6). It is seen that the noise level due to the first contribution is independent of frequency for upward-looking cases and only slightly dependent for downward-looking cases. The independence is due to the negligible attenuation for the short path lengths involved, while the slight dependence in the downward direction is due to the fact that the bottom reflection coefficient  $\beta$  is a decreasing function of frequency [Fig. 7].

This second effect due to contributions from remote sources is heavily dependent on the fact that the surface reflection coefficient  $\gamma$  is assumed to be equal to unity. If this is not the case, but  $\gamma$  differs from unity by  $\delta$ , ( $\gamma = 1 - \delta$ ), then (7) leads to

$$N_{up}(\theta_o) = \frac{DPg(\theta_1)}{\sin \theta_1 [1 - \gamma(1 - 4\alpha R)]} \quad (\theta_o \text{ small}) \quad (24)$$

$$= \frac{DPg(\theta_1)}{\sin \theta_1 [\delta + 4\alpha R\gamma]} \quad (25)$$

Marsh et al. have derived a theoretical dependence for  $\gamma$  on several parameters,<sup>(6)</sup> arriving at

$$\delta = .485 f^{1.5} (1.77 h)^{1.6} \sin \theta_1 \quad (26)$$

where  $f$  is the frequency in kcps and  $h$  is the rms wave height. This dependence is valid for small  $\theta_1$  and low sea state. However, it will have little effect on  $N_{up}(\theta_o)$ , since  $\theta_1$  is very small when  $\theta_o$  is near zero, and consequently  $\gamma \approx 1$ . A sample computer result is shown in Fig. 10, which compares the values of  $N_{up}(\theta_o)$  when  $\gamma = 1$  and when  $\gamma = 1 - \delta$ . It is seen to cause a negligible reduction in ambient noise level.

## VII. Further Discussion of Results

The rather peculiar shape of the vertical noise distributions of Figs. 10-18 merits some discussion. Examining Fig. 10 as an example, it is seen that the noise level drops suddenly as  $\theta_o$  passes beyond  $4^\circ$  or  $5^\circ$ . It is seen that this is true for both the  $g(\theta_1) = 1$  and  $g(\theta_1) = \sin \theta_1$  cases, so that the effect cannot be due to the falling off of the number of noise elements involved (the inverse  $\sin \theta_1$  effect). The effect instead is that of attenuation, for as shown in the table of  $R_1$  and  $R_2$  accompanying Fig. 10 (which applies as well to Fig. 11), there is a sudden jump in  $R_1 + R_2$  as  $\theta_o$  reaches  $5^\circ$ , for a hydrophone at 100 ft. This is due to a jump of the ray from a region 1 type to a region 2 type, as shown in Fig. 6. The angle  $\theta_o = 5^\circ$  is just sufficient to allow the

ray to pass out of the shallow water channel into a deep water path. This causes all contributions but the first to the total noise level to travel much greater distances to the hydrophone. Due to the attenuation of sound in water, these now very remote contributions are much smaller, and the total noise level is consequently reduced.

Beyond this sudden drop there is a gradual decay in the noise, except in the case where  $g(\theta_1) = \sin \theta_1$ , where slight increases are seen due to the fact that  $R_1 + R_2$  again decreases slightly. The decay increases as soon as the bottom is reached (which occurs at  $12^\circ$  in all curves of Figs. 10 and 11), for the bottom reflection coefficient begins to decrease from unity. Finally this levels out as seen from Fig. 7 and thus the  $g(\theta_1) = \sin \theta_1$  case is essentially constant while the  $g(\theta_1) = 1$  case decreases due to the inverse  $\sin \theta_1$  effect.

The difference in hydrophone depths is seen to be unimportant except at small values of  $\theta_0$ , since at small  $\theta_0$  the slightly increased path length for larger hydrophone depths permits a small change in  $\theta_1$ , and  $N_{up}(\theta_0)$  is very sensitive to  $\theta_1$  at small values of  $\theta_0$ . At larger values of  $\theta_0$  the rays are geometrically very similar for different hydrophone depths.

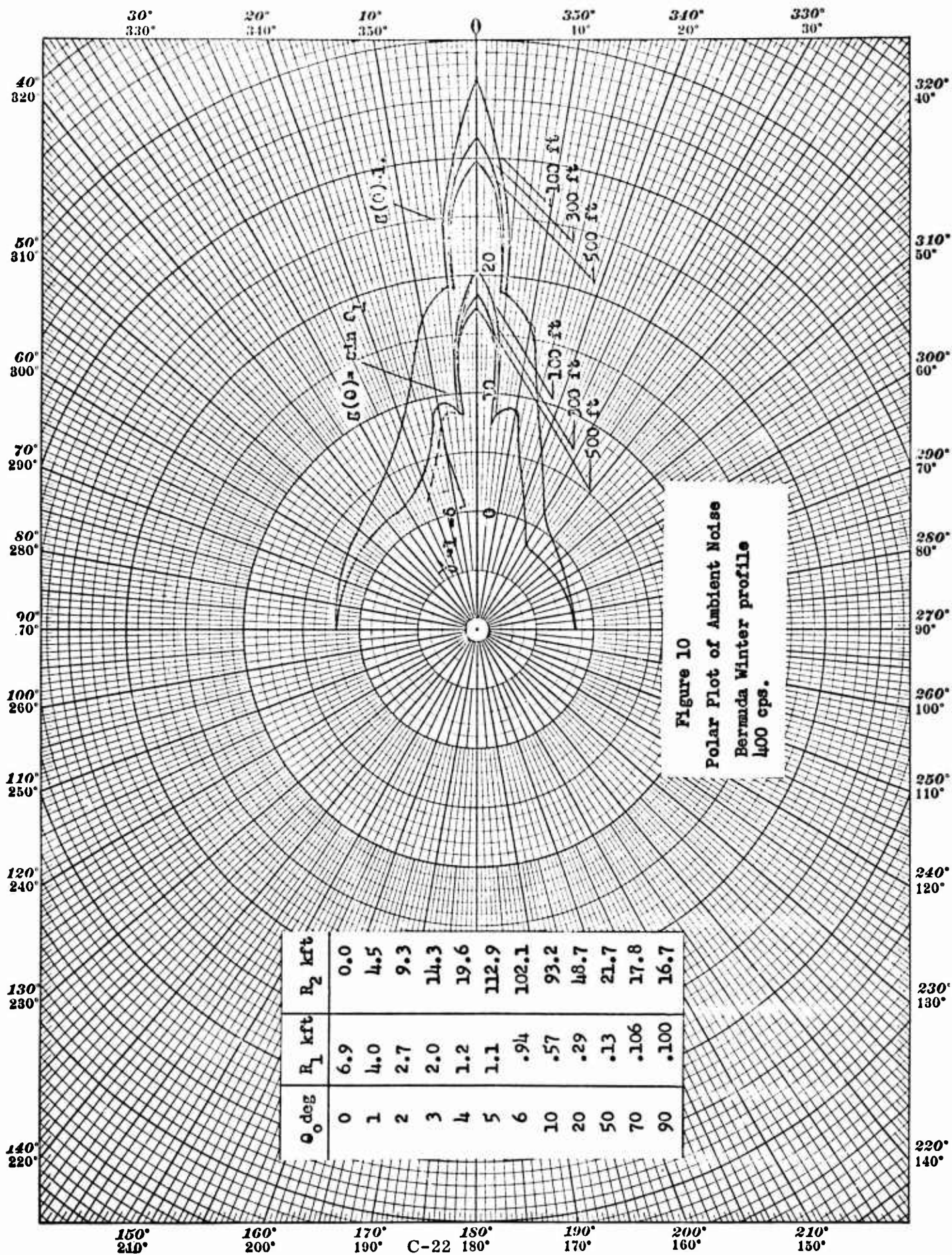
In the summer profile cases of Figs. 12 and 13 the  $g(\theta_1) = \sin \theta_1$  case shows a constant noise level over a range of  $\theta_0$  near  $\pi/2$ . This is due to the fact that  $R_1$  and  $R_1 + R_2$  are essentially constant over this range, as a sketch of ray paths for such a profile will readily show. Since the inverse  $\sin \theta_1$  effect is cancelled in this case, the constancy of the noise is understandable. It ends as soon as the bottom is encountered (at  $8^\circ$  for a hydrophone depth of 100 ft, and at  $11^\circ$  for a depth of 500 ft).

For still larger angles the features mentioned above again apply. The summer cases also exhibit regions in which a null exists in the ambient noise. These are considered in more detail below.

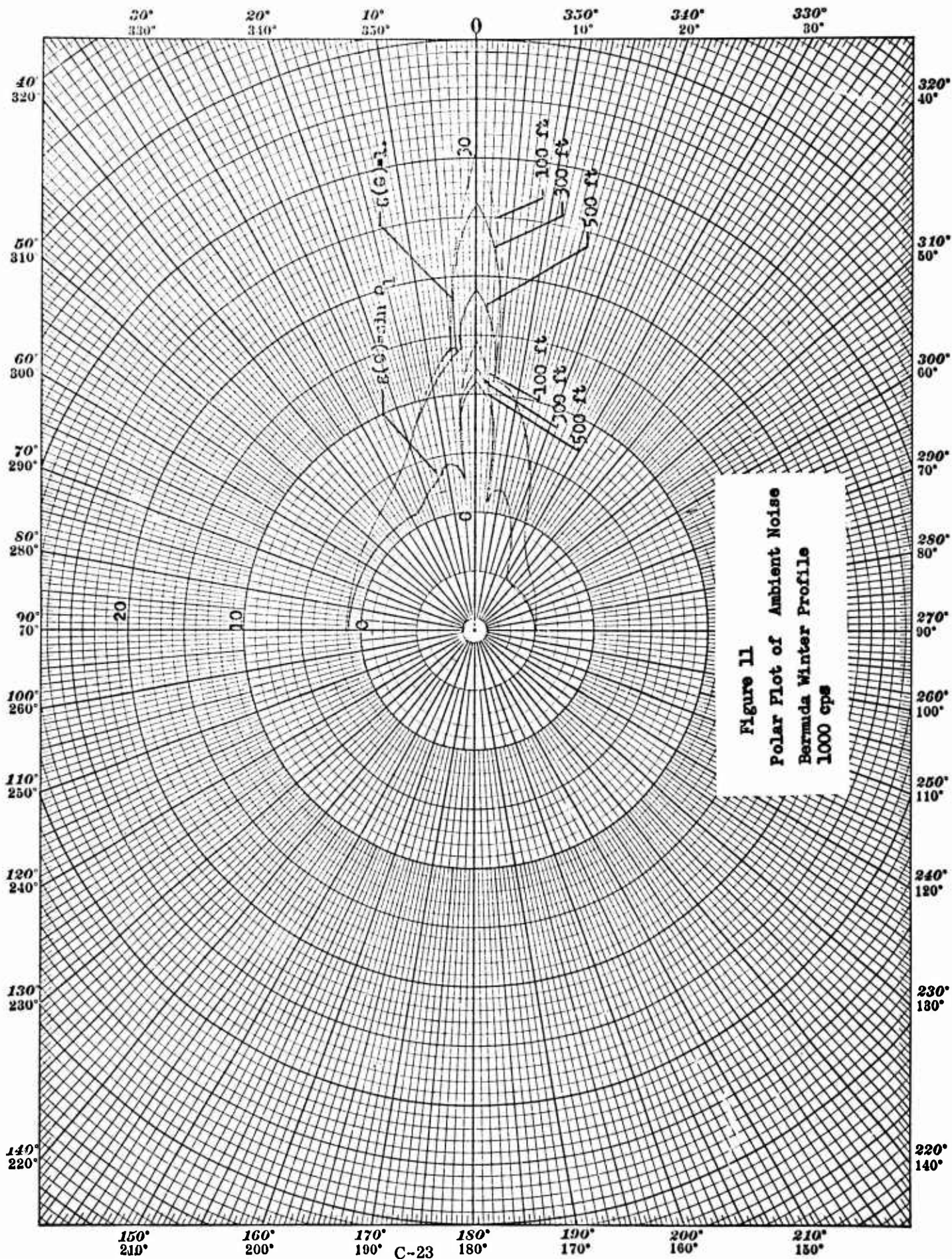
#### VIII. Conclusions

It has been shown that an ambient noise model which assumes a uniform surface distribution of independent noise source elements gives rise to one of two very different noise distributions vs. vertical angle. If the hydrophone lies at a depth where a negative velocity gradient exists, there will be no surface ambient noise received at angles near the horizontal, although at slightly larger angles the noise intensity will rapidly jump to a high level. If the hydrophone lies in a region of positive velocity gradient (and if the sound velocity at the hydrophone is greater than that at the surface), then no shadow region exists and the noise level grows rapidly as the vertical angle approaches the horizontal. This peaking near  $\theta_0 = 0$  is due to two important features. The first occurs because at small values of  $\theta_0$  a small solid angle at the hydrophone covers a very large area of surface due only to the geometry involved. The second arises from contributions to the noise generated far from the hydrophone and propagating to the hydrophone via many surface bounces. This effect may be greatly reduced if the surface reflection coefficient is heavily dependent on sea state. The first effect may be counteracted partially if the surface noise elements are directional, such that more power is transmitted at steep downward angles than at very shallow angles to the surface.

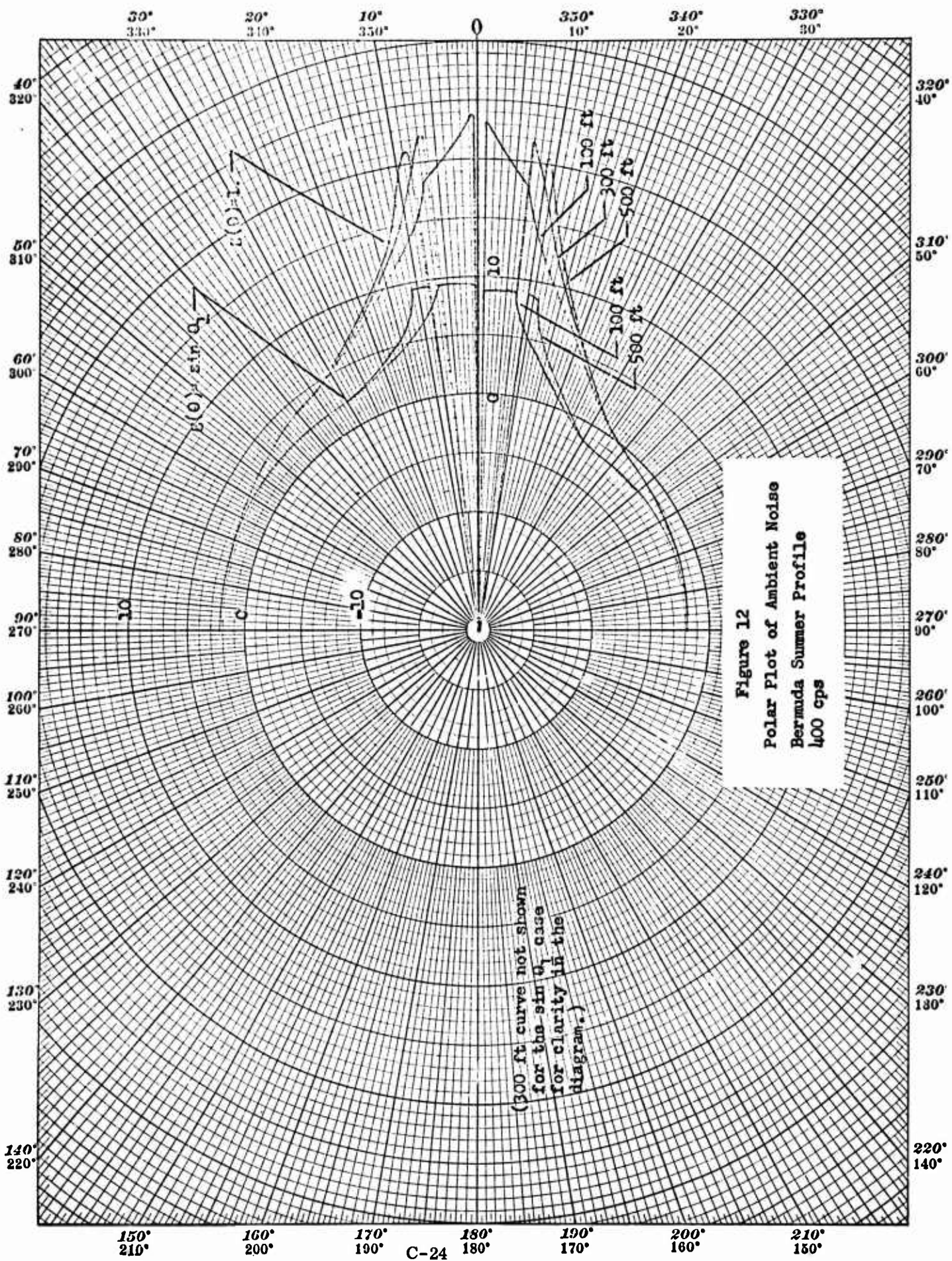
The results in the winter profile cases shown above are seen to depend only to a small extent on frequency and hydrophone depth, for low

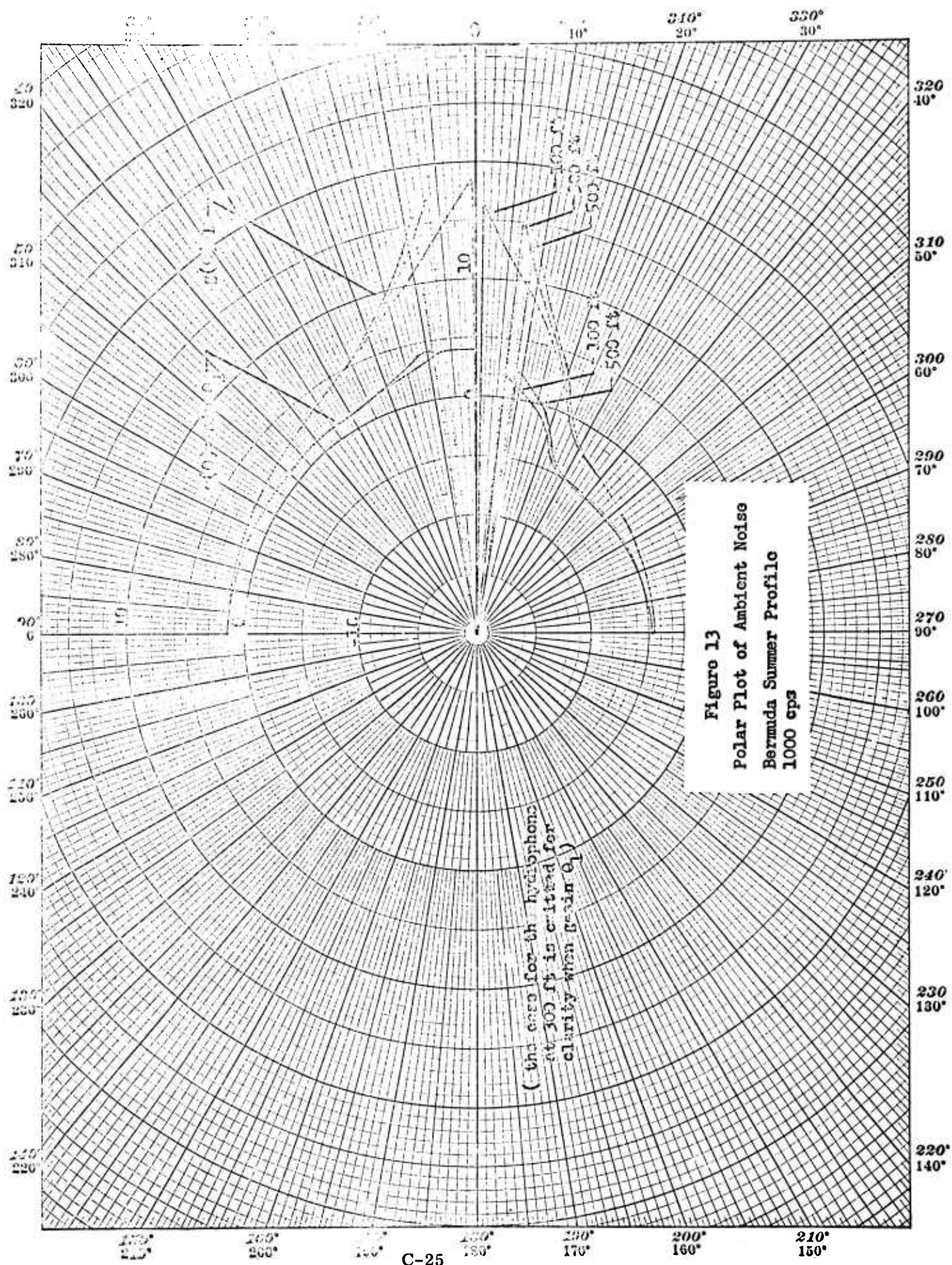




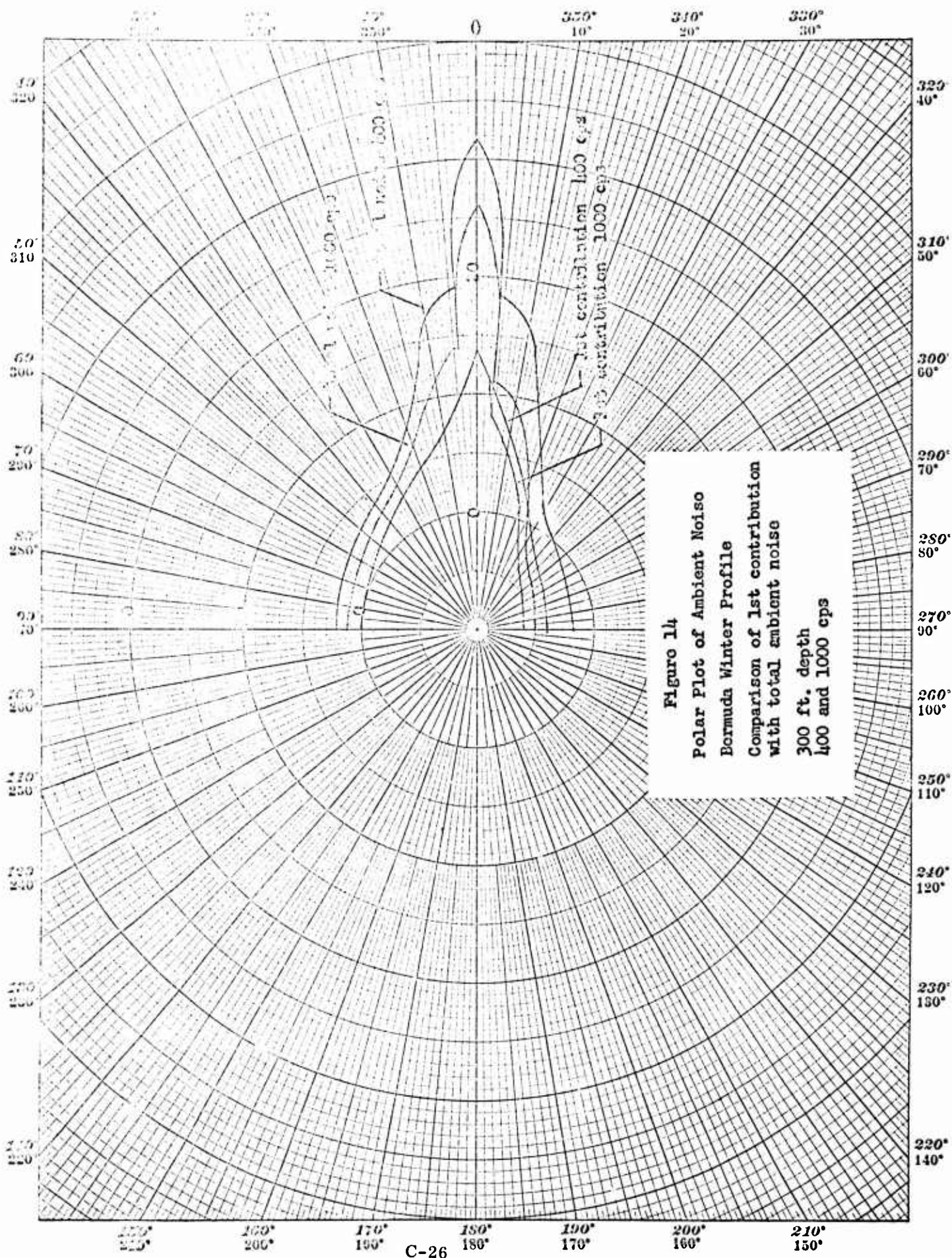


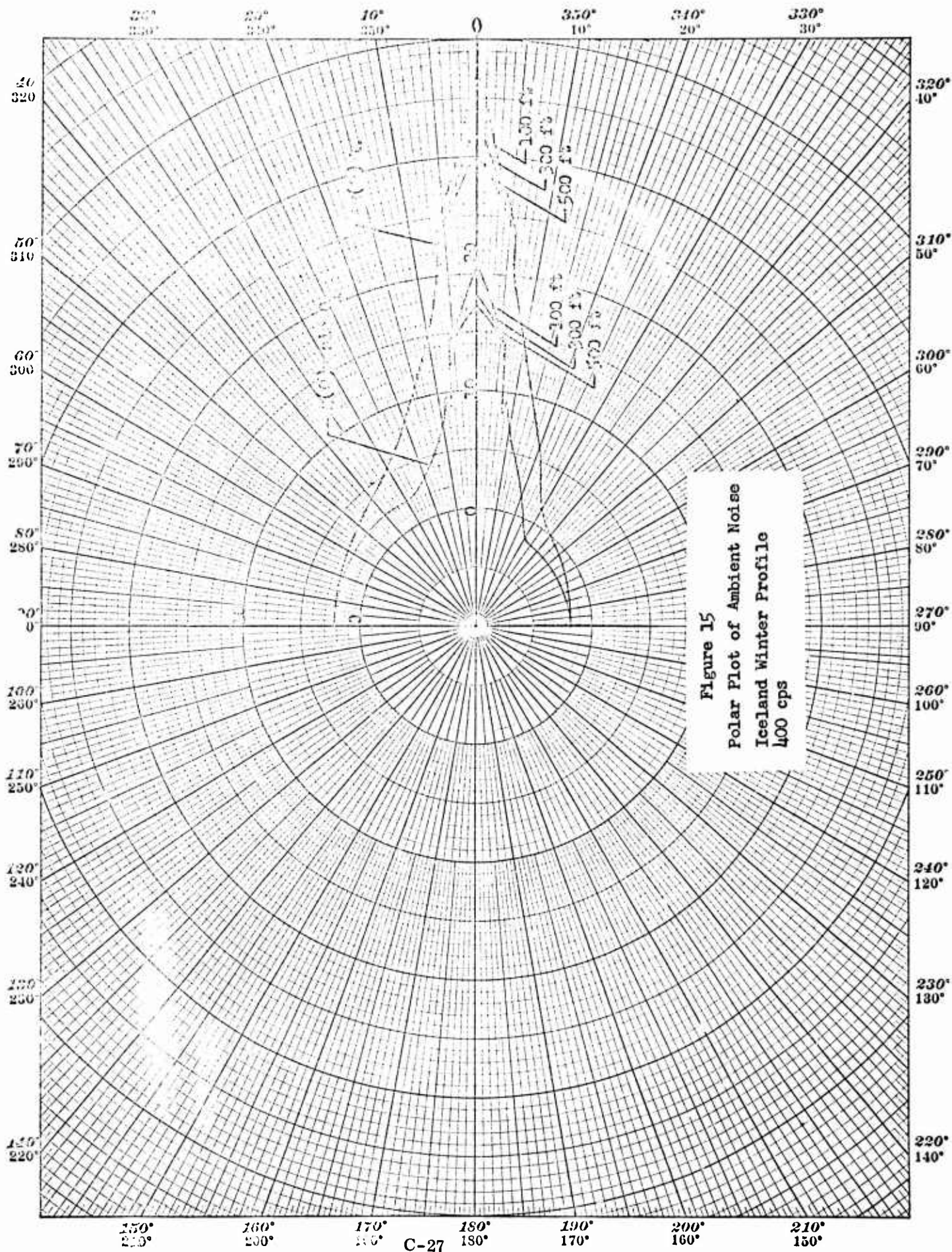




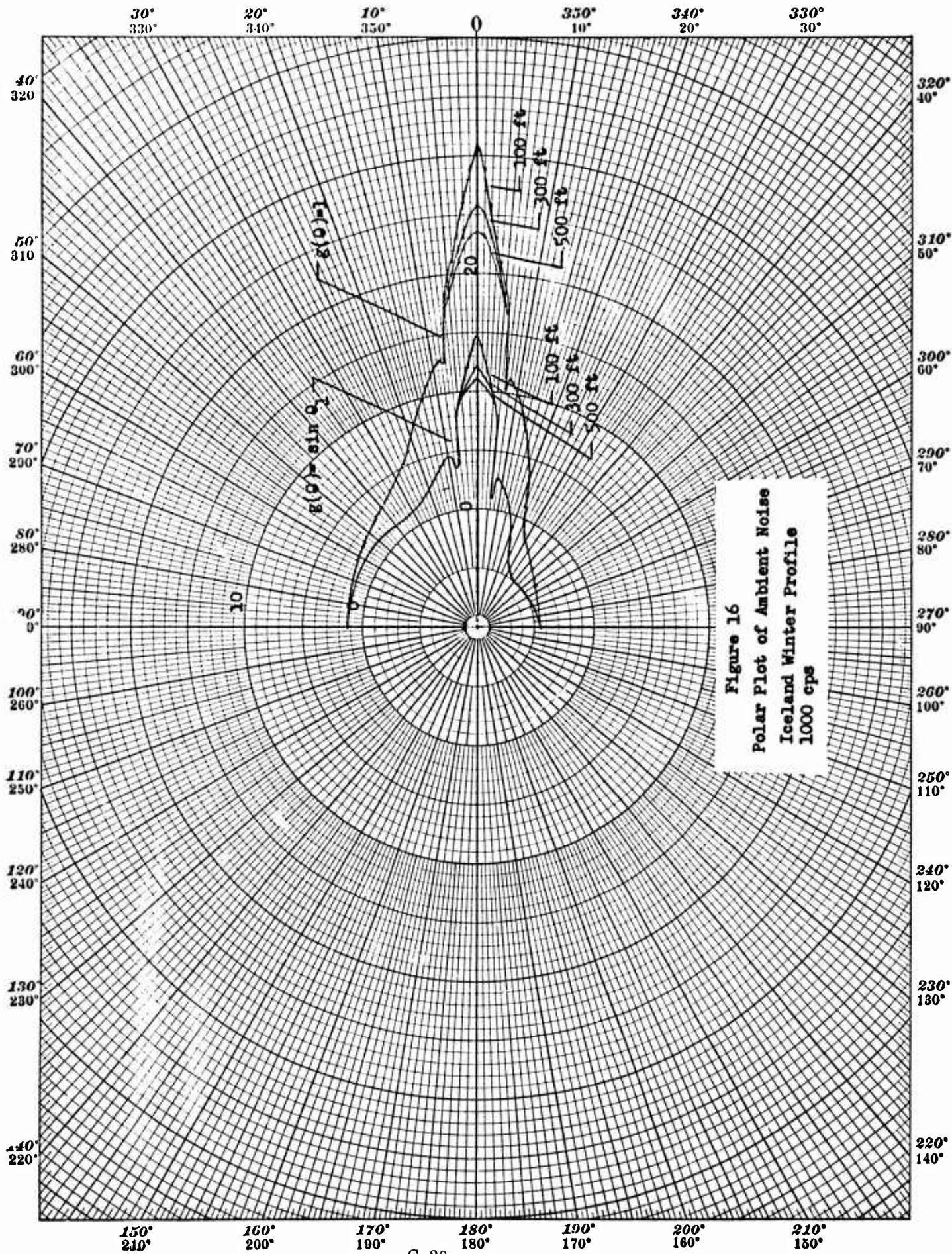


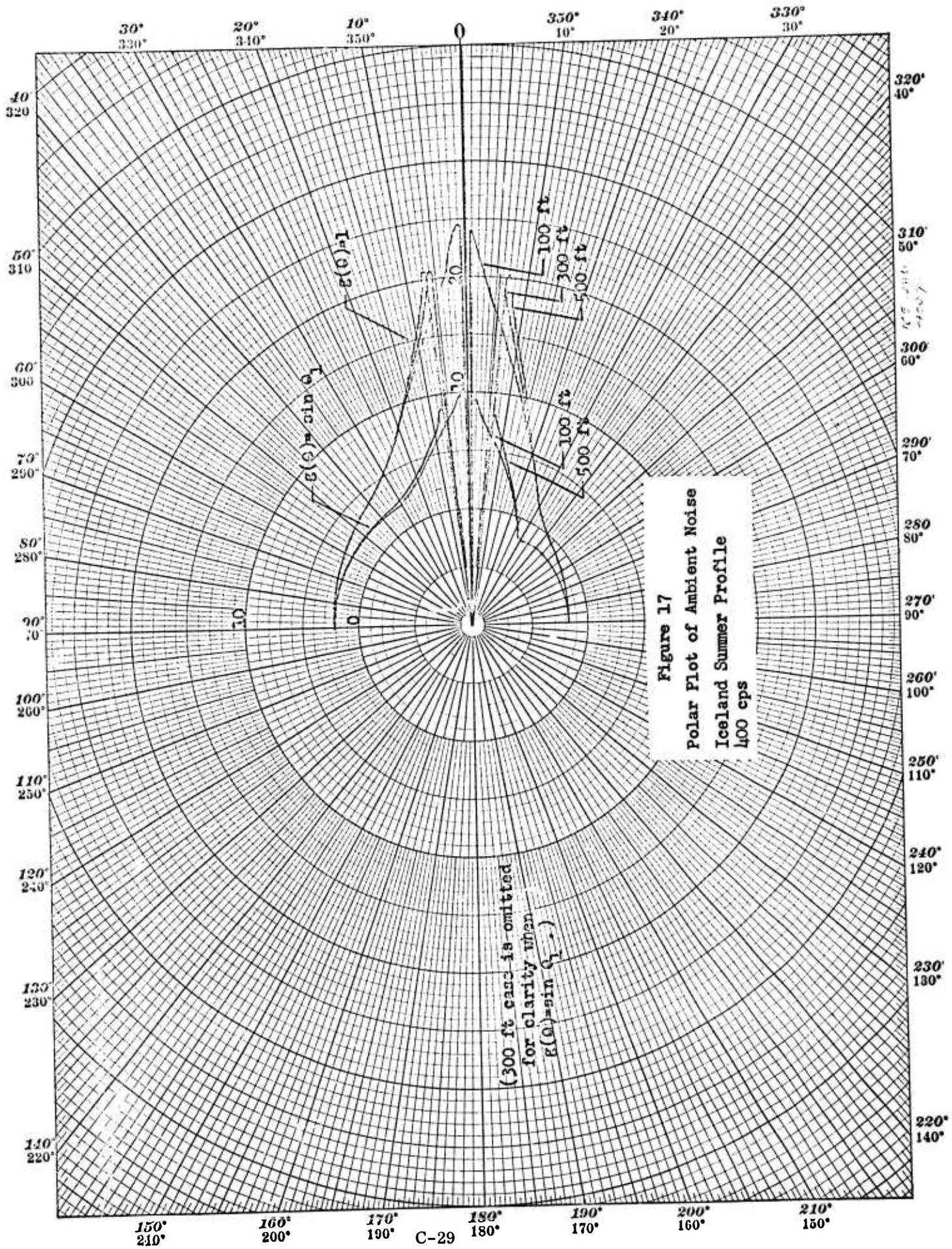




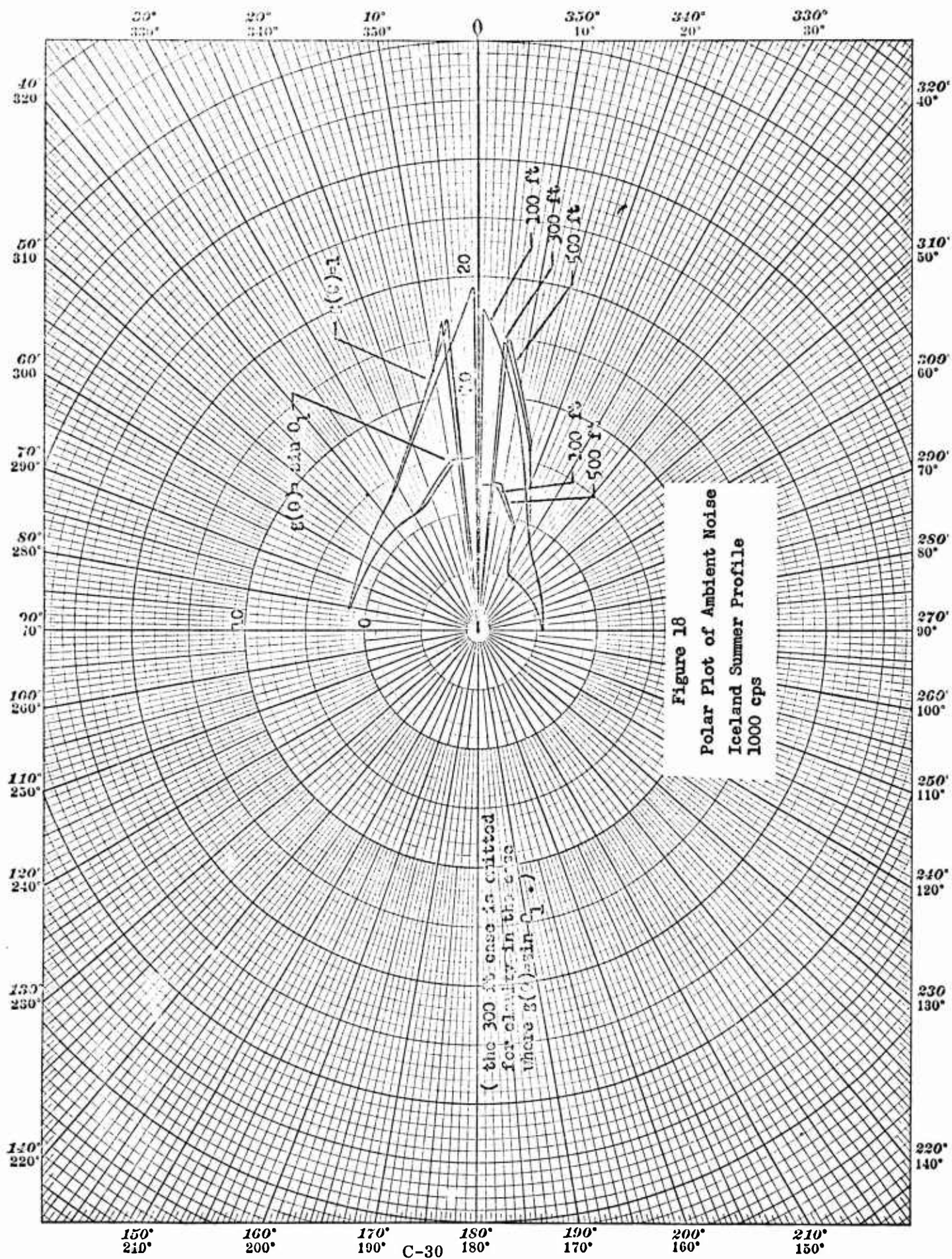












frequencies (100-1000 cps) and shallow depths (100-500 ft). Except for the seasonal shifts in velocity profiles which cause radical changes in the noise distribution, the distribution is rather insensitive to profile, as seen by comparing the Bermuda and Iceland cases in each season.

The superficially promising null in the noise at small values of  $\theta_0$  during the summer months is not actually very helpful, since it is due to sound channeling effects. Thus a target near the surface would also be hidden from the hydrophone. The exception to this would occur if the submarine and hydrophone were both in the negative gradient region (below  $D_{\text{mode}}$  in Fig. 5) and at approximately the same depth. Then the submarine signal would arrive at the hydrophone at an angle near zero, for which there is a null in the surface ambient noise. This case possibly could be taken advantage of, in order to combat such noise.

The results indicate that bottom bounce techniques might be employed in order to take advantage of the greatly reduced ambient noise at angles steeper than about  $20^\circ$ . The noise level at these angles can be as much as 28 db below that at near horizontal angles.

The above results depend strongly on the assumed noise model. The need for careful measurements of the vertical noise distribution near the surface therefore appears to be indicated. By comparing such results with the various cases given in Figs. 10-18, it should be possible to make some judgments as to the functional form of  $g(\theta_1)$ , the surface reflection coefficient  $\gamma$ , and indeed the validity of the basic model concept, that of a uniform surface distribution of noise sources.



#### Appendix The Ray Tracing Program

In order to evaluate  $N_{up}(\theta_o)$  and  $N_{down}(\theta_o)$ , the following quantities must be computed.

$\theta_1$ : the angle of intersection of the ray with the surface

$\theta_{bottom}$ : the angle of intersection of the ray with the bottom

$R_1$ : the ray path length from the hydrophone to the surface

$R_2$ : the ray path length from the hydrophone to the bottom

If the ray does not reach the bottom, then  $R_2$  is the path length of the ray from the hydrophone to its position of maximum depth, at which point, of course, it is moving horizontally.

If the velocity profile is approximated by several straight line segments, the ray path in the region of depth for each segment is uniquely determined by the angle with which it enters the region, the velocity of sound at the depth at which it enters, and the velocity gradient in the region.

By Eq. (4) the angle at each depth is known as soon as  $\theta_o$  and  $c_{hyd}$  are given, and the sound velocity at that depth is computed. Thus  $\theta_1$  and  $\theta_{bottom}$  (when applicable) can be found without any ray tracing as such.

The program used begins at the surface, and taking each linear segment, subdivides the corresponding depth interval into a sufficient number of subintervals. The criterion used was that the ray angle should not change by more than a specified fraction of a degree over the subinterval. A change of one degree was found tolerable. Thus in this subinterval the ray path is essentially straight, and if it is directed at an angle  $\theta_1$  with respect to the horizontal, the path length in the subinterval is

$d_i/\sin \theta_i$ , where  $d_i$  is the change in depth in the subinterval. Thus  $R_1$  is merely the sum of all these contributions, until the depth of the hydrophone is reached. This number is stored and then the computation resumes downward to find  $R_2$ . When either the bottom or an angle  $\theta_i = 0$  is reached, the computation is terminated.

#### References

- (1) R. J. Talham, "Ambient Sea-Noise Model," JASA 36, 1541-1544, 1964.
- (2) G. R. Fox, "Ambient-Noise Directivity Measurements," JASA 36, 1537-1540, 1964.
- (3) H. W. Marsh and M. Schulkin, "Underwater Sound Transmission," Avco Corp. Report, New London, Connecticut, 1962.
- (4) L. T. Einstein, U. S. Navy Underwater Sound Laboratory, Technical Memo.
- (5) J. W. Horton, "Fundamentals of Sonar," U.S. Navy Underwater Sound Laboratory, 1954.
- (6) H. W. Marsh, M. Schulkin, and S. G. Kneake, "Scattering of Underwater Sound by the Sea Surface," JASA 33, 334-340, 1961.



DETECTION OF ACTIVE SONAR SIGNALS BY MEANS OF  
A CROSSCORRELATOR

By

Peter M. Schultheiss

Progress Report No. 27

General Dynamics Electric Boat division  
(8050-31-55001)

January 1966

DEPARTMENT OF ENGINEERING  
AND APPLIED SCIENCE  
YALE UNIVERSITY

### Summary

The detection of a single sonar pulse by means of a correlation detector is analyzed in the absence of Doppler shift due to transmitter, target, or scatterer motion. The returned signal is assumed to be a delayed replica of the transmitted signal. Noise fields consisting primarily of volume reverberation, surface reverberation, and ambient noise are considered separately. The reverberation noise is assumed to be generated by independently located, Poisson distributed scatterers, dispersed throughout the illuminated volume (volume reverberation) or near the illuminated surface (surface reverberation). The transmitted signal is assumed to be a pulse of sinusoidal carrier with or without superimposed linear frequency modulation. The following results are obtained:

- 1) The bandwidth of the transmitted signal imposes an effective range gate on output noise arising from the intermodulation products of signal with reverberation. The width of this gate is of the order of the velocity of sound divided by the bandwidth of the signal. (this ratio may be regarded as the correlation distance in the water of the transmitted signal). Only scatterers whose range differs from that of the target by no more than the gate width contribute to this type of output noise (which is dominant under high signal to noise conditions).
- 2) Output noise consisting of the intermodulation products of reverberation with reverberation is contributed by all scatterers illuminated simultaneously with the target. Contributing scatterers therefore lie within a range gate determined by the pulse duration rather than the (possibly much shorter) signal correlation time. However, the two members of each contributing pair must be separated from each

other by a range difference no greater than the "range gate" defined in 1). Intermodulation of reverberation with reverberation is the dominant noise at low input signal to reverberation ratios. Except for the phenomenon discussed in 3), there is no angular discrimination against either type of reverberation noise aside from the obvious effects of transmitter and receiver beam patterns.

- 3) A special case of 2) is output noise due to the intermodulation of the returns from a particular scatterer to the two receivers. This type of noise is important only when one or a few strong scatterers (false targets) contribute a significant fraction of the total reverberation. False target returns are subject to angular discrimination, being sharply attenuated if they are separated from the target by more than a certain angle. This angle defines the minimum angular resolution of which the detector is capable. For a broadside target it is the arc sine of the ratio of the signal correlation distance to the spacing between receivers. The resolution is best in the broadside direction and poorest in the endfire direction.
- 4) In the absence of a target the average detector output is zero except for a transmitter-receiver combination with very narrow beam patterns trained very close to the axis of the receiving array. In the latter case a non-zero average output may result from the inability of the detector to resolve different scatterer groups within the illuminated area.
- 5) In the absence of strong scatterers (false targets) and for beams trained far enough from the array axis so that the resolution problem mentioned in 4) does not arise, the reverberation may be

regarded as a Gaussian noise process. For a fixed input signal to noise ratio, there is then no difference in performance between a detector operating in a noise field consisting primarily of reverberation and a similar detector operating in an ambient noise field with the same power spectrum. If the ambient noise field is broad-band but is filtered so that its spectrum comes close to matching that of the signal, there is still no important difference between detector performance in reverberation limited and ambient noise limited environments (for fixed input signal to noise ratio). One must keep in mind, however, that the effective input signal to noise ratio tends to vary inversely with the signal bandwidth for ambient noise, whereas it is independent of the signal bandwidth for reverberation. Thus maximum output signal to noise ratio is generally achieved by the use of broadband signals if the primary problem is reverberation and by the use of narrowband signals if the primary problem is ambient noise. In the former case one takes advantage of the range gating effect produced by short signal correlation times, in the latter case one relies on noise reduction through the use of narrow filters matched to the signal spectrum.

- 6) Under the conditions stated in 5) the output signal to noise ratio varies as the square of the input signal to noise ratio for small input signal to noise ratios and as the first power of the input signal to noise ratio for large input signal to noise ratios. Thus the correlation detector operates much like a coherent detector for large input signal to noise ratios but more like an incoherent detector for small input signal to noise ratios. The output signal to noise ratio of a true coherent detector (correlating the output

of one receiver with a delayed replica of the transmitted signal) is precisely twice that of the correlation detector in the limit of high input signal to noise ratio. For one set of reasonable parameter values, the correlation detector requires an input signal to noise ratio 8 db higher than that of the coherent detector in order to achieve an output signal to noise ratio of 6 db.

- 7) The primary difference between surface and volume reverberation is the time dependence of the former, caused by the fact that surface reverberation is a problem only when elements of the surface are illuminated simultaneously with the target. This leads to limitations on desirable pulse length which are not present in the case of volume reverberation.
- 8) Reverberation power varies with range: with the inverse second power of range for volume reverberation and the inverse third power of range for surface reverberation. The input signal power varies with the inverse fourth power of range. Hence, for small input signal to noise ratios, the output signal to noise ratio varies as the inverse fourth power of range for volume reverberation and the inverse second power of range for surface reverberation. When ambient noise dominates, the output signal to noise ratio varies with the inverse eighth power of range. Under conditions of high input signal to noise ratio, the output signal to noise ratio varies with the inverse second power of range for volume reverberation, with the inverse first power of range for surface reverberation and with the inverse fourth power of range for ambient noise.



### I. Detection in a Reverberation Limited Environment

This report is concerned with the detection of an active sonar signal in a noise environment that may be dominated either by reverberation or by ambient noise. The postulated signal processing scheme is outlined in Figure 1. A sonar pulse produced by a transmitter with known beam pattern is reflected by the target and received at two locations, labelled receiver a and receiver b

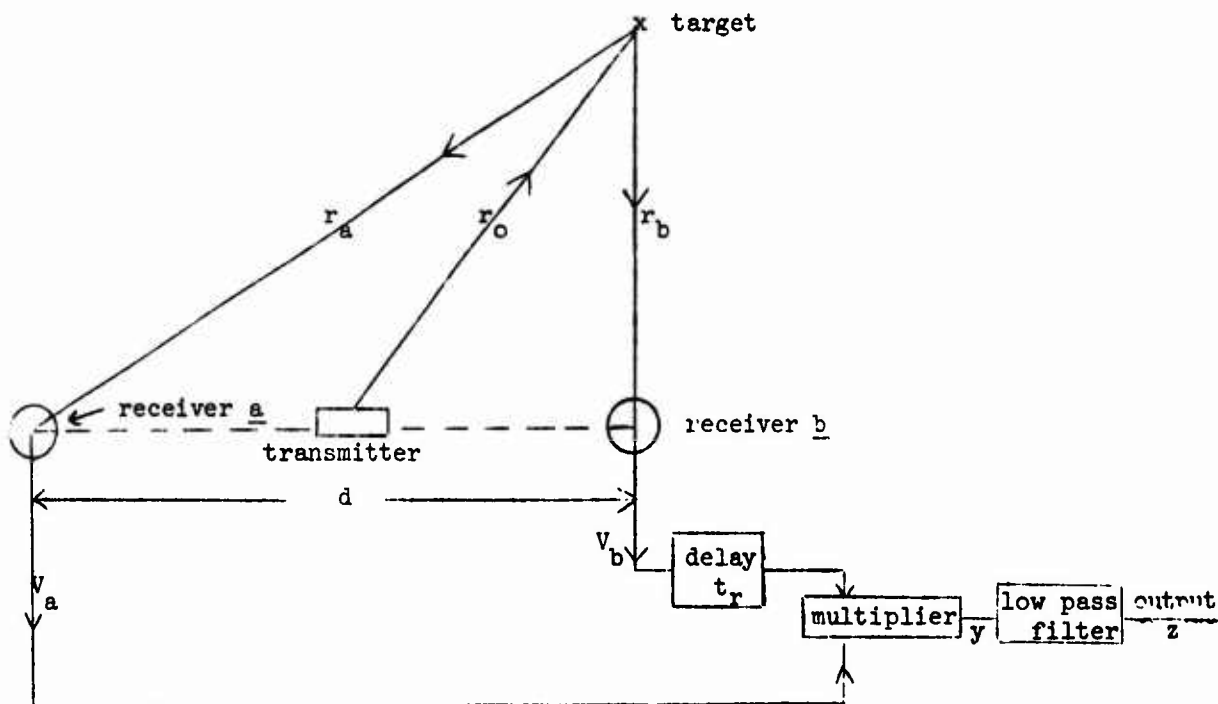


Figure 1

respectively. Whether each of these receivers consists of one hydrophone or of a group of hydrophones is immaterial to the analysis except for the effect on the signal strength received from any given direction. As long as the two receivers are similar and the target is relatively remote ( $r_o \gg d$ ), any beam-forming effects of the receiver can clearly be lumped with those of the

transmitter. The output of one receiver is delayed by an amount  $t_r$ , chosen so as to bring the two target returns into alignment (steering). It is then multiplied by the output of the second receiver and the product is smoothed by means of a low pass filter.<sup>1</sup> Reverberation is assumed to be generated by a series of scatterers randomly distributed in volume and at the surface. The scatterers, as well as the source and target, are assumed to be at rest.<sup>2</sup>

The transmitted signal is taken as a linearly frequency modulated pulse with Gaussian envelope. Thus

$$\text{Transmitted signal} = \exp\left[-\frac{t^2}{\sigma_T^2}\right] \cos(\omega_0 t + \frac{K}{2} t^2) \quad (1)$$

In cases of practical interest the pulse width  $\sigma_T$ , maximum frequency deviation in the pulse  $K\sigma_T$ , and mean carrier frequency  $\omega_0$  satisfy the inequalities

$$\frac{1}{\sigma_T} \ll K\sigma_T \ll \omega_0 \quad (2)$$

In a reverberation dominated environment the output  $v_a$  of receiver a

---

<sup>1</sup>Alternatively one might use transducers a and b for transmission as well as reception. With proper delays in transmitted and received signals the signal component of the output would be identical with that obtained from the configuration of Fig. 1. The formal expression for the reverberation noise would be more cumbersome, since for most scatterers the round trip times to one receiver from the two sources would be different. It is not felt that the inclusion of this added complexity would yield significant additional insight into the detection process.

<sup>2</sup>For the relatively wideband signals considered in much of this report, the Doppler shifts due to scatterer motion (even due to target motion) should be quite small compared with the signal bandwidth.

can now be written as follows:

$$V_a(t) = \frac{A}{t_a^2} \exp \left[ -\frac{(t-t_a)^2}{\sigma_T^2} \right] \cos \left[ \omega_0(t-t_a) + \frac{K}{2}(t-t_a)^2 \right] + \sum_i \frac{a_i}{t_i^2} \exp \left[ -\frac{(t-t_i)^2}{\sigma_T^2} \right] \cos \left[ \omega_0(t-t_i) + \frac{K}{2}(t-t_i)^2 \right] \quad (3)$$

In Equation (3)  $t_a = \frac{r_o + r_a}{c}$  is the round trip time from the transmitter via the target to receiver a.<sup>1</sup>  $c$  is the velocity of sound in water.  $t_i$  is the round trip time from the transmitter to scatterer  $i$  and back to receiver a. The constant  $A$  depends on the scattering cross-section of the target and on the amount of radiation received by the target, i.e. on the beam parameters of the transmitter. In similar fashion,  $a_i$  depends on the scattering cross-section of the  $i^{\text{th}}$  scatterer and on the transmitter beam parameters. The dependence of the signal and noise components of  $V_a(t)$  on  $1/t_a^2$  and  $1/t_i^2$  respectively reflects the usual spherical spreading loss and results in a non-stationarity of the reverberation noise.

In completely analogous fashion the output  $V_b$  of receiver b assumes the form:

$$V_b(t) = \frac{A}{t_b^2} \exp \left[ -\frac{(t-t_b)^2}{\sigma_T^2} \right] \cos \left[ \omega_0(t-t_b) + \frac{K}{2}(t-t_b)^2 \right] + \sum_j \frac{a_j}{T_j^2} \exp \left[ -\frac{(t-T_j)^2}{\sigma_T^2} \right] \cos \left[ \omega_0(t-T_j) + \frac{K}{2}(t-T_j)^2 \right] \quad (4)$$

Here  $t_b$  and  $T_j$  are the signal round trip times from the transmitter to

<sup>1</sup>Strictly speaking, the first term is proportional to  $c^2/(r_o r_a)$ . With  $r_o \approx r_a$  this becomes approximately  $4/t_a^2$

receiver  $b$  via the target and scatterer  $j$  respectively.  $V_b(t)$  is delayed by  $t_r$  seconds and multiplied by  $V_a(t)$  to yield  $y(t)$ . After some algebraic simplification one obtains:

$$\begin{aligned}
 y(t) = & \frac{A^2}{2t_a^2} \exp \left[ -\frac{(t_a - t_b - t_r)^2}{2\sigma_T^2} \right] \exp \left[ -\frac{\left( t - \frac{t_a + t_b + t_r}{2} \right)^2}{\sigma_T^2/2} \right] \\
 & \cdot \cos \left[ \omega_c(t_b + t_r - t_a) + K(t_b + t_r - t_a) \left( t - \frac{t_b + t_r + t_a}{2} \right) \right] \\
 & + \frac{A}{2t_a^2} \sum_j \frac{a_j}{T_j^2} \exp \left[ -\frac{(t_a - T_j - t_r)^2}{2\sigma_T^2} \right] \exp \left[ -\frac{\left( t - \frac{t_a + T_j + t_r}{2} \right)^2}{\sigma_T^2/2} \right] \\
 & \cdot \cos \left[ \omega_c(T_j + t_r - t_a) + K(T_j + t_r - t_a) \left( t - \frac{T_j + t_r + t_a}{2} \right) \right] \\
 & + \frac{A}{2t_b^2} \sum_i \frac{a_i}{t_i^2} \exp \left[ -\frac{(t_i - t_b - t_r)^2}{2\sigma_T^2} \right] \exp \left[ -\frac{\left( t - \frac{t_i + t_b + t_r}{2} \right)^2}{\sigma_T^2/2} \right] \\
 & \cdot \cos \left[ \omega_c(t_b + t_r - t_i) + K(t_b + t_r - t_i) \left( t - \frac{t_b + t_r + t_i}{2} \right) \right] \\
 & + \frac{1}{2} \sum_i \sum_j \frac{a_i a_j}{t_i^2 T_j^2} \exp \left[ -\frac{(t_i - T_j - t_r)^2}{2\sigma_T^2} \right] \exp \left[ -\frac{\left( t - \frac{t_i + T_j + t_r}{2} \right)^2}{\sigma_T^2/2} \right] \\
 & \cdot \cos \left[ \omega_c(T_j + t_r - t_i) + K(T_j + t_r - t_i) \left( t - \frac{T_j + t_r + t_i}{2} \right) \right] \quad (5)^1
 \end{aligned}$$

If the weighting function of the low pass filter is  $w(t)$ , its output  $z(t)$  is given by

---

<sup>1</sup>Sinusoidal terms in  $2\omega_c t$  have been discarded since they will be filtered out by the low pass filter in any case.

$$z(t) = \int_0^{\infty} d\rho w(\rho) y(t-\rho) \quad (6)$$

For computational convenience the weighting function will be chosen as

$$w(t) = \frac{1}{\sqrt{\pi}\sigma_F} \exp\left[-\frac{(t-t_D)^2}{\sigma_F^2}\right] \quad (7)$$

This corresponds to the frequency function

$$G(\omega) = \int_{-\infty}^{\infty} w(t) \exp[-j\omega t] dt = \exp\left[-\frac{\sigma_F^2}{4} \omega^2\right] \exp[-j\omega t_D] \quad (8)$$

As long as the time delay  $t_D$  satisfies  $t_D \gg \sigma_F$ , the filter is approximately realizable.

Substituting Equations (5) and (7) into Equation (6) one obtains after extensive algebraic manipulations:

$$\begin{aligned} z(t) = & \frac{A^2}{2t_a^2 t_b^2} \frac{\sigma_c}{\sigma_F} \exp\left[-\frac{(t_a - t_b - t_r)^2}{2\sigma_T^2}\right] \exp\left[-\frac{\left(t - \frac{t_a + t_b + t_r}{2} - t_D\right)^2}{\sigma_F^2 + \sigma_T^2/2}\right] \exp\left[-\frac{K^2 \sigma_c^2}{4}(t_b + t_r - t_a)^2\right] \\ & \cdot \cos\left\{\omega_0(t_b + t_r - t_a) + K \frac{\sigma_c^2}{\sigma_F^2} (t_b + t_r - t_a)\left(t - \frac{t_b + t_r + t_a}{2} - t_D\right)\right\} \\ & + \frac{A}{2t_a^2} \frac{\sigma_c}{\sigma_F} \sum_j \frac{a_j}{T_j^2} \exp\left[-\frac{(t_a - T_j - t_r)^2}{2\sigma_T^2}\right] \exp\left[-\frac{\left(t - \frac{t_a + T_j + t_r}{2} - t_D\right)^2}{\sigma_F^2 + \sigma_T^2/2}\right] \exp\left[-\frac{K^2 \sigma_c^2}{4}(T_j + t_r - t_a)^2\right] \\ & \cdot \cos\left\{\omega_0(T_j + t_r - t_a) + K \frac{\sigma_c^2}{\sigma_F^2} (T_j + t_r - t_a)\left(t - \frac{T_j + t_r + t_a}{2} - t_D\right)\right\} \end{aligned}$$

$$\begin{aligned}
& + \frac{A}{2t_b} \frac{\sigma_c}{\sigma_F} \sum_i \frac{a_i}{t_i^2} \exp \left[ -\frac{(t_i - t_b - t_r)^2}{2\sigma_T^2} \right] \exp \left[ -\frac{\left( t - \frac{t_i + t_b + t_r}{2} - t_D \right)^2}{\sigma_F^2 + \sigma_T^2/2} \right] \exp \left[ -\frac{K^2 \sigma_c^2}{4} (t_b + t_r - t_i)^2 \right] \\
& \cdot \cos \left\{ \omega_0 (t_b + t_r - t_i) + K \frac{\sigma_c^2}{\sigma_F} (t_b + t_r - t_i) \left( t - \frac{t_b + t_r + t_i}{2} - t_D \right) \right\} \\
& + \frac{\sigma_c}{2\sigma_F} \sum_i \sum_j \frac{a_i a_j}{t_i^2 T_j^2} \exp \left[ -\frac{(t_i - T_j - t_r)^2}{2\sigma_T^2} \right] \exp \left[ -\frac{\left( t - \frac{t_i + T_j + t_r}{2} - t_D \right)^2}{\sigma_F^2 + \sigma_T^2/2} \right] \exp \left[ -\frac{K^2 \sigma_c^2}{4} (T_j + t_r - t_i)^2 \right] \\
& \cdot \cos \left\{ \omega_0 (T_j + t_r - t_i) + K \frac{\sigma_c^2}{\sigma_F} (T_j + t_r - t_i) \left( t - \frac{T_j + t_r + t_i}{2} - t_D \right) \right\} \quad (9)
\end{aligned}$$

where

$$\sigma_c^2 = \frac{\sigma_F^2 \sigma_T^2/2}{\sigma_F^2 + \sigma_T^2/2} \quad (10)$$

Equation (9) indicates that the delay  $t_r$  necessary to maximize the signal component of  $z(t)$  is

$$t_r = t_a - t_b \quad (11)$$

With this adjustment of delay

$$\begin{aligned}
z(t) &= \frac{A^2}{2t_a^2 t_b} \frac{\sigma_c}{\sigma_F} \exp \left[ -\frac{(t - t_a - t_b)^2}{\sigma_F^2 + \sigma_T^2/2} \right] \\
& + \frac{A}{2t_a} \frac{\sigma_c}{\sigma_F} \sum_j \frac{a_j}{T_j^2} \exp \left[ -\frac{(t_b - T_j)^2}{2\sigma_T^2} \right] \exp \left[ -\frac{\left( t - t_a - t_b - \frac{T_j - t_b}{2} \right)^2}{\sigma_F^2 + \sigma_T^2/2} \right] \exp \left[ -\frac{K^2 \sigma_c^2}{4} (t_b - T_j)^2 \right]
\end{aligned}$$

$$\begin{aligned}
& \cdot \cos \left\{ (T_j - t_b) \left[ \omega_o + K \frac{\sigma_c^2}{\sigma_F^2} (t - t_a - t_D - \frac{T_j - t_b}{2}) \right] \right\} \\
& + \frac{A}{2t_b^2} \frac{\sigma_c}{\sigma_F} \sum_i \frac{a_i}{t_i^2} \exp \left[ - \frac{(t_i - t_a)^2}{2\sigma_T^2} \right] \exp \left[ - \frac{(t - t_D - \frac{t_i + t_a}{2})^2}{\sigma_F^2 + \sigma_T^2 / 2} \right] \exp \left[ - \frac{K^2 \sigma_c^2}{4} (t_i - t_a)^2 \right] \\
& \cdot \cos \left\{ (t_a - t_i) \left[ \omega_o + K \frac{\sigma_c^2}{\sigma_F^2} (t - t_D - \frac{t_i + t_a}{2}) \right] \right\} \\
& + \frac{\sigma_c}{2\sigma_F} \sum_i \sum_j \frac{a_i a_j}{t_i^2 t_j^2} \exp \left[ - \frac{[(t_i - t_a) - (T_j - t_D)]^2}{2\sigma_T^2} \right] \exp \left[ - \frac{(t - \frac{t_i + T_j + t_a - t_b}{2} - t_D)^2}{\sigma_F^2 + \sigma_T^2 / 2} \right] \\
& \cdot \exp \left[ - \frac{K^2 \sigma_c^2}{4} [(t_i - t_a) - (T_j - t_b)]^2 \right] \\
& \cdot \cos \left\{ [(t_i - t_a) - (T_j - t_b)] \left[ \omega_o + K \frac{\sigma_c^2}{\sigma_F^2} (t - \frac{t_i + T_j + t_a - t_b}{2} - t_D) \right] \right\} \quad (12)
\end{aligned}$$

The signal component of  $z(t)$  clearly peaks at  $t = t_a + t_D$ . The statistical properties of the random variable  $z(t_a + t_D)$  are therefore of primary importance in any discussion of detector performance.<sup>1</sup> The general expression for  $z(t_a + t_D)$  is from Equation (12)

$$z(t_a + t_D) = \frac{A^2}{2t_a^2 t_b^2} \frac{\sigma_c}{\sigma_F}$$

---

<sup>1</sup>The statement that the output is observed at time  $t_a + t_D$  implies selection of the proper range cell, just as the choice  $t_r = t_a - t_b$  implies selection of the proper bearing cell. If bearing and range are not known a priori, one must clearly examine all possible cells.

$$\begin{aligned}
& + \frac{A}{2t_a} \frac{\sigma_c}{\sigma_F} \sum_j \frac{a_j}{t_j} \exp\left[-\frac{(t_b - T_j)^2}{2\sigma_T^2}\right] \exp\left[-\frac{(t_b - T_j)^2}{4(\sigma_F^2 + \sigma_T^2/2)}\right] \exp\left[-\frac{K^2 \sigma_c^2}{4} (t_b - T_j)^2\right] \cos\left\{(T_j - t_b) \left[\omega_0 + K \frac{\sigma_c^2}{2\sigma_F} (t_b - T_j)\right]\right\} \\
& + \frac{A}{2t_b} \frac{\sigma_c}{\sigma_F} \sum_i \frac{a_i}{t_i} \exp\left[-\frac{(t_i - t_a)^2}{2\sigma_T^2}\right] \exp\left[-\frac{(t_i - t_a)^2}{4(\sigma_F^2 + \sigma_T^2/2)}\right] \exp\left[-\frac{K^2 \sigma_c^2}{4} (t_i - t_a)^2\right] \cos\left\{(t_a - t_i) \left[\omega_0 + K \frac{\sigma_c^2}{2\sigma_F} (t_a - t_i)\right]\right\} \\
& + \frac{\sigma_c}{2\sigma_F} \sum_i \sum_j \frac{a_i a_j}{t_i t_j} \exp\left[-\frac{[(t_i - t_a) - (T_j - t_b)]^2}{2\sigma_T^2}\right] \exp\left[-\frac{[(t_i - t_a) + (T_j - t_b)]^2}{4(\sigma_F^2 + \sigma_T^2/2)}\right] \\
& \cdot \exp\left\{-\frac{K^2 \sigma_c^2}{4} [(t_i - t_a) - (T_j - t_b)]^2\right\} \cos\left\{[(t_i - t_a) - (T_j - t_b)] \left[\omega_0 - K \frac{\sigma_c^2}{2\sigma_F} \left(\frac{t_i - t_a}{2} + \frac{T_j - t_b}{2}\right)\right]\right\}
\end{aligned} \tag{13}$$

For ease in later computations it will be convenient to distinguish between two cases:

- A) The bandwidth of the transmitted signal is determined primarily by the frequency modulation ( $K\sigma_c \gg 1/\sigma_T$ ).
- B) The bandwidth of the transmitted signal is determined by the pulse duration (no frequency modulation,  $K = 0$ ).

In case A) Equation (13) reduces to the expression

$$\begin{aligned}
z(t_a + t_b) &= \frac{A^2}{2t_a t_b} \frac{\sigma_c}{\sigma_F} \\
& + \frac{A}{2t_a} \frac{\sigma_c}{\sigma_F} \sum_j \frac{a_j}{t_j} \exp\left[-\frac{K^2 \sigma_c^2}{4} (t_b - T_j)^2\right] \cos\left\{(T_j - t_b) \left[\omega_0 + \frac{K}{2} \frac{\sigma_c^2}{\sigma_F} (t_b - T_j)\right]\right\} \\
& + \frac{A}{2t_b} \frac{\sigma_c}{\sigma_F} \sum_i \frac{a_i}{t_i} \exp\left[-\frac{K^2 \sigma_c^2}{4} (t_i - t_a)^2\right] \cos\left\{(t_a - t_i) \left[\omega_0 + \frac{K}{2} \frac{\sigma_c^2}{\sigma_F} (t_a - t_i)\right]\right\} \\
& + \frac{\sigma_c}{2\sigma_F} \sum_i \sum_j \frac{a_i a_j}{t_i t_j} \exp\left[-\frac{K^2 \sigma_c^2}{4} (t_i - t_a - (T_j - t_b))^2\right] \exp\left[-\frac{[(t_i - t_a) + (T_j - t_b)]^2}{4(\sigma_F^2 + \sigma_T^2/2)}\right]
\end{aligned}$$



$$\cdot \cos \left\{ \left[ (t_i - t_a) - (T_j - t_b) \right] \left[ \omega_0 + \frac{K}{2} \frac{\sigma_c^2}{\sigma_F^2} (t_a - t_i + t_b - T_j) \right] \right\} \quad (14)$$

The equivalent expression for case B) is

$$\begin{aligned} z(t_a + t_b) &= \frac{A^2}{2t_a^2 t_b^2} \frac{\sigma_c}{\sigma_F} + \frac{A}{2t_a^2} \frac{\sigma_c}{\sigma_F} \sum_j \frac{a_j}{T_j^2} \exp \left[ -\frac{(t_b - T_j)^2}{2\sigma_e^2} \right] \cos (T_j - t_b) \omega_0 \\ &+ \frac{A}{2t_b^2} \frac{\sigma_c}{\sigma_F} \sum_i \frac{a_i}{t_i^2} \exp \left[ -\frac{(t_i - t_a)^2}{2\sigma_e^2} \right] \cos (t_i - t_a) \omega_0 \\ &+ \frac{\sigma_c}{2\sigma_F} \sum_i \sum_j \frac{a_i a_j}{t_i^2 T_j^2} \exp \left\{ -\frac{[(t_i - t_a) - (T_j - t_b)]^2}{2\sigma_T^2} \right\} \exp \left\{ -\frac{[(t_i - t_a) + (T_j - t_b)]^2}{4(\sigma_F^2 + \sigma_T^2/2)} \right\} \\ &\cdot \cos \left\{ [(t_i - t_a) - (T_j - t_b)] \omega_0 \right\} \end{aligned} \quad (15)$$

$$\text{where } \sigma_e^2 = \frac{\sigma_T^2 (\sigma_F^2 + \sigma_T^2/2)}{\sigma_F^2 + \sigma_T^2} \quad (16)$$

The first term in each of the two equations [(14) and (15)] is the signal component, the next two terms are due to the intermodulation of signal from one receiver and reverberation from the other, while the last term results from the intermodulation of the reverberation components.

Several qualitative conclusions concerning detector performance can be drawn immediately from inspection of Equations (14) and (15):

- 1) If the signal is strong compared with the reverberation, the noise consists primarily of intermodulation products of signal with reverberation, and the last noise term can be omitted.
- 2) If the signal is weak compared to the reverberation, the dominant noise term is the last.
- 3) A coherent detector cross-correlates the output as a single receiver

against a properly delayed replica of the transmitted signal. Its output therefore consists of the first two terms of Equation (14) or (15). It follows that the instrumentation of Figure 1 behaves essentially as a coherent detector when the signal to noise ratio is high.<sup>1</sup> When the signal to noise ratio is low, its performance is quite different and will be seen later to approximate more nearly that of an incoherent (power) detector.

- 4) The intermodulation products of signal and reverberation are effectively range gated. In Equation (14) only scatterers located at a range differing from that of the target by no more than about  $\frac{c}{K\sigma_c}$  contribute to the reverberation<sup>2</sup>. For  $K\sigma_c = 2\pi \times 50$  (about 100 cps transmitted bandwidth) this corresponds to a range variation of about 16 feet. In Equation (15) scatterers may deviate in range from the target by roughly  $\frac{1}{\sqrt{2}} \sigma_e c$ . With a transmitted pulse of 0.5 sec duration, this corresponds to a range variation of about 145 feet.
- 5) A somewhat more complicated range gating effect is present in the terms resulting from intermodulation of reverberation with reverberation. According to Equation (14) significant contributions to the last term arise only when the following two inequalities are satisfied.

---

<sup>1</sup>It will be shown later that the cross-correlation between the second and third terms of Equations (14) and (15) is small under most conditions of practical interest. Hence, under conditions of high signal to noise ratio, the instrumentation of Figure 1 may be replaced conceptually by a coherent detector operating in a background of reverberation with twice the actual power.

<sup>2</sup>Note that  $t_i$  is round trip time to scatterer  $i$ . Hence a range increment of  $s$  feet changes  $t_i$  by  $\frac{2s}{c}$  seconds.

$$|(t_i - t_a) - (T_j - t_b)| < \frac{2}{K\sigma_c} \quad (17)$$

$$|(t_i - t_a) + (T_j - t_b)| < 2\sqrt{\sigma_F^2 + \frac{\sigma_T^2}{2}} \quad (18)$$

The spatial region to which these relations restrict the location of contributing scatterer pairs is indicated by the crosshatched region of

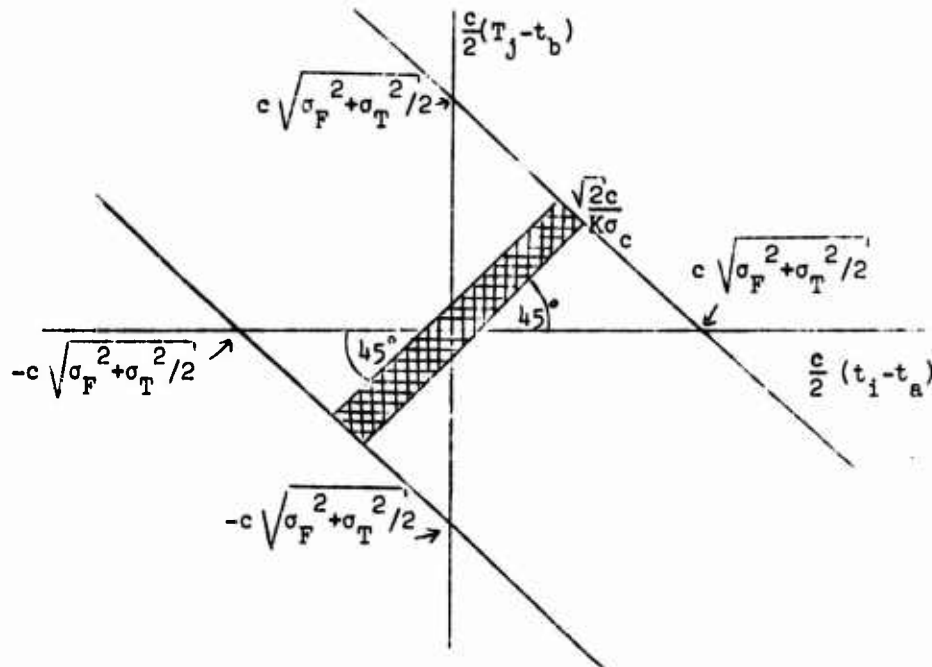


Figure 2

Figure 2. Note that the constraint is one on range only. Scatterer pairs having the proper range relation contribute reverberation regardless of their relative bearing.<sup>1</sup> The origin of Figure 2 denotes a scatterer pair such that scatterer i is located at the same range as the target relative to receiver a while scatterer j is located at the same range as the target relative to receiver b. The total range variation allowed by the crosshatched area is

<sup>1</sup>If they are simultaneously illuminated by the transmitting beam. The beam parameters are introduced later by assigning angular dependence to  $a_i$  and  $A$ .

clearly of the order of  $\sqrt{2} c \sqrt{\sigma_F^2 + \sigma_T^2} / 2$ . However any given intermodulating pair can have a range differential no greater than  $c/K\sigma_c$ .

In the absence of frequency modulation [Equation (15)], the equivalent of Equations (17) and (18) is

$$|(t_i - t_a) - (T_j - t_b)| < \sqrt{2}\sigma_T \quad (19)$$

$$\text{and} \quad |(t_i - t_a) + (T_j - t_b)| < 2 \sqrt{\sigma_F^2 + \sigma_T^2} / 2 \quad (20)$$

The region of contributing scatterer pairs is shown in Figure 3.

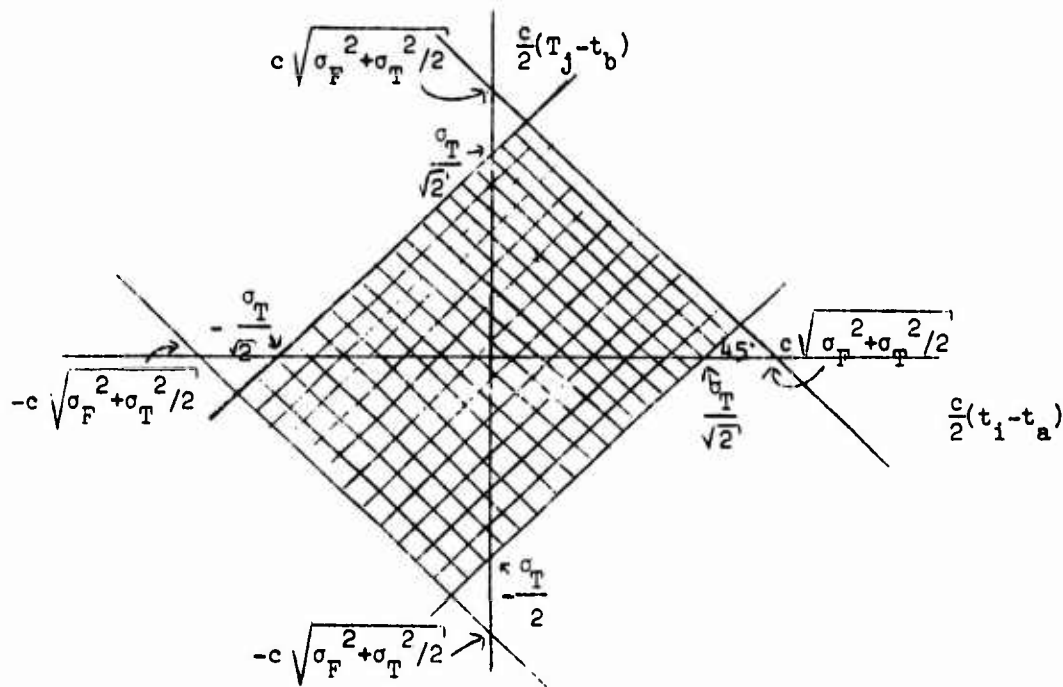


Figure 3

6) An interesting special case of 5) [intermodulation of reverberation with reverberation] arises when  $i=j$ . This means that the returns from a particular scatterer to receivers a and b are intermodulating with each other. If a total of  $N$  scatterers is illuminated, the number of terms of this form is  $N$  whereas the number of modulation products of different scatterers is  $N^2 - N$ . For large  $N$  the latter predominate and the former are of practical

interest only if the return from one or more scatterers is particularly large. In other words, the case  $i=j$  is essentially that of false targets. For  $i \neq j$  Equation (17) can now be decomposed into the two expressions

$$t_1 - T_1 < \frac{2}{K\sigma_c} + (t_a - t_b) \quad (21)$$

$$T_1 - t_1 < \frac{2}{K\sigma_c} - (t_a - t_b) \quad (22)$$

Similarly Equation (18) can be rewritten as follows

$$t_1 + T_1 < (t_a + t_b) + 2\sqrt{\sigma_F^2 + \sigma_T^2}/2 \quad (23)$$

$$t_1 + T_1 > (t_a + t_b) - 2\sqrt{\sigma_F^2 + \sigma_T^2}/2 \quad (24)$$

$ct_1$  is the distance from transmitter to receiver a via the  $i^{\text{th}}$  scatterer and  $cT_1$  is the distance from transmitter to receiver b via scatterer 1. It follows that Equations (21) and (22) define a pair of hyperbolas and Equations (23) and (24) a pair of ellipses between which false targets must lie if they are to be a significant source of confusion. These constraints on false target locations are illustrated in Figure 4.

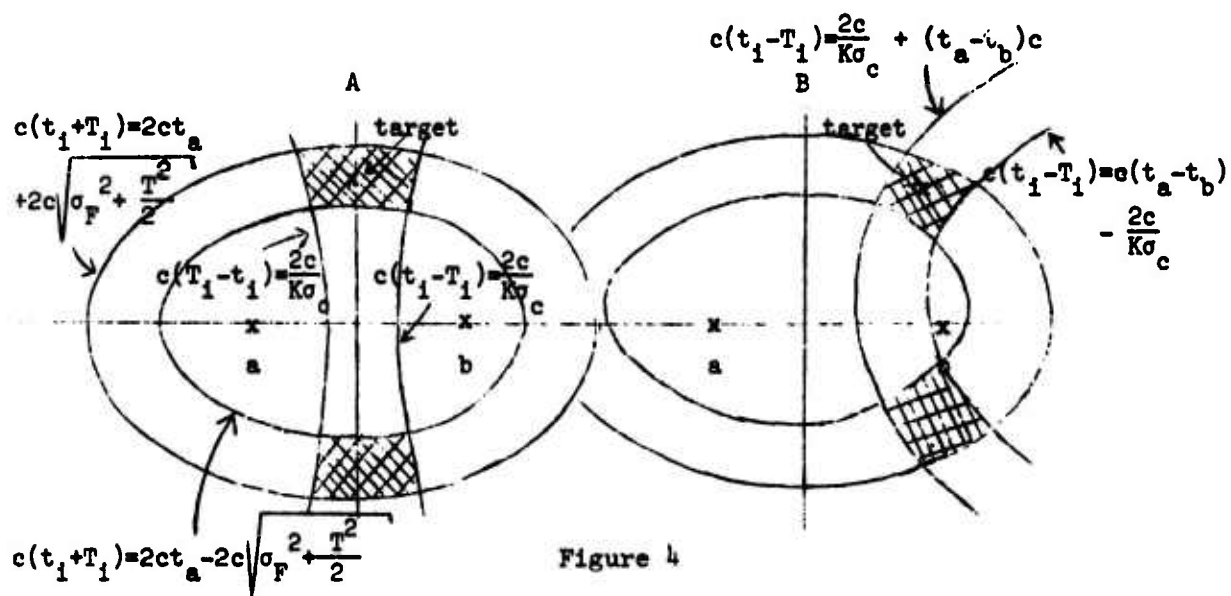


Figure 4

Figure 4A is based on the assumption  $t_a = t_b$  (target broadside), while Figure 4B shows the case  $t_a - t_b > \frac{2}{K\sigma_c}$  (target significantly clockwise from broadside). In each case the region from which false target returns may originate (crosshatched area) is a pair of small curvilinear squares centered at the target location. Thus, as far as false targets are concerned, the postulated instrumentation introduces not only a range gating effect but also a gate in azimuth and elevation.<sup>1</sup> In practice the situation is actually likely to be simpler than suggested by Figure 4, because the target is almost certain to be at a range which is large compared with the spacing between receivers a and b. In that case the ellipses and hyperbolas degenerate into circles and radial straight lines respectively, as indicated in Figure 5. It is now a simple matter of analytic geometry to determine

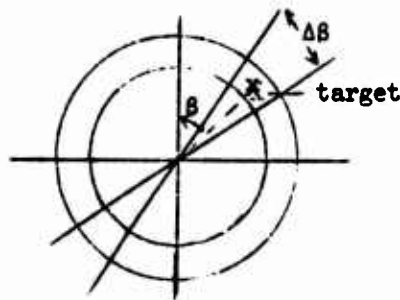


Figure 5

the angular spread ( $\Delta\beta$ ) which might contribute a false target return. With a true target broadside ( $\beta=0$ ) one obtains

$$\Delta\beta = \begin{cases} 2 \sin^{-1} \frac{c/(K\sigma_c)}{d} & \text{for } \frac{c}{K\sigma_c} \leq d \\ \pi & \text{for } \frac{c}{K\sigma_c} > d \end{cases} \quad (25)$$

If  $\frac{c/(K\sigma_c)}{d} \ll 1$

i.e. if the correlation distance of the transmitted signal in the water is much smaller than the spacing between receivers, Equation (25) reduces to

$$\Delta\beta \approx 2 \frac{c/(K\sigma_c)}{d} \text{ radians} \quad (26)$$

With  $c/K\sigma_c = 16$  feet (as postulated before) and  $d = 160$  feet, this leads to an effective aperture  $\Delta\beta \approx 0.2$  radians. Another way of stating this

---

<sup>1</sup>The significant region of false target locations in 3 dimensional space is, of course, the solid of revolution generated by rotating the crosshatched areas about the axis (a,b).

result is that the postulated instrumentation is capable (regardless of beam pattern considerations) of resolving two targets separated in angle by about 0.1 radians. An expression equivalent to Equation (25) for  $\beta \neq 0$

assumes the form

$$\Delta\beta = \sin^{-1}\left|\frac{c/K\sigma}{d} + \sin\beta\right| + \sin^{-1}\left|\frac{c/K\sigma}{d} - \sin\beta\right| \quad (27)$$

where each arc sine is interpreted as  $\pi/2$  when its argument exceeds unity.

## II. Probability Density of Scatterer Location

The detector output  $z(t_a + t_D)$  as described by Equations (14) or (15) is a random variable whose properties are dependent on scatterer location to the extent that scatterer position influences  $t_i$  and  $T_j$ . In order to describe the statistical properties of  $z(t_a + t_D)$  it is therefore necessary to postulate a statistical model of scatterer distribution and to express the properties of  $t_i$  and  $T_j$  in terms of appropriate parameters of this model.

There are two major sources of reverberation

- 1) Scatterering centers distributed throughout the volume of water traversed by the signal (volume reverberation).
- 2) Scatterering centers near the ocean surface or bottom (surface or bottom reverberation).

For the purposes of this report the simplest possible assumptions will be made concerning the distribution of each type of scatterer.

1) Volume reverberation. Consider a large volume  $V$  of ocean surrounding the source and including all of (but encompassing much more than) the volume illuminated by the source. The location of the  $i^{\text{th}}$  scatterer will be taken as a random variable uniformly distributed over  $V$  and independent of the location of any other scatterer. Thus the number  $N$  of scatterers in  $V$  has a Poisson distribution. Each scatterer is assumed to be stationary while illuminated by the transmitted pulse. The scatterer distribution

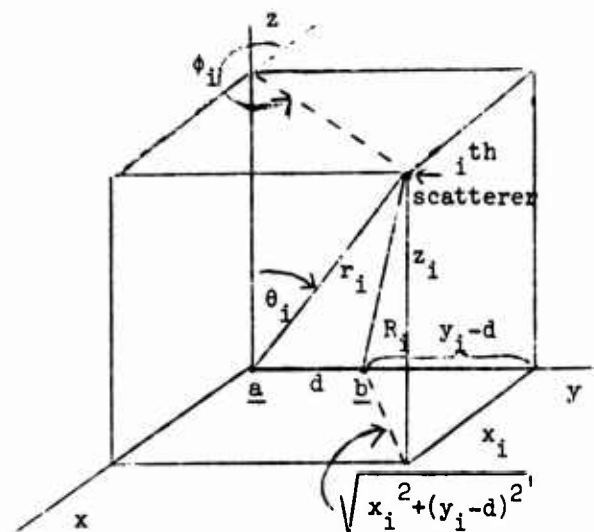


Figure 6

is described most simply in terms of a rectangular coordinate system. Consider such a system set up with origin at receiver a and receiver b located on the y axis as shown in Figure 6. The probability that the  $i^{th}$  scatterer lies in  $[(x_i, y_i, z_i), (x_i + dx, y_i + dy, z_i + dz)]$  is clearly  $(1/V)(dx dy dz)$ . Transforming

this result into a spherical coordinate system centered at receiver a as indicated in Figure 6, one obtains

$$\Pr \{i^{th} \text{ scatterer in } (r_i, \theta_i, \phi_i), (r_i + dr, \theta_i + d\theta, \phi_i + d\phi)\} = \frac{1}{V} r_i^2 \sin \theta_i dr d\theta d\phi \quad (28)$$

Hence the probability density of the  $i^{th}$  scatterer location in spherical coordinates is

$$p(r_i, \theta_i, \phi_i) = \begin{cases} \frac{1}{V} r_i^2 \sin \theta_i & \text{in } V \\ 0 & \text{elsewhere} \end{cases} \quad (29)$$

If, as a matter of computational convenience (and without influencing the results in any significant way), one assumes that the transmitter is located close to receiver a, then

$$t_i = \frac{2}{c} r_i \quad (30)$$

Hence the joint probability density of  $t_i, \theta_i$  and  $\phi_i$  is

$$p(t_i, \theta_i, \phi_i) = \begin{cases} \frac{3}{8V} t_i^2 \sin \theta_i & \text{in } \bar{X} \\ 0 & \text{elsewhere} \end{cases} \quad (31)$$

where  $\bar{X}$  is the space equivalent of  $V$  under the transformation (30).

2) Surface reverberation. The scatterers are now distributed in the



immediate vicinity of a plane (the average surface or bottom) which will be taken as parallel to the xy plane of Figure 6. If Q is an area on the surface much larger than that illuminated by the beam and if one assumes uniform and independent distribution of scatterers in the x and y directions one can write

$$\text{Pr } \{i^{\text{th}} \text{ scatterers in } (x_i, y_i, z_i), (x_i+dx_i, y_i+dy_i, z_i+dz_i)\} = \frac{1}{Q} \frac{1}{\sqrt{2\pi}\Delta} \exp\left[-\frac{(z_i-D)^2}{2\Delta^2}\right] \cdot dx_i dy_i dz_i \quad (32)$$

D is the depth of the array relative to the average surface and  $\Delta$  is the vertical rms spread of scatterer locations. The Gaussian distribution in z is of course an arbitrary model. Variations in the parameter  $\Delta$  can be used to introduce some of the effects of surface roughness. Since scatterer location enters the expression for the received signal only via the time delays  $t_i$  and  $T_j$ , it is clear that vertical spreads  $\Delta$  small compared with the effective illuminated area have little effect on the return signal. The z distribution then degenerates effectively into a delta function at  $z=D$ . This simplification will be introduced at an appropriate point later in the analysis. It should also be pointed out that the primitive model of reverberation used in this report ignores the time dependence of scatterer locations.

Transformation into spherical coordinates converts Equation (32) into the expression

$$p(r_i, \theta_i, \phi_i) = \begin{cases} \frac{1}{Q} \frac{1}{\sqrt{2\pi}\Delta} \exp\left[-\frac{(r_i \cos\theta_i - D)^2}{2\Delta^2}\right] r_i^2 \sin\theta_i & \text{in } Q \\ 0 & \text{elsewhere} \end{cases} \quad (33)$$

which is the equivalent of Equation (29) for surface reverberation. Finally the transformation (30) yields

$$p(t_i, \theta_i, \phi_i) = \begin{cases} \frac{c^3}{8Q} \frac{1}{\sqrt{2\pi\Delta}} \exp \left[ -\frac{\frac{c}{2} t_i \cos \theta_i - D)^2}{2\Delta^2} \right] t_i^2 \sin \theta_i & \text{in } \bar{Y} \\ 0 & \text{elsewhere} \end{cases} \quad (34)$$

where  $\bar{Y}$  is the space equivalent to  $Q$  under the transformation (30).

The joint distribution of  $t_i, \theta_i$ , and  $\phi_i$  is sufficient for the computation of all reverberation statistics because the random variable  $T_i$  can be expressed in terms of  $t_i, \theta_i$ , and  $\phi_i$  by simple geometrical reasoning. From

Figure 6

$$R_i = \sqrt{x_i^2 + z_i^2 + (y_i - d)^2} = \sqrt{x_i^2 + y_i^2 + z_i^2} \sqrt{1 - \frac{2dy_i - d^2}{x_i^2 + y_i^2 + z_i^2}} \approx r_i - \frac{dy_i - d^2/2}{r_i} \quad (35)$$

where use has been made of the assumption  $d \ll r_i$ . In view of the fact that the only scatterers contributing to the reverberation are located at approximately the same range as the target, this assumption should not introduce any significant error.

Omitting  $d^2/(2r_i)$  as negligible compared with  $r_i$  and transforming to spherical coordinates, one obtains

$$R_i = r_i + d \sin \theta_i \sin \phi_i \quad (36)$$

The travel time of sound from the  $i^{\text{th}}$  scatterer to receivers a and b is  $r_i/c$  and  $R_i/c$  respectively. Thus, assuming the source to be located near receiver a

$$T_i = t_i + \frac{d}{c} \sin \theta_i \sin \phi_i \quad (37)$$

### III. Average Detector Output

The DC output of the detector is the expected value of Equations (14) or (15). In each case it consists of a signal component

$$E\{z(t_a + t_D)\} |_{\text{signal}} = \frac{A^2}{2t_a^2 t_b^2} \frac{\sigma_c}{\sigma_F} \quad (38)$$

and a noise component. The second and third terms of Equations (14) and (15) make no significant contributions to the average, because  $\omega_0 \gg K\sigma_c \gg \frac{1}{\sigma_e}$  so that one can invoke the Riemann-Lebesgue lemma. For the same reason all terms of the double sum for which  $i \neq j$  can be ignored. Thus for case A) [bandwidth determined by frequency modulation]

$$E\{z(t_a + t_D)\}_{\text{noise}} = \frac{\sigma_c}{2\sigma_F} \sum_i E \left\{ \left[ \frac{a_i^2}{2T_i^2} \exp \left\{ -\frac{K^2 \sigma_c^2}{4} [(t_i - t_a) - (T_i - t_b)]^2 \right\} \right. \right. \\ \left. \left. \exp \left\{ -\frac{[(t_i - t_a) + (T_i - t_b)]^2}{4(\sigma_F^2 + \sigma_T^2)} \right\} \cos \left\{ [ (t_i - t_a) - (T_i - t_b) ] \left[ \omega_0 + \frac{K}{2} \frac{\sigma_c^2}{\sigma_F^2} (t_a - t_i + t_b - T_i) \right] \right\} \right] \right\} \quad (39)$$

$T_i$  is now expressed in terms of  $t_i$ ,  $\theta_i$ , and  $\phi_i$  by use of Equation (37). Similarly  $t_b$  can be written as

$$t_b = t_a + \frac{d}{c} \sin \theta_0 \sin \phi_0 \quad (40)$$

where  $\phi_0$  and  $\theta_0$  measure target bearing and elevation respectively. For volume reverberation the relevant probability distribution is given by Equation (31). Substituting Equations (31), (37), and (40) into Equation (39) one obtains an expression which must be integrated over the variables  $t_i$ ,  $\phi_i$ , and  $\theta_i$ . The result of the  $t_i$  integration is (after considerable algebraic manipulation)

$$\int_{-\infty}^{\infty} z(t_a + t_D)_{\text{noise}} p(t_i, \theta_i, \phi_i) dt_i = \sqrt{\pi(\sigma_F^2 + \frac{\sigma_T^2}{2})} \frac{\sigma_c}{2\sigma_F} \sum_i \frac{c^3}{8V} \sin \theta_i \frac{a_i^2}{t_a^2} \\ \exp \left\{ -(\sin \theta_0 \sin \phi_0 - \sin \theta_i \sin \phi_i)^2 \frac{K^2 \sigma_c^2 d^2}{8c^2} \right\} \cos \left[ \frac{d\omega_0}{c} (\sin \theta_0 \sin \phi_0 - \sin \theta_i \sin \phi_i) \right] \quad (41)^1$$

<sup>1</sup>The second exponential in Equation (39) differs significantly from zero only over an interval roughly equal to the pulse length, centered at  $2t_a$ . Hence the limit of integration can be taken as  $(-\infty, \infty)$  and  $a_i^2/T_i^2$  can be replaced by  $a_i^2/t_a^2$  without introducing appreciable error.

Before the  $\phi_i$  and  $\theta_i$  integrations can be performed, it is necessary to recall that the coefficient  $a_i$  determines the power returned from the  $i^{\text{th}}$  scatterer.  $a_i$  is therefore dependent on the beam pattern of the transmitter and receiver. This relationship is now made explicit by the following expression

$$a_i^2 = \frac{b_i^2}{\sin^2 \theta_i} \exp \left[ -\frac{(\theta_i - \theta_0)^2}{B_\theta^2} \right] \exp \left[ -\frac{(\phi_i - \phi_0)^2}{B_\phi^2} \right] \quad (42)^1$$

$B_\theta$  and  $B_\phi$  measure the pattern width in the  $\theta$  and  $\phi$  direction respectively while  $b_i$  is the scattering cross-section of the  $i^{\text{th}}$  scatterer. Equation (42) assumes that the beam pattern is centered at the target.<sup>2</sup>

If the beam dimensions  $B_\theta$  and  $B_\phi$  are small compared to one radian, one can approximate the sinusoidal functions in Equation (41) by the linear term of the Taylor Series expansion.

$$\sin \theta_i \sin \phi_i \approx \sin \theta_0 \sin \phi_0 + \cos \theta_0 \sin \phi_0 (\theta_i - \theta_0) + \sin \theta_0 \cos \phi_0 (\phi_i - \phi_0). \quad (43)$$

The averaging operation in  $\theta_i$  extends over  $(0, \pi)$  while that in  $\phi_i$  covers a full two radians. The narrow beam patterns already postulated enable one to extend the limits of integration to  $(-\infty, \infty)$  except for values of  $\theta_0$  near 0 and  $\pi$  (straight up and straight down). Since these particular directions are of little practical interest, the complications arising near  $\theta_0 = 0$  or  $\pi$  will be ignored.

---

<sup>1</sup>The factor  $\sin \theta_i$  in the denominator reflects the fact that the  $\phi$  dimension of a fixed element of area varies inversely with  $\sin \theta$ . Hence for large  $B_\theta$  and  $B_\phi$  Equation (42) corresponds to uniform illumination on any sphere about the transmitter.

<sup>2</sup>If one thinks of a transmitter operating under an average power constraint, it might be reasonable to postulate that the total radiated power is fixed so that the target power would vary inversely as  $B_\theta B_\phi$ . Such an assumption is easily incorporated into the analysis by dividing the right side of Equation (42) by  $B_\theta B_\phi$ . As it stands Equation (42) implies that the power returned from the target is independent of  $B_\theta$  and  $B_\phi$ .

The actual integrations are tedious but quite straightforward. The result, after extensive algebraic simplification, is

$$\int_{-\infty}^{\infty} dt_i \int_0^{\pi} d\theta_i \int_{-\pi}^{\pi} d\phi_i \quad \underset{\text{noise}}{z(t_a + t_D)} \quad p(t_i, \theta_i, \phi_i) = \sqrt{\pi(\sigma_F^2 + \frac{\sigma_T^2}{2})} \frac{\sigma_c}{2\sigma_F} \frac{c^3}{8V} \left( \sum_{i=1}^N \frac{b_i^2}{t_a^2} \right) \cdot \frac{\pi B_{\theta} B_{\phi}}{\sqrt{1 + \frac{K^2 \sigma_T^2 d^2 \rho^2}{8c^2}}} \exp \left\{ - \frac{d^2 \omega_o^2}{4c^2} \frac{\rho^2}{1 + \frac{K^2 \sigma_T^2 d^2 \rho^2}{8c^2}} \right\} \quad (44)$$

$$\text{where} \quad \rho^2 = B_{\phi}^2 \sin^2 \theta_o \cos^2 \phi_o + B_{\theta}^2 \cos^2 \theta_o \sin^2 \phi_o. \quad (45)$$

Equation (44) contains two random variables, the scatterer cross section  $b_i^2$  and N, the number of scatterers in the volume V. Designating the average scatterer cross section as  $\langle b^2 \rangle$  and postulating an average of K scatterers per unit volume the expected value of the detector output noise becomes finally

$$E\{z(t_a + t_D)\} \underset{\text{noise}}{=} \sqrt{\frac{\pi(\sigma_F^2 + \sigma_T^2/2)}{t_a^2}} \frac{\sigma_c}{2\sigma_F} \langle b^2 \rangle \frac{K_V c^3}{8} \frac{\pi B_{\theta} B_{\phi}}{\sqrt{1 + \frac{K^2 \sigma_T^2 d^2 \rho^2}{8c^2}}} \cdot \exp \left\{ - \frac{d^2 \omega_o^2}{4c^2} \frac{\rho^2}{1 + \frac{K^2 \sigma_T^2 d^2 \rho^2}{8c^2}} \right\} \quad (46)$$

If  $(K^2 \sigma_T^2 d^2 \rho^2)/(8c^2) \gg 1$  the argument of the exponential function

becomes  $-\frac{2\omega_o^2}{K^2 \sigma_T^2} = -2 \frac{\text{carrier frequency}}{\text{transmitted bandwidth}}$ . The magnitude of this ratio

is almost certain to be large compared to unity so that the DC output due to noise is negligible. If  $(K^2 \sigma_T^2 d^2 \rho^2)/(8c^2) \ll 1$  the argument of the

exponential becomes  $-\frac{d^2 \omega_o^2 \rho^2}{4c^2}$ . For  $d=100$  ft.,  $\omega_o = 2\pi \times 3500$  rad/sec, and  $c = 5000$  ft/sec,  $d^2 \omega_o^2 / 4c^2 = (70\pi)^2$ . Hence the exponential is of an order no larger than  $e^{-10}$  for  $\rho^2 \geq 0.0002$ . Small values of  $\rho$  occur near  $\theta_o = 0$ ,  $\phi_o = 0$ , and  $\theta_o = \pm \frac{\pi}{2}$ ,  $\phi_o = \pm \frac{\pi}{2}$ . Only the latter combination is of practical interest. Postulating  $B_\phi = B_\theta = 0.1$  and working with the extreme case,  $\theta_o = \frac{\pi}{2}$ , one concludes that the average noise output is very small unless the system is trained on a target no more than  $8^\circ$  from the endfire direction. The appearance of a DC component of noise near the endfire direction is reasonable, for in that condition the difference in signal travel time to the two receivers is very nearly the same for any point in the illuminated volume. In other words, because of poor directivity near endfire, the detector is unable to distinguish between a point target and a volumetric distribution of scatterers. In effect it reports the accumulated return from all those scatterers which it is unable to resolve as an equivalent target.<sup>1</sup>

The derivation of the average noise output in the absence of frequency modulation (case B) follows the same pattern and leads to the result

$$E(z(t_n + t_D))|_{\text{noise}} = \frac{\sqrt{\pi(\sigma_F^2 + \sigma_T^2/2)}}{t_n^2} \frac{\sigma_c}{2\sigma_F} \langle b^2 \rangle \frac{K_V c^3}{8} \frac{\pi B_\theta B_\phi}{\sqrt{1 + \frac{d^2 \rho^2}{2c^2 \sigma_T^2}}} \exp \left\{ -\frac{d^2 \omega_o^2}{4c^2} \frac{\rho^2}{1 + \frac{d^2 \rho^2}{2c^2 \sigma_T^2}} \right\} \quad (47)$$

When  $(d^2 \rho^2) / (2c^2 \sigma_T^2) \ll 1$  the exponent reduces to  $-(d^2 \omega_o^2 \rho^2) / (4c^2)$  as

<sup>1</sup>Caution is in order in any quantitative use of Equation (46) very close to the endfire direction, for the use of only linear terms in Equation (43) becomes inappropriate for  $\theta_o$  and  $\phi_o$  within  $B_\phi$  and  $B_\theta$  of  $(\theta_o = \frac{\pi}{2}, \phi_o = \frac{\pi}{2})$ . Higher order terms must be included if quantitatively accurate results are desired.

under the equivalent approximation on Equation (46) so that the previous comments concerning DC noise output near the endfire condition remain applicable.

Equivalent results for surface reverberation could be obtained by using the distribution of Equation (34) in place of Equation (31). The computation is quite tedious and was judged to be of limited interest in view of the anticipated negligible value in all but the extreme endfire direction.

#### IV. Detector Output Variance

In order to evaluate the performance of the detector, it is necessary to compute the output fluctuation as well as the average output. Since the signal component of Equations (14) and (15) is a constant, the fluctuation is entirely due to the noise. For the frequency modulated case [case (A)] one obtains from Equation (14)

$$\begin{aligned}
 z^2(t_a + t_D) \Big|_{\text{noise}} &= \frac{A^2}{4t_a} \frac{\sigma_c^2}{\sigma_F^2} \sum_j \sum_{j', T_j} \frac{a_j a_{j'}}{t_j^2 T_j^2} \exp \left\{ -\frac{K^2 \sigma_c^2}{4} [(t_b - T_j)^2 + (t_b - t_{j'})^2] \right\} \\
 &\quad \cdot \cos \left\{ (T_j - t_b) \left[ \omega_o + \frac{K}{2} \frac{\sigma_c^2}{\sigma_F^2} (t_b - T_j) \right] \right\} \cos \left\{ (T_j - t_b) \left[ \omega_o + \frac{K}{2} \frac{\sigma_c^2}{\sigma_F^2} (t_b - T_{j'}) \right] \right\} \quad (1) \\
 &+ \frac{A^2}{4t_b} \frac{\sigma_c^2}{\sigma_F^2} \sum_i \sum_{i'} \frac{a_i a_{i'}}{t_i^2 t_{i'}^2} \exp \left\{ -\frac{K^2 \sigma_c^2}{4} [(t_i - t_a)^2 + (t_i - t_{a'})^2] \right\} \\
 &\quad \cdot \cos \left\{ (t_a - t_i) \left[ \omega_o + \frac{K}{2} \frac{\sigma_c^2}{\sigma_F^2} (t_a - t_i) \right] \right\} \cos \left\{ (t_a - t_{i'}) \left[ \omega_o + \frac{K}{2} \frac{\sigma_c^2}{\sigma_F^2} (t_a - t_{i'}) \right] \right\} \quad (2) \\
 &+ \frac{\sigma_c^2}{4\sigma_F^2} \sum_i \sum_{i'} \sum_j \sum_{j'} \frac{a_i a_{i'} a_j a_{j'}}{t_i^2 t_{i'}^2 T_j^2 T_{j'}^2} \exp \left[ -\frac{K^2 \sigma_c^2}{4} \left\{ [(t_i - t_a) - (T_j - t_b)]^2 + [(t_{i'} - t_a) - (T_{j'} - t_b)]^2 \right\} \right]
 \end{aligned}$$

$$\begin{aligned}
& \cdot \exp \left\{ - \frac{(t_1 + T_j - t_a - t_b)^2 + (t_1 + T_j, -t_a - t_b)^2}{4(\sigma_F^2 + \sigma_T^2/2)} \right\} \cos \left\{ [(t_1 + T_j) - (T_j - t_b)] [\omega_0 + \frac{K}{2} \frac{\sigma_c^2}{\sigma_F^2} (t_a - t_1 + t_b - T_j)] \right\} \quad (3) \\
& \cdot \cos \left\{ [(t_1, -t_a) - (T_j, -t_b)] [\omega_0 + \frac{K}{2} \frac{\sigma_c^2}{\sigma_F^2} (t_a - t_1 + t_b - T_j)] \right\} \\
& + \frac{A^2}{2t_a^2 t_b^2} \frac{\sigma_c^2}{\sigma_F^2} \sum_i \sum_j \frac{a_i a_j}{t_i^2 T_j^2} \exp \left\{ - \frac{K^2 \sigma_c^2}{4} [(t_b - T_j)^2 + (t_1 - t_a)^2] \right\} \quad (4) \\
& \cdot \cos \left\{ (T_j - t_b) [\omega_0 + \frac{K}{2} \frac{\sigma_c^2}{\sigma_F^2} (t_b - T_j)] \right\} \cos \left\{ (t_a - t_1) [\omega_0 + \frac{K}{2} \frac{\sigma_c^2}{\sigma_F^2} (t_a - t_1)] \right\} \\
& + \frac{A^2}{2t_a^2} \frac{\sigma_c^2}{\sigma_F^2} \sum_i \sum_j \sum_{j'} \frac{a_i a_j a_{j'}}{t_i^2 T_j^2 T_{j'}^2} \exp \left[ - \frac{K^2 \sigma_c^2}{4} \left\{ [(t_1 - t_a) - (T_j - t_b)]^2 - (t_b - T_{j'})^2 \right\} \right] \quad (5) \\
& \cdot \exp \left\{ - \frac{(t_1 + T_j - t_a - t_b)^2}{4(\sigma_F^2 + \sigma_T^2/2)} \right\} \cos \left\{ [(t_1 - t_a) - (T_j - t_b)] [\omega_0 + \frac{K}{2} \frac{\sigma_c^2}{\sigma_F^2} (t_a - t_1 - T_j + t_b)] \right\} \\
& \cdot \cos \left\{ (T_j, -t_b) [\omega_0 + \frac{K}{2} \frac{\sigma_c^2}{\sigma_F^2} (t_b - T_j)] \right\} \\
& + \frac{A^2}{2t_b^2} \frac{\sigma_c^2}{\sigma_F^2} \sum_i \sum_j \sum_{i'} \frac{a_i a_j a_{i'}}{t_i^2 T_j^2 t_{i'}^2} \exp \left[ - \frac{K^2 \sigma_c^2}{4} \left\{ [(t_1 - t_a) - (T_j - t_b)]^2 + (t_1 - t_a)^2 \right\} \right] \quad (6) \\
& \cdot \exp \left\{ - \frac{(t_1 + T_j - t_a - t_b)^2}{4(\sigma_F^2 + \sigma_T^2/2)} \right\} \cos \left\{ [(t_1 - t_a) - (T_j - t_b)] [\omega_0 + \frac{K}{2} \frac{\sigma_c^2}{\sigma_F^2} (t_a - t_1 - T_j + t_b)] \right\} \\
& \cdot \cos \left\{ (t_a - t_1) [\omega_0 + \frac{K}{2} \frac{\sigma_c^2}{\sigma_F^2} (t_a - t_1)] \right\} \cdot
\end{aligned}$$

(48)



Because of the odd number of indices involved in terms ⑤ and ⑥ one can immediately invoke the Riemann-Lebesgue lemma and assert that these terms make no significant contribution to the mean square value. Similar considerations lead to the conclusion that contributions from other terms arise only for the following combinations of indices.

term ①:  $j=j'$

term ②:  $i=i'$

term ③:  $i=i', j=j', i \neq j$

$i=j, i'=j', i \neq i'$

$i=j', j=i', i \neq j$

$i=i', j=j'$

term ④:  $i=j$

The actual performance of the averaging operations is exceedingly cumbersome but basically straightforward. With approximations similar to those used in Section III one obtains in the case of volume reverberation the following result for the variance of  $z(t_a+t_D)$

$$\begin{aligned}
 D^2\{z(t_a+t_D)\} = & \frac{A^2 \langle b^2 \rangle}{32 t_a^6} \frac{\sigma_c^2}{\sigma_F^2} \frac{\sqrt{2\pi}}{K \sigma_c} \pi B_\phi B_\theta K_V c^3 + \frac{\sigma_c^2}{\sigma_F^2} \frac{c^6}{512} \frac{\langle b^2 \rangle^2}{t_a^4} K_V^2 \pi^3 B_\phi^2 B_\theta^2 \sqrt{\frac{\sigma_F^2 + \sigma_T^2}{2}} \frac{1}{K \sigma_c} \\
 & \cdot \left\{ 1 + \frac{1}{\sqrt{1 + \frac{d^2 \omega_o^2}{4 c^2 \sigma_F^2}}} \sqrt{\frac{1}{K^2 \sigma_c^2 d^2 \rho^2}} \exp \left[ - \frac{d^2 \omega_o^2}{2 c^2} \frac{\rho^2}{1 + \frac{K^2 \sigma_c^2 d^2 \rho^2}{8 c^2}} \right] \right\} \\
 & + \frac{\sigma_c^2}{\sigma_F^2} \frac{\pi}{64} c^3 \frac{\langle b^2 \rangle}{t_a^6} K_V B_\phi B_\theta \sqrt{\frac{\pi}{2} (\sigma_F^2 + \sigma_T^2 / 2)} \sqrt{\frac{1}{K^2 \sigma_c^2 d^2 \rho^2}} \sqrt{1 + \frac{d^2 \omega_o^2}{2 c^2}} \\
 & + \frac{A^2 \langle b^2 \rangle}{32 t_a^6} \frac{\sigma_c^2}{\sigma_F^2} c^3 K_V \pi \frac{\sqrt{2\pi}}{K \sigma_c} B_\phi B_\theta \sqrt{\frac{1}{K^2 \sigma_c^2 d^2 \rho^2}} \exp \left\{ - \frac{d^2 \omega_o^2}{4 c^2} \frac{\rho^2}{1 + \frac{K^2 \sigma_c^2 d^2 \rho^2}{8 c^2}} \right\} \cdot \quad (49)
 \end{aligned}$$

The exponential terms are all similar in form to Equation (46) and are therefore negligible except very near to horizontal and endfire. When they are negligible Equation (49) reduces to

$$\begin{aligned}
 D^2\{z(t_a+t_D)\} &= \frac{A^2 \langle b^2 \rangle}{t_a^6} \frac{c^3}{32} \frac{\sigma_c^2}{\sigma_F^2} \pi B_\phi B_\theta K_V \frac{\sqrt{2\pi}}{K\sigma_c} \\
 &+ \frac{\sigma_c^2}{\sigma_F^2} \frac{c^6}{512} \frac{\langle b^2 \rangle^2}{t_a^4} K_V^2 \pi^3 B_\phi^2 B_\theta^2 \sqrt{\frac{\sigma_F^2 + \sigma_T^2}{2}} \frac{1}{K\sigma_c} \\
 &+ \frac{\sigma_c^2}{\sigma_F^2} \frac{c^3}{64} \frac{\langle b^4 \rangle}{t_a^6} \pi K_V B_\phi B_\theta \sqrt{\frac{\pi}{2} (\sigma_F^2 + \sigma_T^2)} \frac{1}{\sqrt{1 + \frac{K^2 \sigma_c^2 d^2 \rho^2}{8c^2}}} \quad (50)
 \end{aligned}$$

The first term of Equation (50) represents the power of the intermodulation products of signal with the returns from various scatterers [terms ① and ② of Equation (48)]. The second term results from the intermodulation of the returns from different scatterers [term ③,  $i=i', j=j', i \neq j$  in Equation (48)] while the last term gives the total power of intermodulation products from the same scatterer (false target power) [term ③,  $i=j=i'=j'$  in Equation (48)]. The radical in the denominator of the last term reflects the bearing discrimination against false targets discussed qualitatively in Section I. Comparison of the last two terms reveals that the last term is likely to be small compared with the second unless the scatterer density in the illuminated volume is very low (a situation in which the reverberation is composed of returns from a few strong scatterers - which may clearly be regarded as false targets).

In the absence of frequency modulation a completely analogous computation leads to the following equivalent of Equation (50)

$$\begin{aligned}
D^2(z(t_a + t_D)) &= \frac{A^2 \langle b^2 \rangle}{t_a^6} \frac{c^3}{32} \frac{\sigma_c^2}{\sigma_F^2} \pi^{\frac{3}{2}} K_V B_\phi B_\theta \sigma_e \\
&+ \frac{\sigma_c^2}{\sigma_F^2} \frac{c^6 \langle b^2 \rangle^2}{512 t_a^4} \pi^3 K_V B_\phi^2 B_\theta^2 \frac{\sigma_e}{\sqrt{2}} \sqrt{\sigma_F^2 + \sigma_T^2 / 2} \\
&+ \frac{\sigma_c^2}{\sigma_F^2} \frac{c^3 \langle b^4 \rangle}{64 t_a^6} \pi K_V B_\phi B_\theta \sqrt{\frac{\pi}{2} (\sigma_F^2 + \sigma_T^2 / 2)} \frac{1}{\sqrt{1 + \frac{d^2 \sigma_e^2}{c^2 \sigma_F^2}}}
\end{aligned} \tag{51}$$

When the primary noise source is surface reverberation  $p(t_i, \theta_i, \phi_i)$  is given by Equation (34). The averaging operation of Equation (48) with respect to this distribution is basically straightforward but even more cumbersome than the corresponding computation for volume reverberation. It has been carried out only for terms ①, ②, and ③ with  $i=i'$ ,  $j=j'$ ,  $i \neq j$  and under the assumption that the vertical dispersion  $\Delta$  of scatterers satisfies

$$\frac{\Delta / \sin \theta_0}{ct_j / 2} \ll B_\theta \tag{52}$$

Equation (52) demands that  $\Delta / \sin \theta_0$  subtend an angle small compared to  $B_\theta$  at the source [see Figure 7]. The approximation implied by Equation (52)

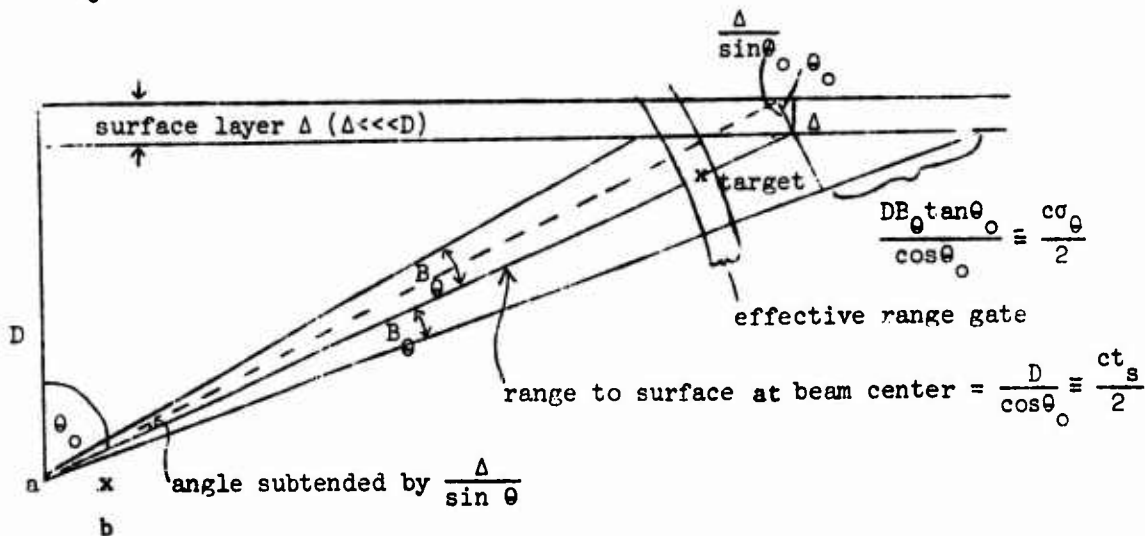


Figure 7

clearly improves with range. For realistic beam widths it should be excellent except at extremely small ranges.

With the stated approximations the averaging operations lead to the following result, equivalent to the first two (generally dominant) terms of Equation (50)

$$D^2\{z(t_a+t_D)\} = \frac{A^2 c^2}{16 t_a^7} \frac{\sigma_c^2}{\sigma_F^2} \frac{\sqrt{2}\pi}{\sin\theta_o} B_\phi \langle b^2 \rangle K_s \frac{1}{K\sigma_c} \exp\left\{-\frac{(t_a-t_s)^2}{\sigma_\theta^2}\right\} \\ + \frac{\pi^2}{\sqrt{2} 128} \frac{c^4}{t_a^6} \frac{\sigma_c^2}{\sigma_F^2} B_\phi^2 \frac{\langle b^2 \rangle^2 K_s^2}{\sin^2\theta_o} \frac{1}{K\sigma_c} \sqrt{\frac{2(\sigma_F^2+\sigma_T^2/2)\sigma_\theta^2}{(\sigma_F^2+\sigma_T^2/2)+\sigma_\theta^2}} \exp\left\{-\frac{(t_a-t_s)^2}{\frac{1}{2}(\sigma_F^2+\sigma_T^2/2+\sigma_\theta^2)}\right\} \quad (53)^1$$

In this equation  $K_s$  is the number of surface scatterers per unit area,

$$t_s = \frac{2D}{c \cos\theta_o} \quad (54)$$

and

$$\sigma_\theta = \frac{2DB_\theta \tan\theta_o}{c \cos\theta_o} \quad (55)$$

Thus  $t_s$  is the signal round trip time between the source and the point on the surface at the center of the beam. Similarly  $\sigma_\theta$  is the differential in round trip time between surface returns from the center of the beam and surface returns from the nominal edge ( $\theta_o+B_\theta$ ) of the beam. [See Figure 7].

The most obvious difference between surface and volume reverberation as expressed by Equations (50) and (53) is the presence of the exponential terms in Equation (53). These simply reflect the fact that surface reverberation is a problem only when the signal round trip time to the surface (nominally  $t_s$ ) is close to the signal round trip time to the target ( $t_a$ ).

---

<sup>1</sup> A factor of the form  $\exp\left\{-\frac{d^2}{8D^2 B_\theta^2} \sin^2\phi_o \cos^4\theta_o \cot^4\theta_o\right\}$  in the second

term has been omitted as negligible under most reasonable operating conditions, particularly when  $D \gg d$ .

It is interesting to observe that the allowed time differential  $t_a - t_s$  is of the order of  $\sigma_0$  for the noise component resulting from intermodulation of signal with reverberation while the differential  $t_a - t_s$  can be as large as  $\sqrt{\sigma_F^2 + \sigma_T^2/2 + \sigma_0^2}$  for the intermodulation products of reverberation with reverberation. Thus the use of very long pulses may create a surface reverberation problem at ranges where it would not otherwise exist if the dominant component of Equation (53) for  $t_a \approx t_s$  is the second term (low signal to noise ratio). This difficulty does not arise when the first term dominates (high signal to noise ratio). The physical explanation for this phenomenon is simple: The frequency modulation imposes a narrow range gate on reverberation (see Section I).

Only scatterers located such that the travel time of the signal to them is almost exactly the same as the travel time to the target can contribute to the intermodulation product of signal and reverberation. Whether the group of scatterers at suitable ranges does, in fact, contribute reverberation depends only on whether they lie within the illuminated surface area. This is purely a matter of geometry and independent of the pulse length. Intermodulation of reverberation with reverberation, on the other hand, occurs for any scatterer pair separated from each other by no more than the effective range gate. Whether a particular combination contributes reverberation at the observation time ( $t_a + t_D$ ) therefore depends both on whether it received illumination and on when it received illumination, i.e. on both geometry and pulse length.

Another interesting point of comparison between volume and surface reverberation is the radical in the second terms of Equations (52) and (53) respectively. When  $\sigma_0^2 \gg (\sigma_F^2 + \sigma_T^2/2)$  the radical in Equation (53) reduces

to  $\sqrt{2} \sqrt{\sigma_F^2 + \sigma_T^2 / 2}$ .<sup>1</sup> Thus the reverberation power is limited by the pulse duration, as in the case of volume reverberation. When  $\sigma_\theta^2 \ll (\sigma_F^2 + \sigma_T^2 / 2)$  the radical in Equation (53) reduces to  $\sqrt{2} \sigma_\theta$ . Thus further increases in pulse length do not increase the peak surface reverberation power. This is, of course, reasonable because the pulse duration is now sufficiently large for reverberation from the entire illuminated surface area to reach the receive simultaneously.

Additional differences between volume and surface reverberation concern the  $t_a$  dependence ( $t_a^{-6}$  and  $t_a^{-4}$  with volume reverberation versus  $t_a^{-7}$  and  $t_a^{-6}$  with surface reverberation) and the appearance of the factors  $\sin \theta_0$  and  $\sin^2 \theta_0$  in the case of surface reverberation. These differences are attributable to the different rate of growth with range of the number of scatterers contributing reverberation in the two cases.

#### V. Output Signal to Noise Ratio

The effectiveness of the detector is characterized by the relation of its output signal to noise ratio with the signal to noise ratio existing in the water. The output signal power is simply the square of the first term of Equation (13). Using  $t_a = t_b$  one obtains from Equation (13) and the first two terms of Equation (50) (volume reverberation, frequency modulated signal)

$$\left(\frac{S}{N}\right)_o = \frac{128 A^4 K \sigma_c}{t_a^4 c^6 \langle b^2 \rangle^2 K_V^2 \pi^3 B_\phi^2 B_\theta^2 \sqrt{\sigma_F^2 + \sigma_T^2 / 2}} \left[ 1 + \frac{16}{c^3} \frac{A^2 \sqrt{2}}{\langle b^2 \rangle \pi \frac{3}{2}} \frac{1}{t_a^2 \sqrt{\sigma_F^2 + \sigma_T^2 / 2}} \frac{1}{B_\phi B_\theta K_V} \right] \quad (56)$$

A simple computation from Equation (4) gives the average reverberation

<sup>1</sup>The effective integration time  $\sigma_F$  of the low-pass filter should clearly be of the order of the pulse width  $\sigma_T$ . A more precise optimum will be obtained later.

power at each receiver.

$$\text{Average reverberation power} = \left(\frac{\pi}{2}\right)^{\frac{3}{2}} \frac{c^3 \langle b^2 \rangle}{8 t_a^2} \sigma_T K_V B_\phi B_\theta \quad (57)$$

If  $t_a \approx t_b$  the peak signal power at each receiver is  $A^2/t_a^4$ .

Hence

$$\left(\frac{S}{N}\right)_{in} = \frac{16\sqrt{2} A^2}{\langle b^2 \rangle^{\frac{3}{2}} \pi^{\frac{3}{2}} c^3 t_a^2 K_V B_\phi B_\theta \sigma_T} \quad (58)$$

Thus Equation (56) can be rewritten in the form

$$\left(\frac{S}{N}\right)_o = \frac{1}{4} \sigma_T (K\sigma_c) \frac{\sigma_T}{\sqrt{\sigma_F^2 + \sigma_T^2/2}} \frac{\left(\frac{S}{N}\right)_{in}^2}{1 + \frac{\sigma_T}{\sqrt{\sigma_F^2 + \sigma_T^2/2}} \left(\frac{S}{N}\right)_{in}} \quad (59)$$

Several features of this expression are interesting.

When  $\frac{\sigma_T}{\sqrt{\sigma_F^2 + \sigma_T^2/2}} \left(\frac{S}{N}\right)_{in} \ll 1$

$$\left(\frac{S}{N}\right)_o \approx \frac{1}{4} \sigma_T (K\sigma_c) \frac{\sigma_T}{\sqrt{\sigma_F^2 + \sigma_T^2/2}} \left(\frac{S}{N}\right)_{in}^2 \quad (60)$$

When  $\frac{\sigma_T}{\sqrt{\sigma_F^2 + \sigma_T^2/2}} \left(\frac{S}{N}\right)_{in} \gg 1$

$$\left(\frac{S}{N}\right)_o \approx \frac{1}{4} \sigma_T (K\sigma_c) \left(\frac{S}{N}\right)_{in} \quad (61)$$

Using the definition of  $\sigma_c$  [Equation (10)] it is a simple matter to determine the optimum  $\sigma_F$  for either case. From Equation (60) one obtains

$$\sigma_F = \frac{\sigma_T}{\sqrt{2}} \quad (62)$$

The optimum  $\sigma_F$  in Equation (61) is infinite. However, it is clear from Equation (10) that only small gains in output signal to noise ratio can be made by increasing  $\sigma_F^2$  above  $\sigma_T^2/2$ . Equation (62) therefore gives a suitable

value of  $\sigma_F$  for all input signal to noise ratios.<sup>1</sup> With this choice

$$\frac{\sigma_T}{\sigma_F^2 + \sigma_T^2 / 2} = 1 \quad (63)$$

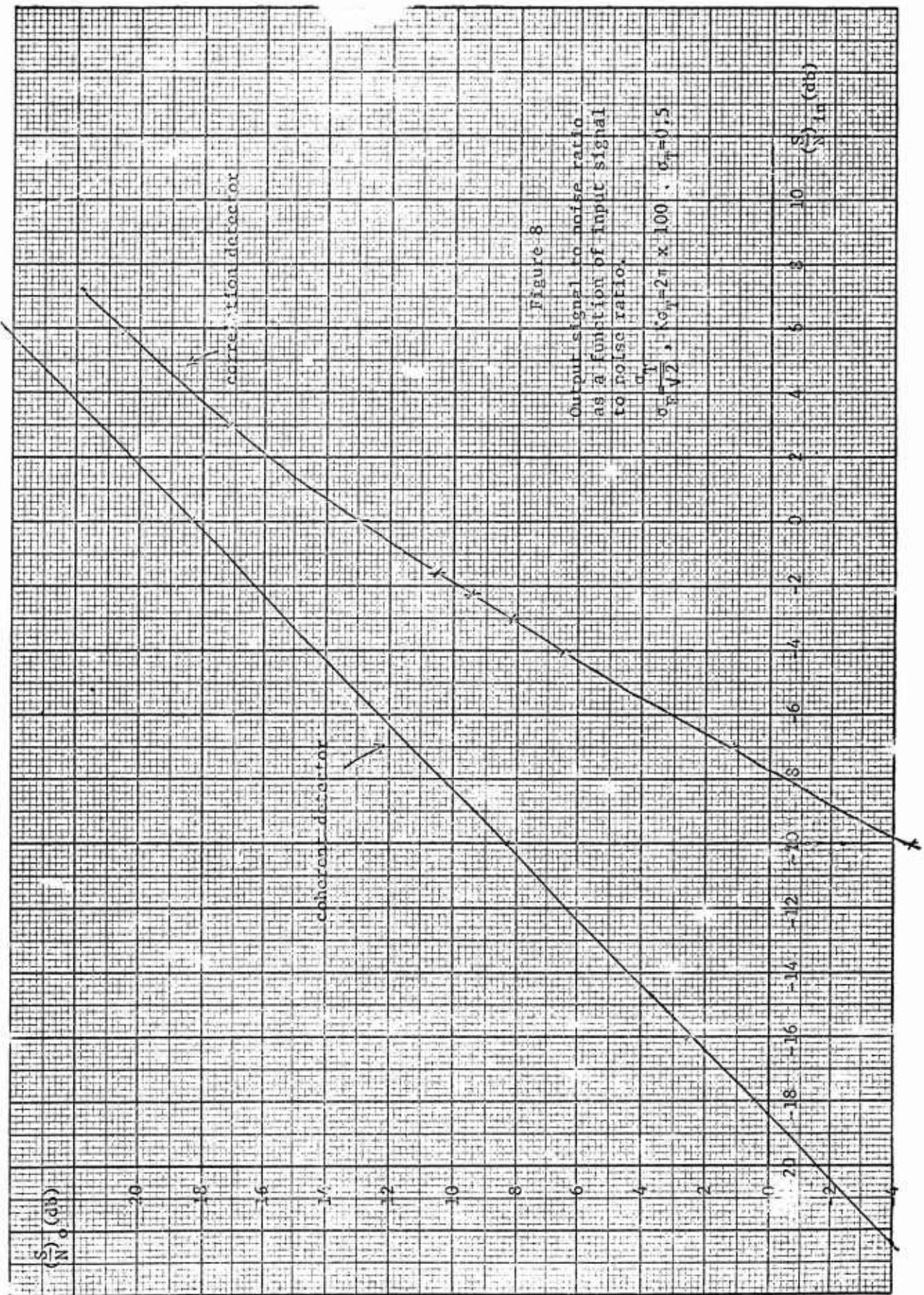
so that Equations (60) and (61) may now be interpreted as follows:

When the input signal to noise ratio is less than unity, the output signal to noise ratio varies with the square of the input signal to noise ratio, a type of behavior generally associated with incoherent detection. When the input signal to noise ratio exceeds unity, the output signal to noise ratio varies linearly with the input signal to noise ratio, a characteristic typical of coherent detection schemes. Equation (61) is, in fact, simply one-half of the output signal to noise ratio of a coherent detector (demodulating the output of a single receiver against a delayed replica of the transmitted signal). The factor of one-half is due to the presence of noise in each channel of the correlation detector. The replica used in the coherent detector is, of course, noise-free. Equation (59) with  $\sigma_F = \sigma_T / 2$ ,  $K\sigma_T = 2\pi \times 100$ , and  $\sigma_T = 0.5$  is plotted in Figure (8). Also shown is the corresponding curve for the coherent detector. If one chooses an output signal to noise ratio of 6 db as the minimum level at which some significant detection capability may be said to exist, Figure (8) indicates that the correlation detector requires about 8 db more input signal to noise ratio than the coherent detector to achieve this minimal performance. Even if one penalizes the coherent detector by 3 db on the grounds that the postulated knowledge concerning carrier phase is almost certainly unavailable in practice, there remains a differential of about 5 db.

---

<sup>1</sup>The presence of ambient noise - ignored thus far - would also mitigate against a choice of effective smoothing times  $\sigma_F$  much larger than the duration of the demodulated signal pulse.





The factor  $\sigma_T(K\sigma_c)$  appearing in Equation (59) can be rewritten

$$\sigma_T(K\sigma_c) = \frac{\sigma_T}{1/(K\sigma_c)} = \frac{1}{2} \frac{\sigma_T}{1/(K\sigma_T)} \text{ (with } \sigma_F = \sigma_T/\sqrt{2} \text{)}. \quad (64)$$

Since  $K\sigma_T$  is a direct measure of the signal bandwidth, its inverse may be interpreted as the correlation time of the signal (and hence of the reverberation). The "processing gain" factor (64) is therefore the ratio of signal duration to signal correlation time. It can be made substantial by the use of wide signal bandwidths. It is, of course, nothing more than the quantitative expression of the range gating effect discussed earlier.

In the absence of frequency modulation the equivalent of Equation (59) is

$$\left(\frac{S}{N}\right)_o = \frac{1}{2} \frac{\sigma_T}{\sqrt{\sigma_T^2 + 2\sigma_F^2}} \frac{\left(\frac{S}{N}\right)_{in}^2}{1 + \frac{\sigma_T}{\sqrt{\sigma_T^2 + \sigma_F^2}} \left(\frac{S}{N}\right)_{in}} \quad (65)$$

With  $\sigma_F = \frac{\sigma_T}{\sqrt{2}}$  (66)

the "processing gain" is of the order of unity. All other comments concerning Equation (59) apply to Equation (65) also.

In order to avoid misinterpretation of Equations (59) and (65) it should, perhaps, be pointed out that the input signal to noise is also a function of  $\sigma_T$ . Thus, from Equation (58)

$$\left(\frac{S}{N}\right)_{in} \propto \frac{1}{\sigma_T} \quad (67)$$

Hence in the presence of frequency modulation [Equation (59)]

$$\left(\frac{S}{N}\right)_o \propto \begin{cases} \frac{K\sigma_c}{\sigma_T} = \frac{K}{2} & \text{for } \left(\frac{S}{N}\right)_{in} \ll 1 \\ K\sigma_c = \frac{K}{2} \sigma_T & \text{for } \left(\frac{S}{N}\right)_{in} \gg 1 \end{cases} \quad (68)$$

In the absence of frequency modulation [Equation (65)]

$$\left(\frac{S}{N}\right)_o \propto \begin{cases} \frac{1}{\sigma_T^2} & \text{for } \left(\frac{S}{N}\right)_{in} \ll 1 \\ \frac{1}{\sigma_T} & \text{for } \left(\frac{S}{N}\right)_{in} \gg 1 \end{cases} \quad (69)$$

The use of short pulses is advantageous in the absence of frequency modulation because the bandwidth (and hence the range gating effect) is determined exclusively by  $\sigma_T$ . In the presence of frequency modulation pulse length is a secondary factor, for the rise in bandwidth offsets the decrease in input signal to noise ratio accompanying an increase in  $\sigma_T$ . For fixed bandwidth (fixed  $K\sigma_T$ ) the output signal to noise ratio increases monotonically as  $\sigma_T$  decreases. Thus the use of short pulses (with large values of  $K$  to maintain constant bandwidth) is indicated. However, once the input signal to noise ratio exceeds unity, further decreases in  $\sigma_T$  cause only a small increase in output signal to noise ratio.

In the case of surface reverberation the signal to noise ratio is critically dependent on the exponential factors in Equation (53). When  $(t_a - t_s)^2 \ll \sigma_\theta^2$  both of these factors are close to unity and one obtains the following equivalent of Equation (59) (frequency modulated signal)

$$\left(\frac{S}{N_o}\right) = \frac{1}{4} \frac{\sigma_\theta \sigma_T^2 \sqrt{\sigma_T^2/2 + \sigma_F^2 + \sigma_\theta^2}}{\sqrt{\sigma_T^2/2 + \sigma_F^2} (\sigma_T^2/2 + \sigma_\theta^2)} (K\sigma_c) \frac{\left(\frac{S}{N}\right)_{in}^2}{1 + \frac{\sigma_T \sqrt{\sigma_T^2/2 + \sigma_F^2 + \sigma_\theta^2}}{\sqrt{(\sigma_T^2/2 + \sigma_F^2)(\sigma_T^2/2 + \sigma_\theta^2)}} \left(\frac{S}{N}\right)_{in}} \quad (70)$$

With  $\sigma_F = \sigma_T/\sqrt{2}$  this result reduces to

$$\left(\frac{S}{N}\right)_o = \frac{1}{4} \sigma_T (K\sigma_c) \frac{\sigma_\theta \sqrt{\sigma_T^2 + \sigma_\theta^2}}{\sigma_T^2/2 + \sigma_\theta^2} \frac{\left(\frac{S}{N}\right)_{in}^2}{1 + 2\sqrt{2} \sqrt{\frac{\sigma_T^2 + \sigma_\theta^2}{\sigma_T^2/2 + \sigma_\theta^2}} \left(\frac{S}{N}\right)_{in}} \quad (71)$$

When  $\sigma_T \ll \sigma_\theta$

$$\sigma_T(K\sigma_c) \frac{\sigma_\theta \sqrt{\sigma_T^2 + \sigma_\theta^2}}{\sigma_T^2/2 + \sigma_\theta^2} \approx \sigma_T(K\sigma_c) \quad (72)$$

so that the "processing gain" is the same as with volume reverberation. On the other hand, when  $\sigma_T \gg \sigma_\theta$

$$\sigma_T(K\sigma_c) \frac{\sigma_\theta \sqrt{\sigma_T^2 + \sigma_\theta^2}}{\sigma_T^2/2 + \sigma_\theta^2} \approx 2\sigma_\theta(K\sigma_c) \quad (73)$$

Thus the "processing gain" rises with increasing pulse length to a maximum determined by the geometry of the illuminated surface area. As in the case of volume reverberation, this  $\sigma_T$  dependence is somewhat deceptive because of the  $\sigma_T$  dependence of the input signal to noise ratio. For surface reverberation

$$\left(\frac{S}{N}\right)_{in} \propto \begin{cases} \frac{1}{\sigma_T} & \text{for } \sigma_T \ll \sigma_\theta \\ \frac{1}{\sigma_\theta} & \text{for } \sigma_T \gg \sigma_\theta \end{cases} \quad (74)$$

Hence for low input signal to noise ratios  $[(\frac{S}{N})_o \propto (\frac{S}{N})_{in}^2]$

$$\left(\frac{S}{N}\right)_o \propto \left\{ \begin{array}{l} \frac{K\sigma_c}{\sigma_T} = \frac{K}{2} \text{ for } \sigma_T \ll \sigma_\theta \\ \frac{K\sigma_c}{\sigma_\theta} = \frac{K\sigma_T}{2\sigma_\theta} \text{ for } \sigma_T \gg \sigma_\theta \end{array} \right\} \sigma_F = \frac{\sigma_T}{\sqrt{2}} \quad (75)$$

Thus the output signal to noise ratio increases with pulse duration only when  $\sigma_T$  exceeds  $\sigma_\theta$ , i.e. the entire surface area within the beam receives illumination simultaneously.

For high input signal to noise ratios  $[(\frac{S}{N})_o \propto (\frac{S}{N})_{in}]$  one finds

$$\left(\frac{S}{N}\right)_o \propto \sigma_T \quad (76)$$

for all values of  $\sigma_T/\sigma_\theta$ . These observations are, of course, also evident from Equation (53).

When  $\sigma_T \gg \sigma_\theta$  and the target is so located that  $\sigma_\theta \ll t_a - t_s \ll \sqrt{\sigma_F^2 + \sigma_T^2/2 + \sigma_\theta^2}$  the first exponential term in Equation (53) vanishes while the second assumes a value close to unity.

In that case

$$\left(\frac{S}{N}\right)_o = \frac{1}{4} \frac{\sigma_\theta \sigma_T^2 \sqrt{\sigma_T^2/2 + \sigma_F^2 + \sigma_\theta^2}}{\sqrt{(\sigma_T^2/2 + \sigma_F^2)(\sigma_T^2/2 + \sigma_\theta^2)}} (K\sigma_c) \left(\frac{S}{N}\right)_{in}^2 \quad (77)$$

or with  $\sigma_F = \sigma_T/\sqrt{2}$

$$\left(\frac{S}{N_o}\right) = \frac{1}{4} \sigma_T (K\sigma_c) \frac{\sigma_\theta \sqrt{\sigma_T^2 + \sigma_\theta^2}}{\sigma_T^2/2 + \sigma_\theta^2} \left(\frac{S}{N}\right)_{in}^2 \quad (78)$$

Thus, it is possible to find operating conditions under which the output signal to noise ratio varies with the square of the input signal to noise ratio for all values of input signal to noise ratio.

#### VI. Comparison With Detector Operating in Ambient Noise Limited Environment

Throughout the preceding discussion the received noise was assumed to consist exclusively of reverberation. It will be interesting, for purposes of comparison, to evaluate now the performance of the same receiver in a noise environment consisting predominantly of ambient noise. The ambient noise will be regarded as a stationary Gaussian random process with the power spectrum.

$$S(\omega) = N_o \left\{ \exp \left[ - \frac{(\omega - \omega_o)^2}{\Omega_N^2} \right] + \exp \left[ - \frac{(\omega + \omega_o)^2}{\Omega_N^2} \right] \right\} \quad (79)$$

or the autocorrelation function

$$R(\tau) = \int_0^{\infty} S(\omega) \cos \omega \tau d\omega = \sqrt{\pi} \Omega_N N_0 \exp\left\{-\frac{\Omega_N^2 \tau^2}{4}\right\} \cos \omega_0 \tau \quad (80)$$

One may think of  $N_0$  as the spectral level of a broadband noise whose spectrum is being shaped by a bandpass filter of halfwidth  $\sqrt{2}\Omega_N$  centered at frequency  $\omega_0$ . In practice, this filter might be the inherent frequency response characteristic of the receiving hydrophones or it might be a narrower filter inserted into the hydrophone outputs to discriminate against frequencies outside of the signal range.<sup>1</sup>

If one designates the noise appearing at the two receiver outputs as  $n_a(t)$  and  $n_b(t)$  respectively, then from Figure 1 and Equation (1)

$$y(t) = \left\{ \frac{A}{t_a^2} \exp\left[-\frac{(t-t_a)^2}{\sigma_T^2}\right] \cos\left[\omega_0(t-t_a) + \frac{K}{2}(t-t_a)^2\right] + n_a(t) \right\} \\ \cdot \left\{ \frac{A}{t_b^2} \exp\left[-\frac{(t-t_b-t_r)^2}{\sigma_T^2}\right] \cos\left[\omega_0(t-t_b-t_r) + \frac{K}{2}(t-t_b-t_r)^2\right] + n_b(t) \right\} \quad (81)$$

The detector output  $z(t)$  is related to  $y(t)$  through Equation (6), the low pass filter weighting function  $w(t)$  being specified by Equation (7). The signal component of  $z(t)$  is the same as in the reverberation limited case. With  $t_r = t_a - t_b$  the noise component assumes the form

$$z(t)|_{\text{noise}} = \frac{A}{t_a^2} \int_0^{\infty} d\rho w(\rho) \exp\left[-\frac{(t-t_a-\rho)^2}{\sigma_T^2}\right] \cos\left[\omega_0(t-t_a-\rho) + \frac{K}{2}(t-t_a-\rho)^2\right] n_a(t-\rho) \\ + \frac{A}{t_b^2} \int_0^{\infty} d\rho w(\rho) \exp\left[-\frac{(t-t_b-\rho)^2}{\sigma_T^2}\right] \cos\left[\omega_0(t-t_b-\rho) + \frac{K}{2}(t-t_b-\rho)^2\right] n_b(t-\rho)$$

---

<sup>1</sup>Any such filter is assumed to be sufficiently broad so that it will have negligible effect on the signal.

$$+ \int_0^{\infty} d\rho w(\rho) n_a(t-\rho) n_b(t-\rho) \quad (82)$$

If receivers a and b are separated by more than a very few feet, it is probably reasonable to assume that  $n_a(t)$  and  $n_b(t)$  are statically independent. It also appears reasonable to assume that each noise component has zero mean. In that case the expected value of  $z(t)$  is zero and its variance is simply the sum of the mean square values of the three terms in Equation (82). Thus

$$\begin{aligned} D^2 \{z(t_a + t_D)\} &= \frac{A^2}{t_a^4} \int_0^{\infty} d\rho \int_0^{\infty} d\sigma w(\rho) w(\sigma) \exp\left\{-\frac{(t_D - \rho)^2}{\sigma_T^2}\right\} \exp\left\{-\frac{(t_D - \sigma)^2}{\sigma_T^2}\right\} \\ &\quad \cos\left[\omega_0(t_D - \rho) + \frac{K}{2}(t_D - \rho)^2\right] \cos\left[\omega_0(t_D - \sigma) + \frac{K}{2}(t_D - \sigma)^2\right] R(\sigma - \rho) \\ &+ \frac{A^2}{t_b^4} \int_0^{\infty} d\rho \int_0^{\infty} d\sigma w(\rho) w(\sigma) \exp\left\{-\frac{(t_D - \rho)^2}{\sigma_T^2}\right\} \exp\left\{-\frac{(t_D - \sigma)^2}{\sigma_T^2}\right\} \\ &\quad \cdot \cos\left[\omega_0(t_D - \rho) + \frac{K}{2}(t_D - \rho)^2\right] \cos\left[\omega_0(t_D - \sigma) + \frac{K}{2}(t_D - \sigma)^2\right] R(\sigma - \rho) \\ &+ \int_0^{\infty} d\rho \int_0^{\infty} d\sigma w(\rho) w(\sigma) R^2(\sigma - \rho) \end{aligned} \quad (83)$$

where  $R(\tau)$  is given by Equation (80). The first two terms differ only in the attenuation factor  $A/t_a^4$  vs  $A/t_b^4$ . Since  $t_a \approx t_b$  for all cases of interest this difference will be ignored. The averaging operation can now be performed without difficulty. After algebraic simplification the result is

$$D^2 \{z(t_a + t_D)\} = \frac{A^2}{t_a^4} \Omega_N N_o \sqrt{\pi} \frac{\sigma_T}{\sigma_F} \frac{1}{\sqrt{4 \frac{(\sigma_T^2 + \sigma_F^2)^2}{\sigma_T^2 \sigma_F^2} + 2\Omega_N^2 (\sigma_T^2 + \sigma_F^2) + K^2 \sigma_F^2 \sigma_T^2}} + \frac{\frac{\pi}{2} \Omega_N^2 N_o^2}{\sqrt{1 + \sigma_F^2 \Omega_N^2}} \quad (84)$$

The output signal power is still given by the square of the first term

of Equation (13). Hence

$$\left(\frac{S}{N}\right)_o = \frac{1}{2} \frac{\sigma_c^2}{\sigma_F^2} \Omega_N \sigma_F \frac{A^4 \sqrt{1 + \frac{1}{\sigma_F^2 \Omega_N^2}}}{\pi t_a^8 \Omega_N^2 N_o^2} \frac{1}{1 + \frac{2A^2}{t_a^4 \sqrt{\pi}} \frac{\sigma_T}{N_o} \sqrt{\frac{1 + \frac{1}{\sigma_F^2 \Omega_N^2}}{4 \frac{(\sigma_T^2 + \sigma_F^2)^2}{\sigma_T^2 \sigma_F^2} + 2\Omega_N^2 (\sigma_T^2 + \sigma_F^2) + K^2 \sigma_F^2 \sigma_T^2}}} \quad (85)$$

The input signal to noise ratio at each receiver is easily computed to be

$$\left(\frac{S}{N}\right)_{in} = \frac{A^2}{t_a^4 \sqrt{\pi} \Omega_N N_o} \quad (86)$$

The output signal to noise ratio can now be written in a form equivalent to that of Equations (59) and (65)

$$\left(\frac{S}{N}\right)_o = \frac{1}{2} \frac{\sigma_c^2}{\sigma_F^2} \sqrt{1 + \Omega_N^2 \sigma_F^2} \frac{\left(\frac{S}{N}\right)_{in}^2}{1 + \frac{2\Omega_N \sigma_T \sqrt{1 + \frac{1}{\Omega_N^2 \sigma_F^2}}}{\sqrt{4 \frac{(\sigma_T^2 + \sigma_F^2)^2}{\sigma_T^2 \sigma_F^2} + 2\Omega_N^2 (\sigma_T^2 + \sigma_F^2) + K^2 \sigma_F^2 \sigma_T^2}}} \left(\frac{S}{N}\right)_{in} \quad (87)$$

In order to obtain a comparison with the reverberation limited case, it is necessary to select a suitable value for the noise spectral width  $\Omega_N$ . The best value for this purpose is that which gives the ambient noise spectrum the form of the reverberation spectrum.

The reverberation autocorrelation can be obtained from Equation (3)

$$R_{rev}(\tau) = E \left\{ \sum_i \sum_j \frac{a_i a_j}{t_i^2 t_j^2} \exp \left[ -\frac{(t-t_i)^2}{\sigma_T^2} \right] \exp \left[ -\frac{(t+\tau-t_j)^2}{\sigma_T^2} \right] \cos \left[ \omega_o(t-t_i) + \frac{K}{2} (t-t_i)^2 \right] \cos \left[ \omega_o(t+\tau-t_j) + \frac{K}{2} (t+\tau-t_j)^2 \right] \right\} \quad (88)$$



Carrying out the averaging operation over all random variables one obtains

$$R_{\text{rev}}(\tau) = \frac{\langle b^2 \rangle c^3 \pi^{\frac{3}{2}}}{16\sqrt{2} t_a^2} K_V B_\theta B_\phi \sigma_T \exp \left\{ - \left( \frac{1}{2\sigma_T^2} + \frac{K^2 \sigma_T^2}{8} \right) \tau^2 \right\} \cos \omega_0 \tau \quad (89)$$

Thus the reverberation autocorrelation function [Equation (89)] and the ambient noise autocorrelation function are identical in form if

$$\Omega_N = \sqrt{\frac{2}{\sigma_T^2} + \frac{K^2 \sigma_T^2}{2}} \quad (90)^1$$

With this value of  $\Omega_N$  Equation (87) becomes

$$\left( \frac{S}{N} \right)_o = \frac{1}{2\sqrt{2}} \frac{\sigma_c^2}{\sigma_F} \frac{1}{\sigma_T} \sqrt{4\sigma_F^2 + 2\sigma_T^2 + K^2 \sigma_T^4 \sigma_F^2} \frac{\left( \frac{S}{N} \right)_{\text{in}}^2}{1 + \sqrt{2} \frac{\sigma_c}{\sigma_F} \sqrt{\frac{4\sigma_F^2 + 2\sigma_T^2 + K^2 \sigma_T^4 \sigma_F^2}{4\sigma_F^2 + 4\sigma_T^2 + K^2 \sigma_T^4 \sigma_F^2}} \left( \frac{S}{N} \right)_{\text{in}}} \quad (91)$$

It is a simple matter to demonstrate that Equation (91) reduces to Equation (59) when the bandwidth of the transmitted signal is determined primarily by the frequency modulation [case (A)]. In the absence of frequency modulation [case (B)] Equation (91) reduces to Equation (65). There is no reason to doubt that a similar check could be obtained for frequency modulated signals of a bandwidth comparable to  $1/\sigma_T$ , for which no formal computations were carried out in the reverberation limited case. Thus it appears that Equation (91) may be regarded as a generalization of Equations (59) and (65), covering intermediate values of frequency deviation  $K\sigma_T$  as well as the extremes represented by cases (A) and (B). One therefore concludes that the detector responds in identical fashion to reverberation and to ambient noise of the same power

---

<sup>1</sup>If  $\sqrt{2}\Omega_N$  is indeed the halfwidth of a bandpass filter as suggested earlier, then choice of the value given by Equation (90) would, of course, result in some modification of the signal spectrum.

and spectral shape as long as the assumptions common to Equations (59) and (65) are valid. These are basically the assumptions permitting the reduction of Equation (49) to the first two terms of Equation (50). In physical terms they are

- 1) No significant percentage of the total reverberation power must be contributed by any small collection of scatterers with large cross-section (false targets).
- 2) The parameter  $\rho$ , a combination of looking angle and beam dimensions given by Equation (45), must be sufficiently large so that accumulation of unresolvable small scatterers do not contribute a significant percentage of the total reverberation power. Practically speaking, this is likely to be a problem only for narrow beams directed very close to horizontal and endfire.

Requirements 1) and 2) are, of course, precisely the conditions under which one can invoke the Central Limit Theorem and argue that the combined returns from many small scatterers form a Gaussian random process whose statistical properties are then completely determined by its autocorrelation function.<sup>1</sup>

The above remarks should not be interpreted to mean that there is no significant difference between reverberation and ambient noise, even when conditions 1) and 2) are satisfied. What they do mean is that any differences in performance are due to differences in the input signal to noise ratio. Perhaps the most important feature of the input signal to noise ratio in the ambient noise case is its inverse dependence on  $\Omega_N$  [see Equation (86)]. If

---

<sup>1</sup>See, for instance, H.L. Van Trees, "Optimum Signal Design and Processing for Reverberation Limited Environment" IEEE Transactions on Military Electronics Vol. MIL 9, pp. 212-229, July, Oct. 1965.

$\Omega_N$  is adjusted in accordance with Equation (90), i.e. in accordance with the signal bandwidth, one does not obtain the improvement of output signal to noise ratio with increased bandwidth (frequency modulation) observed in the reverberation limited case. Thus Equation (60) [low input signal to noise ratio] now varies inversely with bandwidth ( $K\sigma_T$ ) while Equation (61) [high input signal to noise ratio] is independent of ( $K\sigma_T$ ). The use of narrowband transmitted signals is therefore indicated for ambient noise limited operation, provided that Doppler shift considerations (which have been ignored in this analysis) permit the use of a sufficiently narrow filter bandwidth  $\Omega_N$ .

#### VII. Concluding Remarks

One of the primary purposes of this report is to provide an analytical framework or future studies of various problems in active sonar detection. Some of the specific assumptions used here (stationary target and scatterers, independence of location of different scatterers, absence of distortion or multipath effects in the return signal) are clearly unrealistic in many cases and will have to be modified in subsequent investigations. In the meantime the detection problem has been analyzed at least under highly idealized conditions and insight has been gained into such questions as the conditions under which reverberation can be regarded as equivalent to Gaussian ambient noise with a known spectrum. The results of the present analysis should therefore permit simplifications of later analyses employing more realistic models of the transmission and reverberation mechanisms.

The first steps towards the generation of a better model should probably be the inclusion of Doppler shifts due to source, target, and scatterer motion and recognition of the fact that the target return may not be simply a delayed and Doppler shifted replica of the transmitted signal. Work along these lines is now in progress.

Unclassified

Security Classification

DOCUMENT CONTROL DATA - R & D

(Security classification of title, body of abstract and indexing annotation must be entered when the overall report is classified)

1. ORIGINATING ACTIVITY (Corporate author) General Dynamics Corporation Electric Boat division Groton, Connecticut		2a. REPORT SECURITY CLASSIFICATION Unclassified	
		2b. GROUP —	
3. REPORT TITLE PROCESSING OF DATA FROM SONAR SYSTEMS VOLUME IV, SUPPLEMENT 1			
4. DESCRIPTIVE NOTES (Type of report and inclusive dates) Annual Report, 1 July 1965 to 1 July 1966			
5. AUTHOR(S) (First name, middle initial, last name) Morton Kanefsky, F.S. Hill, Jr., and Peter M. Schultheiss			
6. REPORT DATE December 27, 1967		7a. TOTAL NO. OF PAGES 137	7b. NO. OF REFS —
8a. CONTRACT OR GRANT NO. NONr 2512 (00)		9a. ORIGINATOR'S REPORT NUMBER(S) U417-67-084	
b. PROJECT NO.		9b. OTHER REPORT NO(S) (Any other numbers that may be assigned this report)	
c.			
d.			
10. DISTRIBUTION STATEMENT Each transmittal of this document outside the agencies of the U.S. Government must have prior approved of Office of Naval Research.			
11. SUPPLEMENTARY NOTES		12. SPONSORING MILITARY ACTIVITY Office of Naval Research Washington, D. C.	
13. ABSTRACT This Supplement and Volume IV examine performance of digital optimal and suboptimal detectors in an interference-dominated environment. Costs of clipping and sampling and the problem of recovering clipping losses are evaluated. Detection threshold variations dependent on measured noise parameters are also studied. Using noise power as a parameter shows non-parametric properties asymptotically independent of the noise amplitude distribution. Reduced dependency on noise properties can also be achieved by a zero count at each hydrophone. An active receiver using widely separated receivers for reverberation and noise-dominated conditions, and the effect of linear frequency modulation on the transmitted signal, are examined. Computation of ambient noise directivity is reported for shallow depths.			

DD FORM 1473 (PAGE 1)

1 NOV 65  
S/N 0101-807-6801

Unclassified

Security Classification

